Molecular Engineering Directives for Nano-Level Architectures with Aromatic $\pi - \pi$ Systems

A thesis submitted

in Partial Fulfillment of the Requirements

for the Degree of

DOCTOR OF PHILOSOPHY

by

Sajitha Sasidharan

Department of Biosciences and Bioengineering

Indian Institute of Technology Guwahati

Guwahati 781039, India

November 2018

Molecular Engineering Directives for Nano-Level Architectures with Aromatic $\pi - \pi$ Systems

A thesis submitted

in Partial Fulfillment of the Requirements

for the Degree of

DOCTOR OF PHILOSOPHY

by

Sajitha Sasidharan

Supervisor

Dr. Vibin Ramakrishnan

Department of Biosciences and Bioengineering

Indian Institute of Technology Guwahati

Guwahati 781039, India

November 2018

“ You have never lived until You
have almost died,
And for those who choose to fight,
Life has a special flavor,
The protected will never know!!! ”

-Capt R Subramanium

DEDICATED TO MY PARENTS AND TO ALL THE BRAVE SOULS OF MY COUNTRY WHO LAID DOWN THEIR LIVES TO MAKE THE TRICOLOR FLY HIGH. . .

...Sajitha Sasidharan

STATEMENT

I hereby declare that this Ph.D. thesis entitled "Molecular Engineering Directives for Nano-Level Architectures with Aromatic $\pi - \pi$ Systems" was carried out by me for the degree of Doctor of Philosophy under the guidance and supervision of Dr.Vibin Ramakrishnan and Dr. Nitin Chaudhary.

I hereby declare that this dissertation is my own original work and has not been submitted before to any institution for assessment purposes. Further, due acknowledgements have been made and the research findings referred have been cited in the reference section.

Date: 3/12/2018

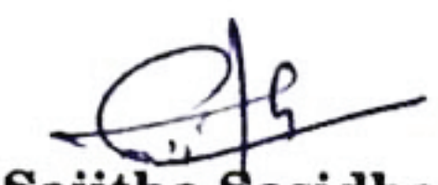

Sajitha Sasidharan

CERTIFICATE

It is certified that this work described in the thesis entitled "Molecular Engineering Directives for Nano-Level Architectures with Aromatic $\pi - \pi$ Systems" by Ms. Sajitha Sasidharan, a student of the Department of Biosciences and Bioengineering, IIT Guwahati was carried out under my supervision and has not been submitted elsewhere for the award of any degree.

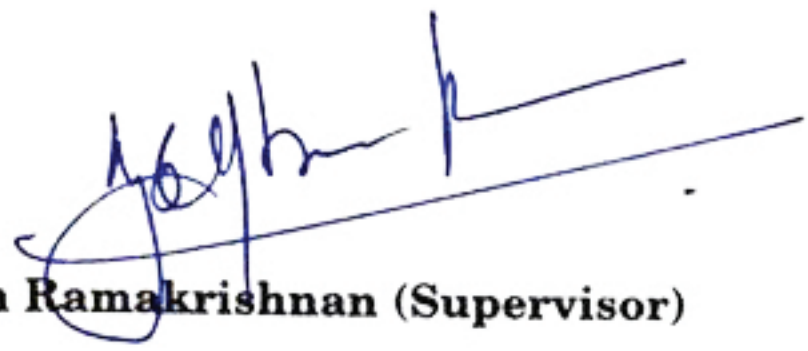

Dr. Vibin Ramakrishnan (Supervisor)

Dr. Nitin Chaudhary (Co-Supervisor)

ACKNOWLEDGEMENT

First and foremost, I would like to acknowledge my thesis Supervisor, Dr. Vibin Ramakrishnan, without whom this doctoral degree would have remained a dream. His creativity and passion towards the field of interdisciplinary science has always inspired me and his constant support has been a driving force to explore different areas of research in my doctoral research.

I wish to thank my Co-Supervisor Dr. Nitin Chaudhary, doctoral committee Chairman Prof. Vishal Trivedi, and doctoral committee members Dr. B. Anand, and Prof. Sreedeep for their participation and valuable insights to pursue my research in the right direction.

I would also like to thank all faculty members and technical staff of the department who extended their help when required. I would like to acknowledge CIF, IIT Guwahati for supporting us with instrumental facilities.

I would like to acknowledge MHRD for research fellowship, DST-SERB for travel assistance and DBT (Grant no. BT/350/NE/TBP/2012, BT/565/NE/U-Excel/2016) for research funding.

I am grateful to Mr. Alex P. Andrews and Dr. M.M. Shaijumon from IISER Thiruvananthapuram, Dr. Babu Varghese and Dr. Sudha for their technical help in Single Crystal Analysis. I also thank Dr Sudeep, University of Toronto for helping me in the synthesis of nanoparticles. I am indebted to Prof. P.K. Iyer and Prof. Roy Paily and their lab members Anwesha and Rajan Singh for helping with the electrical measurements.

I would like to thank my fellow research members Dr. Prakash Kishore Hazam and Gaurav Jerath, Gaurav Pandey, Yvonne, Mukesh, Akhil, Jahnu Saikia and Rishi Sreedhar for their constant support. I would specially like to thank Ruchika Goyal, Vivek Prakash and Franklin for helping me in my research and dissertation work.

I would also like to acknowledge the group members of Dr. Nitin Chaudhary for their constant co-operation and support .

I would like to mention special thanks to Dr. S. Murugavelh, who has guided me right

from my bachelor's studies and giving me right suggestions when required.
I thank my friends, Himakshi,Varsha, Somya, Deepak, Ajay, Ashok, Tejveer, Anjali Singh, Feba, Anshuman, Nethi, Vishnu, Sangkha Borah, Bijita and the entire athletics team of IIT Guwahati for giving me beautiful memories to cherish.
I would also like to acknowledge Karabi Saikia, Anamika Kalita, Anjali Pillai, Avinash Kumar, Prem Bhardwaj and Kranthi Rupavath, for their emotional support, understanding and constant motivation during my ups and downs.
I would like to thank my parents and family for their support, encouragement and love and the values they have instilled in me, which always I abide by. I thank my brother Saravanan for being my wonderful friend and my moral support during my tough times.

SYNOPSIS

Aromatic $\pi - \pi$ interactions, known as π-stacking involves interactions of aromatic rings of individual molecules, forming functional nanoassemblies. Among all the aromatic systems reported, benzene dimer is considered to be the prototypical system for the study of $\pi - \pi$ stacking. π-stacking systems are important building blocks in the design of peptide and small organic molecules as it dominates significant number of the supramolecular assembly and recognition process. External perturbations are believed to influence the π-stacking interactions through their impact on the π-electron density of the aromatic ring. Self-assembling peptide and organic systems containing quadrupole and dipole ring systems are chosen as the model systems for our experiments described in this thesis. Though it is a spontaneous process, where no further input of information is required, the final structures cannot be directed as it happens in macroscopic engineering. Fabrication at the nanoscale is a process at which the atoms are placed specifically at its designated sites. An attempt to direct the fabrication process was made i) where the basic units are sequences of amino acids with different symmetry elements and ii) where the basic units are Triphenylmethyl based organic systems. The resulting nano-assemblies forming organic nanoflowers and stimulus responsive hybrid systems can potentially be harnessed in the fabrication of devices, especially for heavy metal sequestration, capacitors and field-effect transistors (FETs).

TABLE OF CONTENTS

CHAPTER 1

INTRODUCTION

Self-organization is envisaged as a spontaneous process which involves development of an order or a recurring pattern as a result of local interactions between smaller subunits of an initially disordered system. A classic case of self-organization is folding and aggregation of a protein chain to its functional and dysfunctional forms respectively [1]. 1n 1641, Galileo made a foreseeing observation that "book of nature is written in the language of geometry" [2]. Almost all biological systems are assemblies of one or more molecules from nano to macro level. Robustness and efficient functioning of these assembled architectures are well established. John Von Neumann in his article entitled "The Mathematician" makes a far reaching statement; "The most vitally characteristic fact about mathematics is, in my opinion, is it's quite peculiar relationship to the natural sciences, or, more generally, to any science which interprets experience on a higher than purely descriptive level" [3]. It is hence logical to assume that the geometry of assemblies is a derivative of the individual geometry of the basic constituent. Helmholtz in one of his recorded lectures makes an observation that, "the forces so far as they cause chemical and mechanical influence in a living system, must be quite the same character as inorganic forces" [4]. We therefore through this

investigation makes a minimal attempt to understand the specific role of symmetry of the basic building block and effect of electrostatic interactions in determining the geometry of growth while individual units assemble to form nano to macro level assemblies, with combinations of phenyl group based molecular constructs as basic model system.

1.1 Philosophical Formulation of this Thesis

In this thesis, we attempt to understand the connection between physical and chemical characteristics of basic building blocks, its shape and stability, and finally, the nano and micro level associations of such assemblies. One inspiration to conduct such an investigation is the book "On Growth and Form" by D'Arcy Wentworth Thompson [4] written at the beginning of last century, attempting to quantitatively assess structural patterns and formations in biological systems.

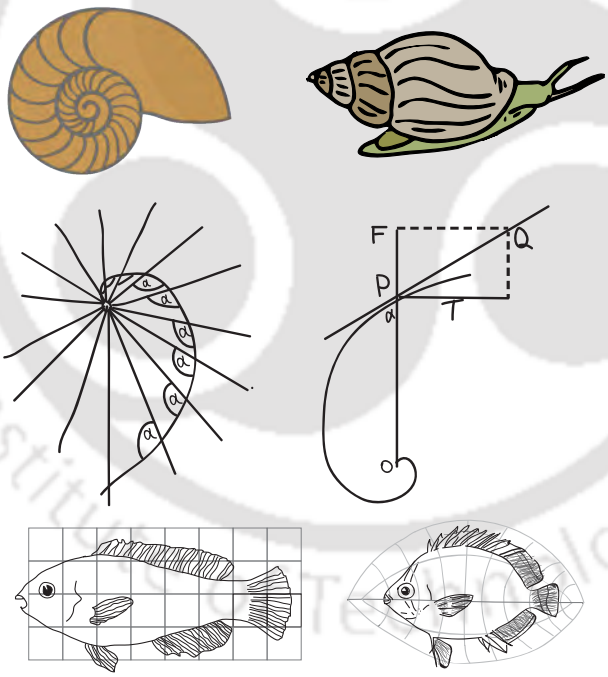

Figure 1.1: Mathematical study of growth and form in various organisms by D'Arcy Thompson.

Thompson in his book argue that all organic forms are in conformity with physical and mathematical laws, and Charles Darwin's natural selection was not the only major influence on the origin and development of species and their unique forms. In a classic example, illustrated by Thompson, the surface of any shell, whether discoid or turbinate,

may be imagined to be generated by the revolution about a fixed axis of a closed curve. By remaining in always geometrically similar to itself, it increases its dimension continually; and, since the scale of the figure increases in geometrical progression while the angle of rotation increases in arithmetical, and the center of similitude remains fixed, the curve traced in space by corresponding points in the generating curve is, in all such cases, an equiangular spiral. The interesting point in his observation is the replication of a self-consistent smaller object forming assemblies, resulting in objects of higher dimension (Figure 1.1).

The fundamental concept of 'nanotechnology' was first discussed by Richard Feynman in his talk "There's Plenty of Room at the Bottom" [5]. Feynman was one of the renowned theoretical physicists in the world, and his work in the early 1940's earned him Nobel Prize in 1965. In his lecture, he described the possibility of "a staggeringly small world that is below". Norio Taniguchi introduced the term "nano-technology" in 1974 [6]. Invention of scanning tunneling microscope, by Gerd Binnig and Heinrich Rohrer in 1981 facilitated unprecedented visualization of smaller objects at molecular scale [7]. Binnig, Quate and Gerber's invention of Atomic Force Microscope (AFM) in 1986 [8] and discovery of fullerenes by Harry Kroto [9] have contributed in solidifying the base of this futuristic discipline.

Drexler in his book "Engines of Creation: The Coming Era of Nanotechnology" [10] first proposed the possibility of a nanoscale "assembler". A nanoscale assembler can in principle build a copy of itself and of other items of arbitrary complexity. Drexler's theoretical work on the concept of molecular manufacturing with 'self replicators' is the therefore the basic philosophical framework of this thesis work.

1.2 Geometric Variations of Phenyl Embraces

The most common aromatic compound is benzene. The structural representation for benzene has a six membered ring, represented usually as a hexagon, which includes three double bonds. Each of the carbons is bonded to one hydrogen atom. The double bonds and single bonds are in conjugation completing a cyclic hexagonal structure, proposed by kekule. An alternative symbol uses a circle inside the hexagon to represent the six pi electrons. The benzene dimer is the standard prototype for the study of pi stacking and is experimentally bound by 8–12 kJ/mol (2–3 kcal/mol) in the gas phase. The model system is a T-shaped dimer with a separation of 4.96 Å between the centers of mass. The

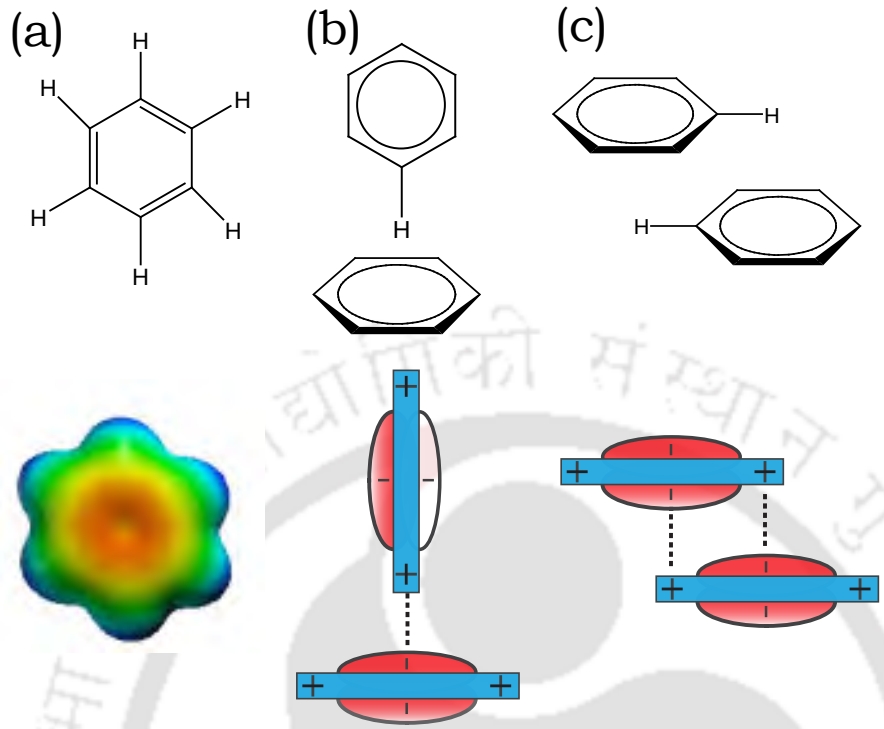

Figure 1.2: (a) Electrostatic surface potential of a benzene molecule and different types of aromatic stacking interactions,(b) Edge-to-face and (c) Parallel displaced interactions possible in an benzene dimer.

dimer is experimentally bound by a small binding energy in the range of 8-12 kJ/mol in the gas phase, and is therefore stable only at low temperatures, with a marked tendency to cluster [11].

The π–π interactions or π-stacking is defined as an attractive interaction between two stacked aromatic rings, resulting from electrostatic interactions described by Hunter and Sanders model [12]. Electrons in π bonds of aromatic rings form a quadrupole moment, with two dipoles aligned such that no net dipole can be distinguished. In phenyl systems, such a quadrupole emanating from the aromatic ring creates a partial negative charge on both face (in fact both faces) of the planar π system and a partial positive charge around the aromatic ring along hydrogen atom covalently linked to the carbon atom. A face-centered stacking of π systems on top of each other would create electrostatic repulsion creating instability. T-shaped and offset parallel configurations of phenyl rings (Figure 1.2) are observed in the crystal structures of aromatic compounds [13]. Geometries of similar kind were observed in X-ray protein crystal structures [14]. Earlier studies have

provided ample evidence that diphenylalanine (phe-phe/FF) nano-assembly is mediated through quadrupolar interactions involving phenyl embraces self-arranged in parallel displaced and T-shaped configurations for maximum stability [15]. Independent analysis of amino-acids with other aromatic sidechains such as tyrosine, histidine, and tryptophan, and their possible combinations have opened up a new field of research known as Peptide nano-assemblies (PNA's). The two most stable conformations of a typical dimer are the parallel displaced (PD) and T-shaped, which are essentially isoenergetic. The sandwich configuration on the other hand, maximizes overlap of the π system is much less stable, representing an energetic saddle point.

Nanotoxicology is developing as an important discipline and toxic effects of nano-materials are developing as a major concern among nano researchers [16]. Difficulty in modulating nano level assemblies and composites are prompting researchers to look up more to materials of organic and biological origin, while designing nano level architectures for generating smart materials of future times. The flexibility of self-assembled architectures can be employed as a tool for the design and development of molecular devices and functional nanomaterials. Ironically, the merit and limitation of such structures point to the singular fact, that such assemblies are modulated by weak intermolecular forces and not by relatively more stable and rigid bonding interactions. In this thesis, efforts have been made to modulate such interactions constructively, resulting in generating new assemblies, which are stable and stimulus-responsive, so that they can be more effectively used in developing new materials.

CHAPTER 2

LITERATURE REVIEW

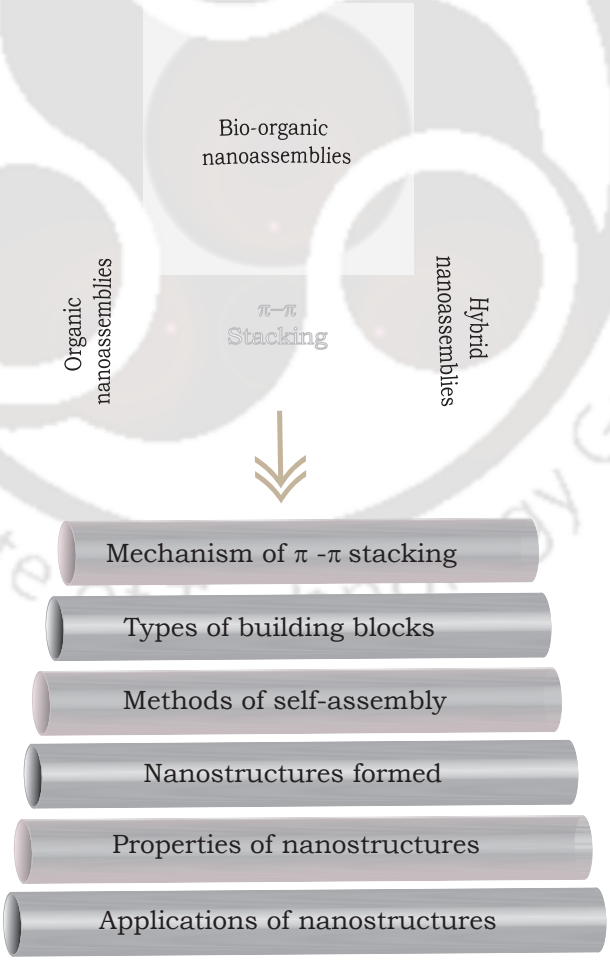

2.1 Organic Nanoassemblies

Supramolecular chemistry originally defined as "the chemistry of molecular assemblies and intermolecular bonds" constitutes supramolecular architectures constructed through self-assembly of individual building blocks. As functional soft materials, supramolecular materials have gained attention over the years in different fields of science. There is a recent surge of interest to get an insight into the ordering and growth phenomena of such molecular organizations in both the solution state (i.e. self-assembly) and the solid state (i.e. crystal engineering). It has led researchers to recognize increasingly the importance of weak noncovalent interactions, because of their ability to manipulate the ordered structures at the molecular scale. Among all the non-covalent interactions, aromatic π–π stacking is considered as the information vectors of molecular interactions. They define and rule the self-assembly processes leading to the formation of the desired molecular and supramolecular architectures. Aromatic stacking interactions, sometimes called phenyl stacking, not only controls the dynamic processes occurring within supramolecular structures, but also directs the self-assembly of a variety of complexes and interlocked molecular compounds in both solid and solution states. Molecular systems involving (i) interactions between p-donors, such as hydroquinone, resorcinol or dioxynaphthalene residues, (ii) host– guest interactions, and (iii) aggregation of porphyrin, phthalocyanines, and perylenes in solution are mediated by π-stacking interactions [17].

Aromatic moieties, involving π-stacking interactions which are central to the chemical and biological processes, plays a pivotal role in many areas of chemistry and biochemistry [17, 18]. In biology, π-stacking interactions stabilize the double-helix structure of deoxyribonucleic acid (DNA) involved in core packing [19] and the tertiary structure of proteins [20]. Aromatic interactions also contribute to the self-assembly forming architectures like liquid crystals, [21] molecular crystals, hydrogen-bonded aggregates, [21] receptor– substrate complexes [22] and Langmuir–Blodgett films [23] in both solid and solution states. In search of such molecules capable of self-assembling in solution and self-organizing in the solid state, chemists could synthesize a wide variety of molecular and supramolecular architectures. In crystal engineering and designing, arranging molecular building blocks using aromatic $\pi - \pi$ stacking along with hydrogen bonding is considered to be one among the most flexible strategies used. In nanotechnology, $\pi - \pi$ interactions is an important factor in designing nanomaterials with structural diversity, which in turn led to the fabrication of various fundamental supramolecular devices or

functional materials [22]. Recent studies of aromatic interactions on their driving force, stability and selectivity, makes it clear that the hydrophobic effect is not the sole factor for attractive interactions, but also its geometry, influenced by the electrostatics. Electrostatics determines the magnitude of the interaction and contributes to the selectivity and stability of aromatic interactions [23].

Stacking, also referred to as $\pi-\pi$ interaction, occurs due to the presence of planar conjugated π systems. In few interactions, when the number of aromatic ring systems are less in number as in DNA, the contribution of aromaticity will be less in the stacking forces. In such cases, the other intermolecular forces also get involved in driving the molecules towards a final stable architecture [24, 25]. The contribution of the other weak interactions helps in fine tuning the morphology of the same molecule into different nanostructures. Although each of the individual non-covalent interactions are considered weak, combination of such weak interactions can contribute to the self-assembly of building blocks into superior and ordered structures. Each of the components belonging to attractive (electrostatic, dispersive, and inductive) and repulsive forces (exchange repulsion) show prominent differences in physical origin, magnitude, and directionality that determine the strength of the π-interactions. On precise control of non-bonded interactions, smart materials, such as reversible self-assembled nanostructures with less defects and self-healing properties can be fabricated [26, 27].

2.2 Mechanism of Aromatic $\pi-\pi$ Stacking

Aromatic interactions were initially proposed to consist of van der Waals, hydrophobic and electrostatic forces [28]. In supramolecular chemistry, it refers to a noncovalent interaction between organic compounds containing aromatic moieties. Among all aromatic interactions, $\pi-\pi$ interactions are considered to be stronger than other noncovalent interactions, and it is of significant importance in supramolecular chemistry. Aromatic $\pi-\pi$ interactions involves two π- electron rich systems (aromatic rings) [12] and becomes stronger as the number of π-electrons increases. The strong electronegativity of Sp^2 carbons creates a quadrupole moment in the benzene ring. The quadrupole moment, with the uneven distribution of charges created by the π- electrons in aromatic rings has a larger electron density around the top and bottom faces of the ring and a reduced electron-density on the edges [29]. Extensive theoretical and empirical studies show that the presence of such partial charges around the aromatic rings favors the formation of

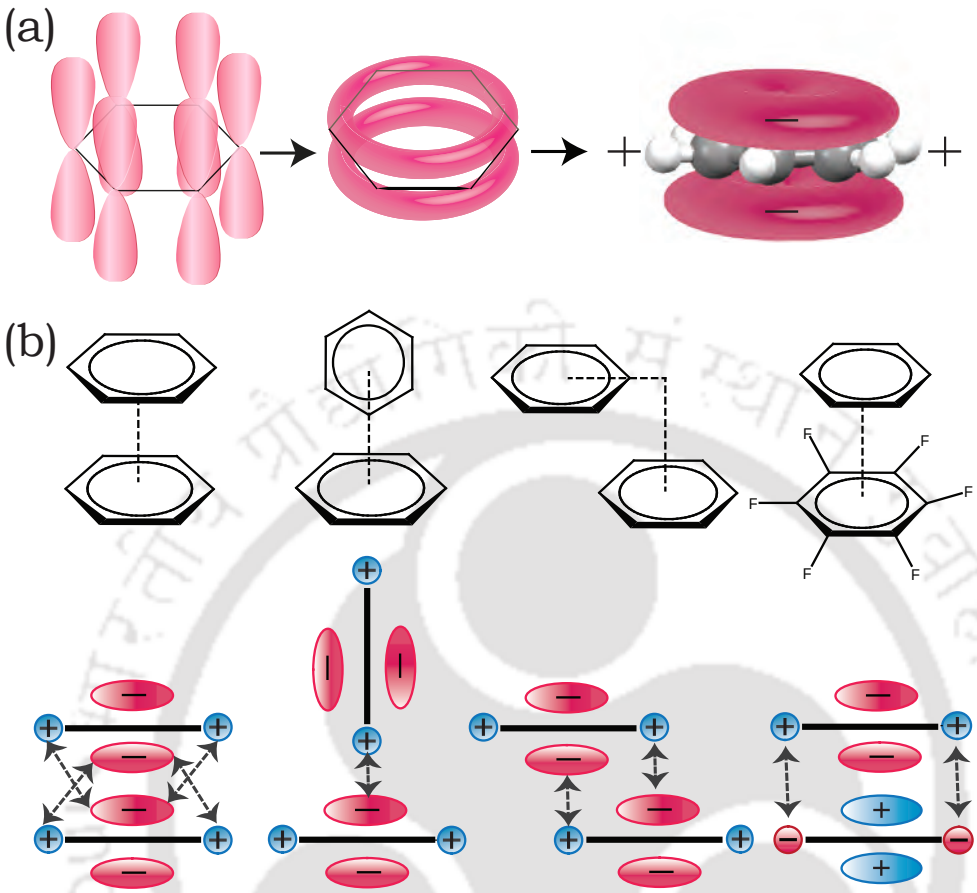

Figure 2.1: (a) Benzene rings with sp^2 hybridized orbitals, and the overlapping of p orbitals to form extended π bond. (b) Different types of $\pi - \pi$ stacking observed in aromatic systems

high-order clusters of four different types: parallel displaced, T-shaped, parallel staggered, or Herringbone [30] (Figure 2.1). In the four types of stacking, the partially charged regions with opposite potentials interact with each other, avoiding the energetically unfavourable self-centered stacking [12, 17]. It attains a potential minimum configuration in the Lennard-Jones-Coulomb empirical potential calculations with a typical bond energy between 5-40 kJ mol^{-1} [30]. The geometry of interaction depends upon the nature of the aromatic rings involved in the reactions. Hence aromatic $\pi - \pi$ interaction, is considered along with hydrogen bonding, as it has the advantages of directional interactions, that can lead to hierarchical structures [31]. For instance, aromatic molecules with functional groups like amides and carboxylic acids can form different hydrogen bonded networks or patterns along with aromatic interactions [32].

2.3 Scope of this Review

In this literature review, we present the development of different types of nanomaterials. In particular, we try to understand better, the specific role of the aromatic $\pi - \pi$ interactions in fabricating functional nanomaterials.

The review is divided into three sections, (i. Organic, ii. Bio-organic and iii. Hybrid nanomaterials) where, the crucial role played by the aromatic interactions in three different types of nanomaterials and their resulting physical properties and applications are highlighted. The chapter begins with an introduction on the role of aromatic $\pi - \pi$ interactions in the self-assembled nanostructures. Then each of the different type of nanomaterial, formed by means of aromatic $\pi - \pi$ stacking are reviewed: organic, bio-organic and hybrid materials by origin and in bioorganic materials, special focus is given to peptide based materials. Under each type of nanomaterial, a brief survey of different types of building blocks and the methods by which they form into functional nanomaterials are described. Finally, it also covers the different types of function materials formed by means of aromatic $\pi - \pi$ interactions, the properties exhibited by them, the means of their characterization and applications.

2.4 Different types of nanomaterials self- assembled by aromatic $\pi - \pi$ interactions

In nanochemistry, there is increasing interest in connecting the structure to function by design and further extending the function to the different nanostructures. Prior to designing and synthesizing a compound, to be fabricated as a nanomaterial, three important factors have to be considered (i) properties of individual building blocks, (ii) interactions among the functional units and the neighboring molecules, and the resultant effect in properties on discrete ensembles of the molecules (iii) interactions based on the environmental changes [33]. Altogether, the criteria in designing a nanomaterial to produce hierarchies of structures with different types of order involves both the optimization of the functional units and the control of their supramolecular order. The quest to find the simplest biomaterial building blocks with the best functionality and properties further expanded the field of nanotechnology leading to many new materials and branches of nanotechnology. Self-assembled nanomaterials can be formed by a

variety of building blocks, both organic and inorganic. A few among the well-ordered nanomaterials formed through the self-assembly of diverse organic, bioorganic and the combination of organic-inorganic hybrid building blocks are discussed in the following sections.

2.4.1 Organic Nanomaterials

The development of nanotechnology using organic materials is considered to be one of the intellectual way of developing nanomaterials. Advancement in supramolecular chemistry was catalyzed by synthetic chemistry, to produce major advances in the field of organic nanomaterials by generating organic nanostructures with diverse morphology and function. Organic molecules, with the versatility in molecular design, diversity, multifunctionality, and tailorability are the most promising candidates for self-assembly. Organic molecules are held together by a combination of weak forces, such as hydrogen bonding, π–π stacking, and van der Waals interactions. Great efforts are invested in synthesizing and manipulating organic nanomaterials through a variety of building blocks like lower molecular weight organic molecules, π-conjugated systems, macromolecules or polymers, dendrimers, etc. In this following session, the basic organic building blocks mediated through aromatic π–π interactions to form nanostructures, the methods involved in fabricating them are discussed. Further the properties and applications of the self-assembled nanostructures are also discussed.

2.4.1.1 Different types of organic building blocks

In order to aid the self-assembly of molecules into functional nanostructures, it is very important to design the building blocks based on nature and strength of the intermolecular interactions. Molecular self-assembly of organic building blocks through aromatic π–π interactions is a versatile method to manufacture different types of nanostructures (Figure 2.2).

Amphiphiles

A typical amphiphilic molecule possesses a polar hydrophilic head group linked to a nonpolar hydrophobic tail moiety through covalent bonds. Amphiphiles self-assembles in solution to yield a rich number of diverse morphologies ranging from simple micelles, vesicles, fibres, helices and tubes. Nanomorphologies depends upon the molecular shape

and experimental conditions such as lipid concentration, electrolyte concentration, pH, and temperature. Amphiphiles are usually classified based on the number and charges of the polar head(s), hydrophobic tail(s) and nature of connection between them [34]. Among all types of amphiphiles, only the molecules which can interact though π–π stacking to form nanoassembled structures are discussed here.

(i) Typical Amphiphiles: A typical amphiphile is the most conventional amphiphile, with a single head and tail. Based on the polarity in the head region, the typical amphiphilic molecules are further divided into ionic and nonionic amphiphiles. Amphiphilic molecules self-assemble into nanostructures as observed in proteins and peptides of biological systems. Huang et al. rationally designed and synthesized a sugar amphiphile bearing a sugar moiety, azobenzene group and butyl chain, which self-assembled into double helical nanostructures. The nanostructures are formed as a result of non-covalent interactions, such as hydrophobic effect, π–π stacking, and multiple H-bonds between the sugar heads [35].

(ii) Gemini Amphiphiles: Gemini amphiphilic molecules contains two identical sets of a hydrophilic head which can be cationic, anionic, zwitterionic, or nonionic in nature and a hydrophobic tail linked by a spacer. It is the spacer which defines the amphiphile's properties through variations in its size, shape, rigidity, and polarity. Gemini amphiphiles can be used to study interfacial assemblies. In such a study, a series of gemini amphiphiles with pyridinium head group and rigid spacers were designed. The interfacial assemblies formed with cyanine dyes through the air–water interface was mainly contributed to the larger conjugated aromatic ring and stronger $\pi-\pi$ interaction in the cyanine dyes [36]. The gemini amphiphiles usually tend to aggregate at a very low concentrations and are used as carriers.

(iii) Triangular Amphiphiles: Triangular amphiphilic molecules with C3 symmetric design represents an intriguing structural deviation from the conventional head-to-tail amphiphiles. It has three peripheric parts with hydrophilic and hydrophobic entities and the core part always a benzene ring or only a nitrogen atom. With the intriguing C3 symmetry and presence of more acting sites in the triangular architecture, triangular amphiphiles are explored as an interesting molecule in self-assembly for the construction of novel architectures. A set of chiral, amphiphilic, self-assembling triangular

molecules based on the 3,3´- bis(acylamino)-2,2´-bipyridine-substituted benzene-1,3,5-tricarboxamide motif, was designed. Solvent effect and intermolecular interactions like $\pi-\pi$ stacking and hydrophobic interactions fine-tuned the morphology of aggregates into self-assembled triple helical fibers [37]. On modification of polarity of the solvent system, triangular amphiphilic molecule like oligo (phenylene ethynylene) can self-assemble into a series of nanostructures like hollow vesicles and rod-like structures [38].

Triphenyl derivatives

Triphenylmethyl (trityl) group is the first stable radical reported by M. Gomberg in 1900 [39]. Trityl cations with a positive charge on the α-Carbon atom is one of the most versatile and stable molecule widely used in biomedical applications such as neurotransmission measurements oligonucleotide arrays (DNA chips) and as organic dyes. Triphenyl group exhibits a non-planar geometry and the positive charge on α-Carbon atom is stabilized by the resonance effect of three aromatic rings. The acid labile nature of trityl group is utilized in serving as a class of protective group widely used in nucleoside, oligonucleotide, peptide and carbohydrate chemistry. With three benzene groups, triphenyl derivatives are potential molecules to self-assemble through π–π stacking. Triphenyl derivatives are used as building blocks to generate nanostructures such as nanoflower [40], hydrogel [41] etc.

Dendrimers

“Dendrimers”, the word arises from the Greek term dendron meaning “tree” are a class of molecules with hyper branched architectures. First synthesized by Vögtle’s group [42], the dendrimer architecture is divided into three parts: (i) core, (ii) internal branches with repeat units called “generations,” and (iii) multivalent surface with reactive sites. Dendrimers, the elegant examples of bottom-up approach can be precisely controlled using the synthesis methods. Dendritic structures are chemically synthesized by using two different approaches, the divergent method and the convergent method. In the divergent approach, the dendrimer is built in a stepwise fashion from the core as the starting point, to form highly branched oligomeric structure of nanometric dimensions [43]. In the alternate convergent approach, the synthesis of dendrimer starts from the surface by attaching segments of pre-formed dendritic arms and ends at the core [44, 45]. The attachments mediated by covalent and noncovalent interactions to form a supramolecular

dendrimer are considered to be more efficient as they yield dendrimers with less impurities resulting from incomplete reactions. Different attempts are made on the synthetic strategies to develop new dendritic molecules with well-defined molecular structure. Synthetic strategies, mainly focused on supramolecular chemistry, is considered to be central for the design of intermolecular interactions. From the dendritic architectural viewpoint, the three parts of the dendrimer can be tailored to exhibit unique properties. Due to these architectural properties, dendrimers are of interest in a variety of contexts in host-guest chemistry for encapsulation of guest molecules, in pharmacology for drug delivery and catalysis [46].

Fréchet's group reported host-guest binding through π–π interactions between the electron-rich polyaryl ether dendrimeric network and an aromatic guest molecule pyrene in water [47]. Diederich et al. created a group of dendrimers named 'dendrophanes', tailored in such a way to bind the hydrophobic guests to the core. The water soluble dendrophanes designed to be centered around a 'cyclophane' core, bind the aromatic guest compounds through π–π interactions and were shown to be excellent carriers of steroids [48, 49]. With well-defined tunable supramolecular properties, dendrimers are also widely used as building blocks in the self-assembly of supramolecular gel-phase materials. Kim et al.synthesized a series of bis-dendritic gelator molecules consisting of benzamide and alkyl dendrons to study the relationship between gelation effect and intermolecular interactions. The gelators with a first-generation benzamide (benzamide-G1) dendron or a first-generation alkyl (alkyl-G1) dendron self-assembled by means of hydrogen bonding and π–π stacking to form stable gels with fibrillar networks. But the unbranched molecule (G0-G0), though having a balanced molecular structure, did not form gels owing to its weak intermolecular interactions in solution [50].

π- Conjugated Systems

Construction of different supramolecular assemblies from π-conjugated systems offers an excellent tool to fabricate different electronic components at the nanoscale. The π-conjugated systems with large delocalized π-electrons, are versatile building blocks, as their physical properties can be fine-tuned by manipulating their chemical structures. The molecular architecture of the conjugated materials also strongly influences the supramolecular organization, and the resulting morphologies of the structures. Among all the molecules of π- conjugated systems for organic nanomaterials, porphyrin, phthalo-

cyanines, and perylenes, have been extensively studied due to their electronic, magnetic and optical properties. Porphyrin molecules with a rigid and planar geometry and with its electronic features is used as a building block to self-assemble into various nanostructures. Most pursuits of porphyrin assemblies are constructed by connecting the porphyrin units with strong bonds such as covalent and coordination bonds considering intermolecular interactions to be too weak to maintain the superstructures. But a few reports have shown that only by using the intermolecular π–π stacking interaction of porphyrins and without using the other bonds/interactions novel supramolecular architectures can be fabricated. Porphyrin molecules are extensively used in applications like catalysis and sensor systems. A list of perylene derivatives self-organizing in organic solvents to form different structures is mainly attributed to π–π molecular orbital overlaps [51].

Other π-conjugated systems like poly(p-phenylene), polyfluorenes and polyindenofluorenes have attracted interest as light emitting materials in the fabrication of devices. Polyfluorenes are good candidates for light-emitting diodes (LED) applications because of their high solid-state photoluminescence properties, excellent solubility and film-forming capability [52]. The nanostructures of the π- conjugated systems formed by self-assembly through π–π stacking, shows excellent optical and electronic properties, including luminescence, charge carrier mobility, and electronic conductivity. Therefore, π-conjugated molecules are extensively used as active materials in organic electronic devices such as LEDs, FETs, and plastic solar cells.

π-Conjugated Gelators: Self-assembly through intermolecular $\pi - \pi$ stacking is a key driving force for the formation of organic gels. Commonly used gelators are π-conjugated systems like anthracene, pyrene, perylene, and other fused aromatic systems like, oligo-phenylenevinylene, oligo- polythiophene, and oligo-polymeric pyrrole groups with photoelectric properties. In addition to that large conjugated molecules such as porphyrin, phthalocyanine, and fullerene have also been widely used for the design of low molecular weight gelators (LMWGs). The strong π–π stacking between these conjugated molecules facilitates the formation of linear aggregates and gelation. The functionalization of molecular gels can be easily achieved through rational design of the gelators with selective π-conjugated systems. For instance, some azobenzene, phenanthroline, or porphyrin-based gelators display reversible assembly–disassembly under light, protons, metal ions, and thermal treatment to support the construction of intelligent materials. On the other hand, the induction of π-conjugated systems such as oligo-p-phenylenevinylenes, oligo-polythiophene, and oligo-polymeric pyrrole groups with

specific optical, electrical, and magnetic properties to LMWGs leads to the gelation of organic solvents and allows the design of a new class of photonically and electronically active supramolecular architectures [53].

2.4.1.2 Nanostructures Formed through Aromatic $\pi-\pi$ Interactions

Modulating nanomaterials for different functional applications has been an interesting topic in materials science and supramolecular chemistry. Self-organization as a tool has been used to develop a variety of organic nanostructures. A substantial amount of work has been done in the previous years to control the self-assembly of organic molecules through molecular interactions and external stimulus into highly ordered architectures.

Nanotubes

Rationally designed organic molecules, like amphiphiles, dendrimers etc. forms well-defined nanotubes through molecular self-assembly. Organic nanotubes have attracted much interest due to the ability of encapsulating guest molecules. The guest molecules are tailor made and can be fine-tuned based on the functional requirement. Organic nanotubes with functionalizable inner and outer surfaces can encapsulate and release any guest molecules in aqueous solutions. The events occur in attoliter volume nanospace of nanotubes and are of profound interest for applications in biological, medical, and industrial areas. A porphyrin derivative 5,10,15,20-tetra(4-pyridyl)porphyrin synthesized through vaporization-condensation-recrystallization process formed single crystalline rectangular nanotubes. Single Crystal X-ray analysis of the tubular structures revealed that the singular units self-stacked through hydrogen-bonding, H–π, and $\pi-\pi$ intermolecular interactions [54].

Nanofibers

Using the supramolecular designs, nanostructures can be created by a variety of building blocks. Among them, nanofibers is the simplest supramolecular aggregates formed by the amphiphiles. A triangular amphiphilic molecule designed, based on the 3,3´-bis(acylamino)-2,2´-bipyridine-substituted benzene-1,3,5-tricarboxamide self-assembled into helical fibers in apolar and polar solvents, due to $\pi-\pi$ stacking and hydrophobic interactions [37]. In another work based on a novel amphiphile of glucose-based lipid, a series of molecules with azobenzene was synthesized and it self-assembled into helical

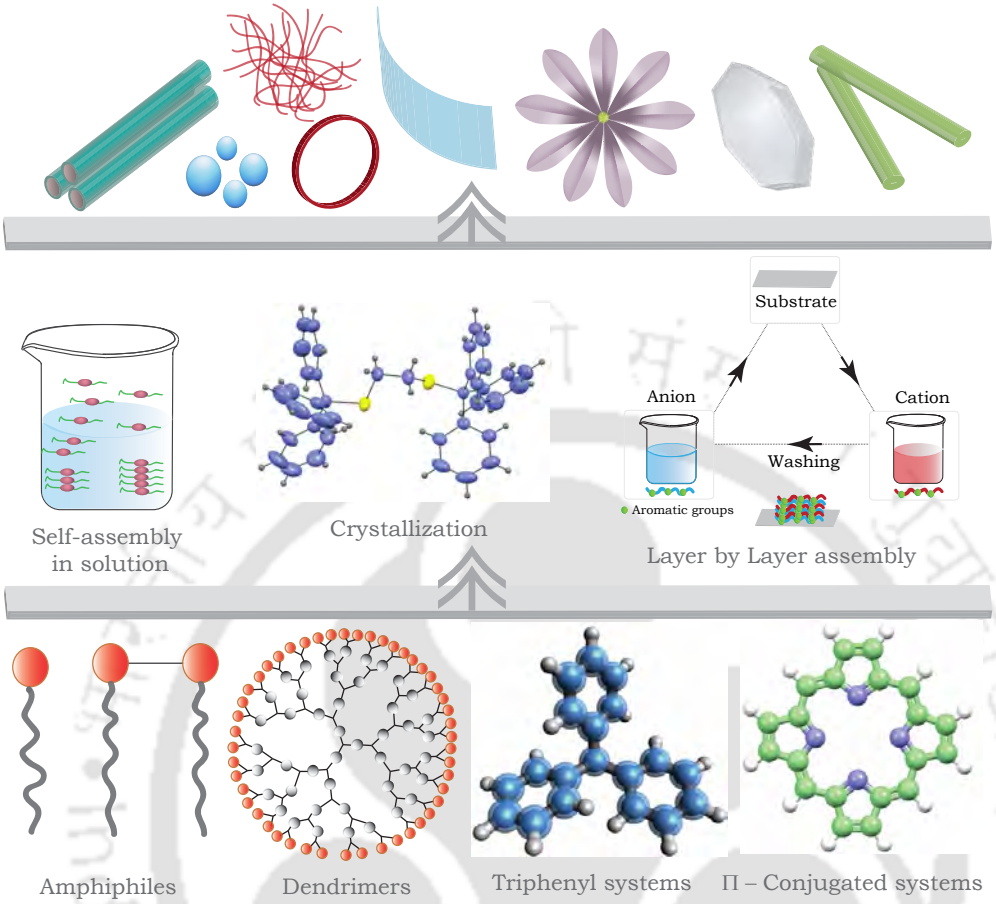

Figure 2.2: Different types of building blocks, methods of self-assembly and nanostructures formed as a result of aromatic $\pi - \pi$ interactions.

nanofibers. To understand the importance of aromatic $\pi - \pi$ interactions, when the azobenzene group was replaced by a saturated aliphatic chain, no fibrillary structures were observed [35]. Amphiphiles are designed with both aromatic and covalent interactions, where the non-covalent interactions are used for first level locking of the structures. The structures packed through non-covalent interactions are further locked by covalent interactions. An example is DPDA-10, an amphiphile containing $\pi - \pi$ interaction groups and polymerizable diacetylene, self-assembles into nanofibers primarily driven by $\pi - \pi$ interactions [55]. Kim et al. synthesized a series of bis-dendritic gelator molecules consisting of benzamide and alkyl dendrons to study the relationship between gelation effect and intermolecular interactions. The gelators with a first-generation benzamide (benzamide-G1) dendron or a first-generation alkyl (alkyl-G1) dendron self-assembled by means of hydrogen bonding and $\pi - \pi$ stacking formed stable gels with fibrillar networks.

But the unbranched molecule (G0-G0), though having a balanced molecular structure, did not form gels owing to its weak intermolecular interactions in solution [50]. Thin deposits of polyfluorenes when substituted with linear alkyl groups, the substituents allowed a close packing of the conjugated chains into very long, regular $\pi-\pi$ stacks to form long fibrils [56]. A propeller-shaped perylene diimide trimer self assembles in solution to form fluorescent nanofibers ranging from 4-150 nm in diameter [57].

Vesicles

Self-assembly of small amphiphilic molecules yields a variety of nanostructural morphologies on the experimental conditions. Hollow vesicles with an internal cavity containing the aqueous solution are considered interesting due to their potential application as molecular containers. A triangular amphiphilic molecule oligo (phenylene ethynylene) self-assembles into a variety of structures based on solvent polarity and associates together to form vesicles with acetonitrile as a solvent [38]. The concept of using both covalent and non-covalent interactions in designing amphiphiles were used in a triblock amphiphilic polymer. The polymer which forms spherical structures through non-covalent interactions, self-assembled into cylindrical structures on addition of covalent interactions.

Nanorods, Nanosheets and Nanoflower

Square porphyrin nanosheets have been synthesized for the first time by Shelnutt's group using a reprecipitation method [58]. 1, 2-bis(tritylthio)ethane, a trityl derivative was crystallized using diethyl ether as a solvent system. The single crystal organic compound assembles to form a sheet like morphology. The sheet like morphologies on vortexing, by means of a supra-molecular interaction, comes together to form organic nanoflowers [40]. 1, 2-bis(tritylthio)ethane molecule with six phenyl rings, forms multiple phenyl embraces (MPE) and engage each other through edge-to-face, (or T-shaped) and parallel offset face-to-face or parallel displaced (PD) interactions [13]. The nano-level assemblies formed may be attributed to the attractive interactions between aromatic systems, as the distance between typical T-shaped phenyl embraces are 4.06 and 7.08 Å respectively between the closest and farthest carbon atoms. Hasobe et al. have reported formation of supramolecular nanorods of meso-diaryl-substituted porphyrins, aided by sonication method and controlled by intermolecular interactions such as $\pi-\pi$ stacking [59].

Thin Films

Polyflourenes which forms long thin fibrils on substitution with linear alkyl groups, branched alkyl or aromatic substituents form homogeneous, featureless thin films [56]. Poly(3-hexylthiophene) or P3HT on spin coating forms thin film of well-ordered lamellar structures, which depends upon regioregularity. P3HT with high regioregularity (>91%HT linkages) forms lamellar structures through edge-on orientation $\pi - \pi$ stacking [60]. A group of molecules with 2′-pyridyl-2-pyridinecarboxamide units exhibited a dynamic interconversion between single and double molecular helices in solution, through spiral sliding of the synthetic oligomer strands. The helical shapes of the molecules result from the intramolecular H-bonding and extensive intermolecular aromatic stacking [61]. A novel supramolecular building block called Dendron rod−coil, comprising of a dendritic, rod-like, and a coil unit, with aromatic groups that self-assembles to form nanoribbon like structures [62].

2.4.1.3 Different Methods for Construction of Organic Nanoassemblies through Aromatic Stacking Interactions

Molecules self-assembles spontaneously in solutions or substrates to form a large non-covalently bound aggregate. The preconditions for the self-assembly, the external factors and the methods of self-assembly is important to obtain defined nanostructures. Few methods of self-assembly involving aromatic $\pi - \pi$ interactions, namely reprecipitation, gelation, crystallization, layer-by-layer Assembly and self-assembly in solutions are discussed below.

Crystallization

Crystallization is also a process of organic synthesis where the outcome of process can be rationalized from the analysis of the nature and properties of the molecular building blocks. The architecture of crystals is governed by the chemistry and geometry of the intermolecular interactions which acts as a supramolecular cement. The emergence of the field of crystal engineering helped in understanding about the intermolecular interactions in the context of crystal packing, so that new molecules with defined geometry and topology can be synthesized. It also helped in establishing connections between molecular and supramolecular structure in terms of intermolecular interactions. Crystallization aims at producing molecules of defined shapes such as rods, tubes, sheets, layers etc. so

that they can find applications as materials. The individual sub-units self-assembles to form a supramolecule and the final patterns obtained usually defines the optical, magnetic and electronic properties of the supramolecular structure.

Aromatic molecules in crystals generally have a greater tendency to stack themselves so as to increase the C...C and C...H interactions. In case of planar aromatic molecules such interactions result in characteristic T-shaped herringbone pattern [63]. In the crystals formed by p-terphenyl, the molecules tilt along their lengths and form parallel slabs in order to optimize the herringbone interactions in them. On the other hand, the dimers of benzoic acid prefer stacking themselves rather than titling to form slabs in order to optimize the herringbone interactions in them [64]. The strategies adopted by the crystal structures due to the geometric consequences can be adopted in crystal engineering.

Self-assembly in Solution

The process of self-assembly in solution to form hierarchical structures is driven by the specific and local molecular interactions governed by thermodynamic and kinetic conditions in order to achieve energy minima. A number of solvent studies on self-assembling systems containing aromatic amino acids has been published to address the importance of such intermolecular interactions. In an attempt to address the nature of the aromatic interactions in solvent, Iverson and co-workers have performed an experiment with three different aromatic pairs in a solvent system [65]. The three different aromatic pairs based on the type of the electrostatic interaction have shown varying degrees of sensitivity to solvent polarity, the following conclusions were derived:

(i) Donor- acceptor pair: Interaction was observed through face-to-face stacked orientation and a strong solvent effect was observed, in which the interaction was stronger in more polar solvents. This suggests that dispersion and/or hydrophobic interactions dominate.

(ii) Electron-poor aromatic pair: Although with the possibility of having greater burial of surface area, the molecules stacked through offset orientation in the solid state, as predicted by the electrostatic model. And the solvent effect was one order less in magnitude.

(iii) Electron-rich aromatic ring: The weakest of all the three interactions, the molecules interacts through edge-face orientation and has almost no solvent dependence.

From the studies it is evident that the electrostatic component influences the geometry of the interactions, and the geometry inturn decides the magnitude of the solvent effect on the interactions and the strength of the interactions in water is approximately – 6.7 to – 18.8 kJ mol^{-1}. The above study also suggests that solvent effect, solvent polarity and the solvent–solute interactions are crucial for regulating the assembly process to get assembled nanostructures of different size, shape, and morphology. Moreover, the choice and design of molecular structures also plays a key role in determining the final self -assembled nanostructure. In another study with water as the solvent system, it was suggested that H-bonding of water with aromatic rings plays a crucial role by influencing the propensity of stacking in the interactions [66]. The nature of the substituents in the aromatic rings was also believed to influence the stacking of the aromatic rings. The substituents tune the nature of the interactions through minimization of repulsive, quadrupole - quadrupole interactions [67].

Among the different types of self-assembly in solution, the surface assisted self-assembly has organic units dissolved in a guest solvent, and are organized with the help of surfactants in the host solvents. By means of surfactant assisted self-assembly, and with oil/aqueous medium, porphyrin self-assembled into various nanostructures like nanospheres, nanorods, nanotubes, and nanofibers [68]. Amphiphiles, triphenyl derivatives and many π-conjugated molecules like porphyrin and pyrelene, self-assembles in solution into structurally well-defined structures which is governed by the delicate balance between different noncovalent interactions [40, 69].

Reprecipitation Method

Reprecipitation method was first reported by Nakanishi and coworkers [70, 71], involves rapid mixing small amount of concentrated molecules in a good solvent with excess of poor solvent to prepare organic nanoparticle dispersions. As a solvent displacement method with no chemical reactions involved, this method is usually employed to obtain zero dimensional and one-dimensional nanostructures. A series of aromatic pyrazoline compounds forming organic nanoparticles through aromatic $\pi - \pi$ stacking was synthesized using co-precipitation method. The organic nanoparticles exhibited size-dependent optical properties which may be used in device applications [72, 73].

Layer by Layer Assembly

The layer-by-layer (LBL) process is based on the strong electrostatic interaction between alternate layers of polyelectrolytes which are sequentially adsorbed on a solid support by simple dipping into an aqueous solution. The polyelectrolytes of opposite charges held through electrostatic interactions results in highly ordered nanostructures or patterns with excellent functionalities and activities. Inspired by the concept of LB membranes invented by Blodgett and Langmuir, Iler discovered the method of layer-by-layer self-assembly in 1996. He established the method by binding a monolayer of negatively charged particles on the surface modified with cationic surfactants. Decher and Hong were the first researchers to extend the concept of LBL process to fully buildup LBL films with positively and negatively charged bolaform molecules. In the developed technology, building blocks like dendrimers, proteins, clays, and nanoparticles were used to self-assemble into diverse functional nanostructured materials. The versatility of the method to be combined with other techniques, easy and low cost operational procedures makes them one of the most effective tools for synthesis of nanomaterials. Nanomaterials like films, capsules, nanotubes, nanoporous particles, macroporous and biomimetic structures etc. synthesized using LBL methods has great potential in nanoelectronic, optoelectronic, magnetic, and chemical or biosensing technologies [74–78]. One such example is the fabrication of self-assembled thin films using perylene diimides. PDI moieties with four positive or negative charges (p-PDI and n-PDI, respectively) are deposited on quartz substrates using molecular layer-by-layer (MLBL) deposition from aqueous solution [79]. A strong $\pi-\pi$ interaction facilitates the self-assembly of perylene diimides [80], into thin films. The individual perylene moieties as such are potential candidates for photon-harvesting arrays (photovoltaic cells) and OLEDs. In addition, the aromatic $\pi-\pi$ interaction is expected to facilitate energy or charge transport in such molecular constructs [81].

2.4.1.4 Properties of the Materials Resulting from Aromatic $\pi-\pi$ Interactions

The material properties of nanoscale objects originate from the type of building blocks and the mechanism through which they interact to form supramolecular materials.

Electronic Properties

Single crystal organic molecules have highest charge carrier motilities due to the molecular ordering that permits good overlapping of $\pi - \pi$ orbitals. For example, pentacene [82], rubrene [83] and dithiophene-tetrathiafulvalene [84] has a mobility of 1.5 cm^2/Vs, 8 cm^2/Vs and 1.4 cm^2/Vs respectively. Synthesis of single crystals are generally tedious; hence alternative ways of synthesizing low-cost electronic materials were explored. Aromatic molecules with π-conjugated systems showed different carrier mobility based on the types of intermolecular $\pi - \pi$ stacking. Percentage of regioregularity in some molecules decides type of π-stacking orientation and the rate of charge mobility in them. For example, P3HT forming lamellar structures through 96% regioregularity with edge on orientation $\pi - \pi$ stacking has charge mobility of 0.05 to 0.1cm^2 $V^{-1}s^{-1}$, whereas with 96% regioregularity and face on orientation, the charge mobility increased to 2 x 10^4 cm^2 $V^{-1}s^{-1}$. Along with the degree of order of the structures, the thin film deposition methods which decides the orientation of the $\pi - \pi$ stacking with respect to the substrate, decides the field-effect mobility and the electron transport direction of Organic Thin Film Transistor (OTFT) devices [60]. The different type of substrate modification prior to film deposition [85] and the solvent systems [86] also influences the charge carrier mobility. Garnier et al. synthesized and crystallized polycrystalline [87], and α–ω-dihexyl-sexithiophene film [88] based OTFT's and showed that crystals containing large π-conjugation length along the long axis of the molecule and close molecular packing of the molecules along at least one of the short molecular axes (π -stacking) are two important conditions for high carrier mobility. Organic thin film transistors are envisioned as an alternative to the traditional inorganic thin film transistors. But the charge carrier mobility of inorganic materials is almost thrice that of organic molecules [89]. But the unique properties of organic thin film transistors like design flexibility and low cost - low temperature processing are used in many such devices.

Optical Properties

Aromatic $\pi - \pi$ stacking determines the optical properties in self-assembled planar aromatic molecules. One dimensional nanobelt like structures of PTDCI exhibited uniaxial optical properties along the $\pi - \pi$ stacking directions, the property of which can be used to generate optical sensors or switches that can be used to yield higher sensitivity [90].

In π-conjugated systems, porphyrin based nanoscale superstructures are generally

known for their light harvesting functions. One such meso-diaryl-substituted porphyrins formed nanorods and nanofibers by sonication method. Based on the spectroscopic studies, photoelectrochemical cell composed of nanorod-modified optically transparent electrode (OTE) was constructed. From the experiments, the nanorods were found to harvest light energy and generate photocurrent during the operation of photoelectrochemical cell [59]. Photoconductive nanorods self-assembled from a porphyrin derivative, acted as a switch in the presence of light. The nanorods appeared insulating in the dark, upon excitation with light exhibited photoconductive behavior [91].

Polyfluorenes based π-conjugated systems, on substitution with different substituents exhibited different morphologies. Photoluminescence properties are strongly co-related with the resulting morphologies. Alkyl chain substituents forming nanofibril like structures exhibited long wavelength emission in the green region, while non-organized structures like granular and smooth films formed by bulky substituents retained pure blue emission. The optoelectronic properties in the materials is attributed to the competition between steric hindrance and π-stacking in them[56]. The optical emission color of a perylene-derivative molecular assembly can be tuned by dynamic $\pi-\pi$ stacked molecular assembly in solution [51].

2.4.1.5 Applications

Drug Delivery

Vesicles are spherical or ellipsoidal structures with internal cavity in them, and the commonly used aspect of this hollowness is targeted drug delivery. Diederich and coworkers designed a group of dendrimers called “dendrophanes” specifically designed for binding hydrophobic guests to the core. Dendrophanes are water soluble in nature and centered around a ‘cyclophane’s core. The dendritic strutures binds compounds, through $\pi-\pi$ interactions were shown to be excellent carriers of steroids [48].

Nanoelectronics

Supramolecular electronics constitutes of electronic components made of supramolecular assemblies, and it bridges the gap between molecular electronics and bulk, ‘Plastic electronics’ [92]. Though initial excitements on single molecule based nanosized devices existed due to miniaturization, the limitation of shape selectivity hampered their application in the field of electronics. Self-assembled molecules formed through co-operative

and specific interactions are considered ideal building blocks for electronic applications. LED: Many organic nanomaterials are used as active semiconductors in light-emitting diodes, and many prototype devices are fabricated which meet realistic specifications for applications. Organic blue-emitting conjugated polymers, can be used for color display applications. First reported molecule with blue emission is poly(p-phenylene) [93] and studies with many polypheylene derivatives blue luminescence followed [52]. OLET: The first organic light-emitting field-effect transistors were fabricated using tetracene polycrystalline as a charge transport and emitting layer. The device with inter-digitated gold source and drain electrodes were fabricated on a Si/SiO_2 substrate on which the organic crystal was deposited as a film [94]. The prototype device had few drawbacks due to the electron transport issues in tetracene, but based on this optimization for the device characteristics has been performed. When thoiopene-derived molecular system was used as an active layer and with a channel width of 0.8 μm, the electroluminescence increased to a value nine times higher than that of the one obtained with a channel width of 9.8 µm. Advantages of organic molecules in terms of electronic applications is that, the molecules can be assembled or deposited on any substrate followed by which, the post processing layers can be added for device fabrication. Organic materials are compatible with low-cost fabrication techniques, and with inherent versatility, it offers the possibility of fabrication of multifunctional devices.

2.4.2 Bio-Organic Nanomaterials

Upon careful examination of short functional fragments of amyloid forming proteins, a common factor was observed. In all the diverse fragments, few aromatic residues were present, which raised the question of the possible role of $\pi - \pi$ interactions in amyloid formation. It was speculated that the π-stacking interactions well known for its contribution in the self-assembly of aromatic units, may provide energetic distribution, order and directionality in the self-assembly of amyloid fibrils [95]. The suggested π-stacking hypothesis, inspired the design of new peptide sequences, which helped in understanding the self-assembly mechanism [96] and the development of a series of functional peptides [97, 98].

2.4.2.1 Aromatic Interactions in Biomolecules

Aromatic interactions, ubiquitous in nature, plays an important role in stabilizing the structure of biomolecules like double stranded DNA [99] and a variety of proteins [95]. It was considered to be one among the less studied and less understood interactions, until the mechanism of aggregation through π-stacking has been elucidated. Extensive investigations about the nature and significance of aromatic interactions followed, employing theoretical [28] and experimental methods [100, 101].

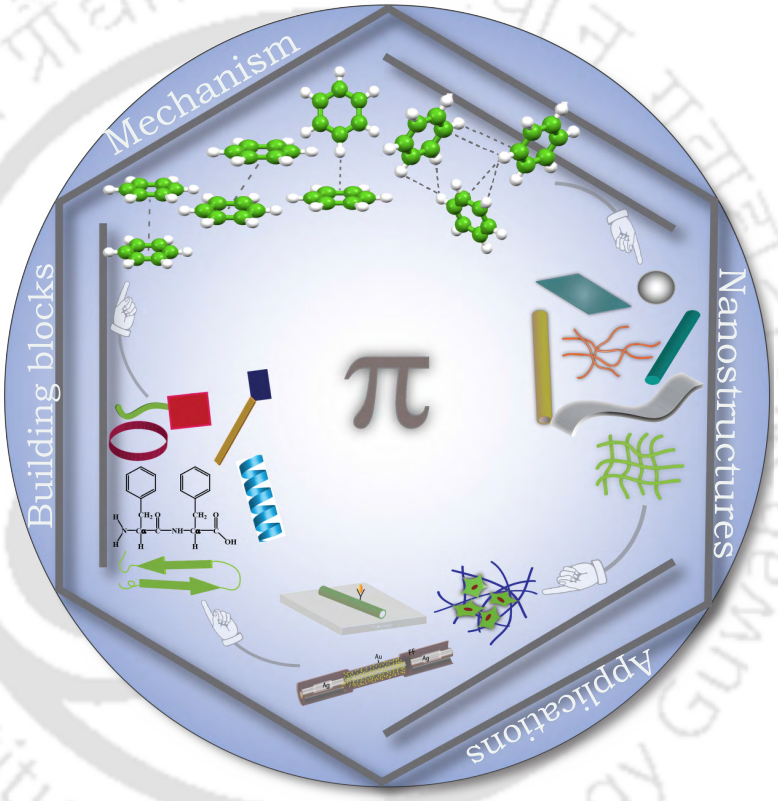

Figure 2.3: Role of aromatic interactions in directing the self-assembly of basic peptide building blocks to functional nanostructures.

Traditionally, though DNA molecules were adapted for applications in nanotechnology, the appeal for peptide and proteins have been intensified due to their versatility and specificity in molecular recognition. In the biological world, many molecular mechanisms at nano, micro and macro scales are governed by proteins and peptides. Among all, self-assembled nanostructures by proteins and peptides remained as one of the most promising directions for many reasons. Inspired by the mechanisms adopted by

the biomolecules, many peptides based nanomaterials have been designed and fabricated [102–104](Figure 2.3). Though protein offers many advantages, draw backs like (i) instability and inability to design and synthesize proteins, (ii) sensitiveness to environmental conditions like pH, solvent and temperature remains as challenges in designing bio-nano devices [105]. Unlike proteins, peptides were recognized as versatile building blocks for self-assembly, owing to their chemical diversity, ease of synthesis, flexibility in design, stability and bio-compatibility.

2.4.2.2 History of Aromatic Stacking

The well-known role of π-stacking in molecular recognition and self-assembly [17, 18, 20] led to various investigations on aggregation patterns in amyloid proteins. Since amyloid formation also involves the process of molecular recognition and self-assembly, it was hypothesized that (i) the energetic contribution from the π-stacking can thermodynamically drive the self-assembly process and (ii) the directionality and orientation for the ordered aggregation is provided by the specific pattern of π-stacking [95]. Analysis of the functional fragments of various aggregating sequences of amyloid peptides revealed an interesting commonality (Figure 2.4). A notable frequent occurrence of aromatic residues in all the functional fragments, raised the possibility of their role in the amyloid formation. With the known fact that the frequency of occurrence of aromatic amino acids in normal proteins is relatively very low, the observation suggests the significant role of the aromatic amino acids in the aggregating sequences.

The first striking examples of the aromatic amino acids was observed in the 15 residue amino acids of the 37 amino acid islet amyloid polypeptide (IAPP), or amylin [106]. Shorter fragments of 6(NFGAIL) and 5(FGAIL) residues formed ordered amyloid fibrils, whereas, the sequence GAIL did not form any fibrils [107]. By means of various analysis like near-ultraviolet circular dichroism (UV CD) spectrum of IAPP, [108] and alanine scan of the 'basic amyloidogenic unit' of IAPP [109], physicochemical properties of the three short residues and the significant role of phenylalanine as a structural element has been demonstrated.

Another example is the minimal fragment of the Alzheimer's β-amyloid (Aβ) polypeptides (QKLVFF) containing two phenylalanine residues. The short peptide specifically binds and inhibits the amyloid formation of the full-length Aβ polypeptide [110]. A few other inhibitors like LVFFA and its derivatives [111] and LPFFD [112] were also

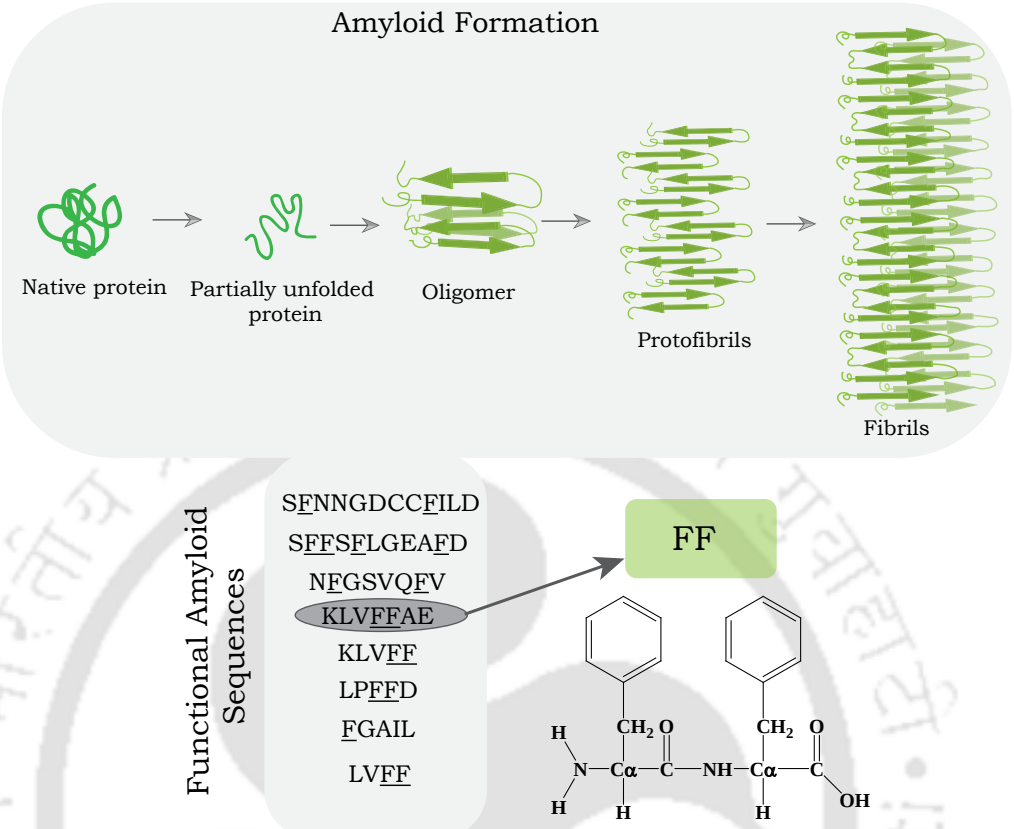

Figure 2.4: Mechanism of amyloid formation through stacking of β-sheets and aromatic interactions. Common features of aromatic amino acids in different amyloid forming sequences and how it led to the discovery of FF is shown.

found to inhibit Aβ peptide. Another study on the sequence KLVFFAE, derived from Aβ peptide forming well-ordered fibrils [113], further confirmed the role of FF motif as a molecular recognition element in the ordered amyloid fibril formation (Figure 2.4). Diphenylalanine happens to be the first shortest dipeptide to self-assemble into rigid nanotubular structures [96].

A short functional octapeptide fragment (NFGSVQFV) of the 5.5 kDa peptide component of the aortic medial amyloid formed amyloid fibrils as the parent peptide [114]. Few other examples of the presence of phenylalanine residues are (i) near the carboxyl terminus of a 35 residue peptide fragment of α-synuclein [115], (ii) in calcitonin a short peptide which forms amyloid fibrils both in vivo and in vitro [116, 117], and (iii) the amyloid fibrils formed by chromosome 13 of human BRI gene, which are associated with neuronal dysfunction and dementia [118].

2.4.2.3 Mechanism of Amyloid Formation through Aromatic $\pi - \pi$ Stacking

Understanding the mechanism of the biomolecules is of prime importance in peptide engineering, as it allows the rationale design of peptides targeting specific applications. As mentioned in section 1, there are four possible ways of π-stacking and each of the four possible stacking interaction with precise planar orientation may regulate the well-ordered formation of the amyloid structures. The suggested mechanism is a stepwise assembly process - in the first stage - only two structural elements containing aromatic amino acid residues forms a bimolecular structure. In the following stage, monomers with the same recognition elements are further added in a stepwise process. From the initial formation of the biomolecular structure to the stepwise addition of the monomers, the process is directed by the restricted geometries of the stacking interactions. The mechanism associated with $\pi - \pi$ stacking plays a crucial role in supramolecular association as it forms highly stable self-assembled structures with the desired precision.

2.4.2.4 Geometry of Aromatic Stacking in Aromatic Rings

In protein folding, based on the interactions involved, aromatic rings can either serve as acceptors or donors in H-bonding [119]. Other than H-bonding, interaction of aromatic groups with other aromatic moiety is considered important, as on an average, 60 % of aromatic chains in proteins are involved in such aromatic pairing interactions [20]. As per the observation by Burly and Petsko, phenyl ring centroids in such interactions are separated by a preferential distance of 4.5 - 7 A$^{\circ}$ and dihedral angles approaching 90^{o} are most common. Among all the abundant structures in contact, most of the interactions involving aromatic groups have a contact distance less than 6 A$^{\circ}$. Whereas in interactions involving isolated Phe rings, which makes 5 % of all the studied structures have a centroid separation distance of 7 A$^{\circ}$.

The geometry of the aromatic resulting from the translation of the crystallographic axis with angle between aromatic planes as 0^{o}, can be calculated using the vertical and horizontal offsets of the aromatic rings. As shown in figure 2.5, the horizontal and vertical offsets of the aromatic rings in parallel displaced contacts are calculated using D sin θ and D cos θ. From the calculations, it was shown that the bulk interactions have the values of H and V in the range of 3 – 6 A$^{\circ}$ and 1.5 – 3.5 A$^{\circ}$ respectively. It was observed that a situation H=0 A$^{\circ}$, representing the direct stacking of amino acids on the top of the each other never occurred in the crystal structures. But the situation corresponding to

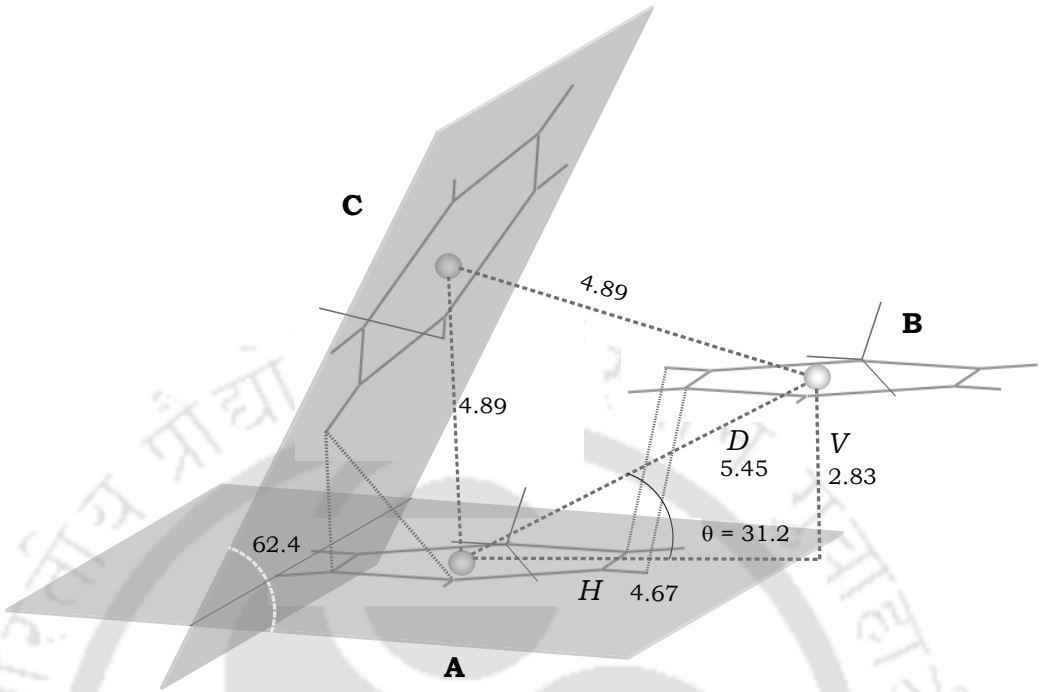

Figure 2.5: Vertical and horizontal offset interactions between the phenyl groups in peptides. Stacking interactions observed in the structure cyclo (N-methyltaurine-Phe-D-Pro). D (the centroid distance) and H•••C distances are represented with dotted lines.

V= 0 A˚ was observed in very few cases which had distinct electrostatic characteristics. At conditions where the amino acids are not related by translations, the angle between the two aromatic rings may vary between 0º (parallel) - 90º (perpendicular) and there will not be any correlation between the centroid distance and plane angle. In short aromatic interactions, with parallel displaced geometry, H-atoms will not be placed on the top of the aromatic ring but with a little displacement pointing out the π – electrons of H...C(π) for contacts down to 2.9 A˚ [120].

2.4.2.5 Strategies adopted and types of building blocks for construction of bioorganic nanoassemblies

Peptides with 20 natural amino acids, have the same basic structure and can adopt different configurations with the varying R group. Though chirality is a choice for amino acids other than Gly, all amino acids exists in L-configuration. Amino acids interact through non-covalent interactions - ionic, hydrophobic, hydrogen bonding and π–π stacking, to from supramolecular structures and with the possibility of 2^n configurations, (n= num-

ber of amino acids) the possible sequences are enormous. On addressing the challenge linking the peptide sequence to structure, design rules are made and central concepts like Ramachandran plots have been developed. In general, peptides can de designed by two ways (i) Natural peptides are designed by imitating the biological assemblies in nature and (ii) non-natural – de novo designs of peptides which are either linked through co-valent or non-covalent interactions (Figure 2.6).

Concepts derived from Nature (Natural Design)

The limitations in the top-down approach has provided an alternative route of 'bottom-up' approaches in the fabrication of nanomaterials. Initial attempts of man-made designs in the bottom-up process using peptides weren't much successful, as the multiple functions of the biomolecules incorporated, created a chaos by interfering with each other and generating unexpected functions. Hence, researchers started mimicking the natural designs of functional nanomachines, fabricated with an outstanding degree of organization and efficiency in task accomplishments. The important design feature of nature is the hierarchical self- assembly of small elementary building blocks of biomolecules into highly ordered functional supramolecular architectures.

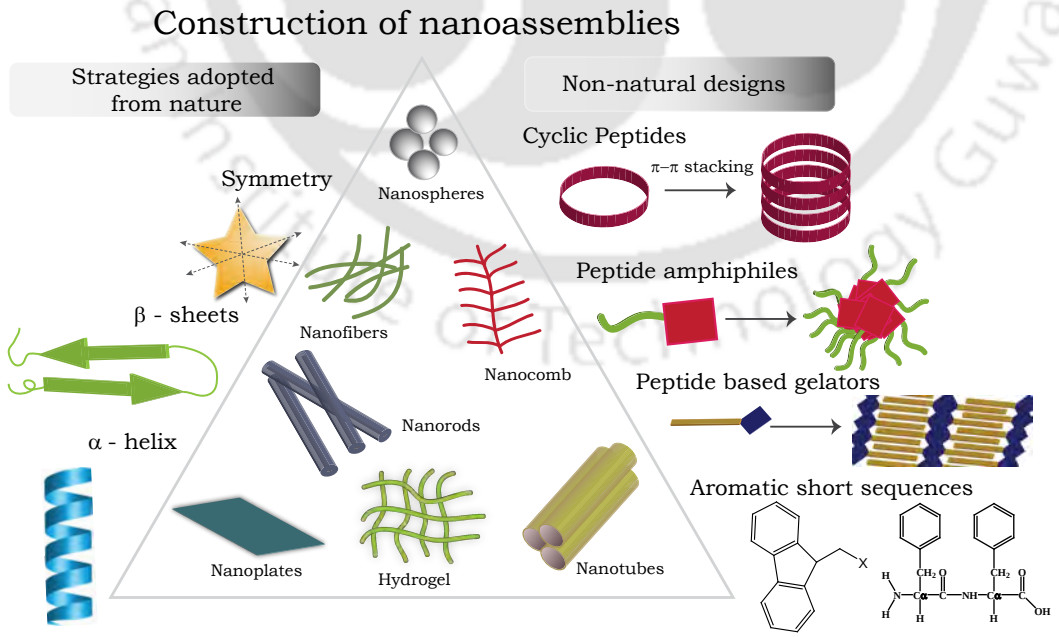

Figure 2.6: Various strategies employed for the design of peptide based nano-assemblies.

(i) Symmetry: Evolution in nature has produced a range of nano-objects self-assembled through bottom-up approach. Among all the concepts adopted by nature, the concept of symmetry provides many functional advantages in the biomolecules. A few examples of different types of symmetry found in biomolecules are listed below in Table 2.1. The common types of symmetry observed in biomolecules are (i) Point group symmetry which is further classified into cyclic, dihedral and cubic symmetry and (ii) translation symmetry and Quasi-symmetry. Inspired by the concept, symmetry as a design variable along with aromatic $\pi-\pi$ interactions and end to end electrostatic interactions have been used in peptide model systems. Peptide systems with same electrostatics and symmetrical elements, tend to form similar crystalline nanotube like structures. When the symmetrical element was changed along with the increase in the distance between the aromatic rings of the basic unit, it formed nanocomb like architectures. The hypothesis that asymmetrical elements will prohibit the epitaxial growth of supramolecular assemblies, was evident with peptide system with asymmetrical design forming no pronounced architecture. Another peptide design was based on the gramicidin helix with both intramolecular as well as intermolecular interactions, assembled forming nanofibers [121]. The observations from the experiments suggest that symmetry along with charge distributions can be used as a design parameter for modulating nano-assemblies.

(ii) Secondary structures

β-sheets: β-Sheets well known for their ability to form ordered amyloid fibrils in amyloid diseases, was initially identified by Pauling and Corey and others in 1950s [122]. β-sheets contains parallel and antiparallel strands with an extended backbone, that permits hydrogen bonding between the backbone amides and carbonyls. The arrangement of C and N-termini on the strands (on the same side-parallel and alternate sides-antiparallel) has an important impact on the H-bonding, side chains and orientations in the structure. In the literature, β-Sheets peptides either natural or designed ones dominates the α-helical peptides as they can form long-range interactions. Zhang in 1900, first demonstrated the use of β-sheets in the design of materials [123]. The hypothesis of aromatic stacking in the β-Sheets of amyloid proteins [124], further inspired the design of series of β-Sheets forming peptides interacting through aromatic $\pi-\pi$ stacking. But the main challenge faced in designing a self-assembled system mediated through β-sheets is to control the assembly, to form uniform and reproducible architectures. Self-assembled β-sheets formed a hierarchy of structures such as tapes, ribbons, fibrils and fibres [129]. Studies done on systematic variation of peptide sequences containing different number

Types of symmetry		**Biomolecules**
Point group symmetry	Cyclic	Pepsin, Max protein, Porin, Potassium Channel, Complement C1
	Dihedral	Phosphofructokinase, Aspartate carbamoyltransferase, Glycolate oxidase, Glutamine synthetase
	Cubic	Ferritin, Protocatechuate 3,4-dioxygenase, Satellite tobacco necrosis virus
Translational symmetry	Line symmetry	Actin filaments
	Plane Symmetry	S-layer proteins
	Space group symmetry	Catalase
Quasi symmetry		Viral capsids

Table 2.1: The common types of symmetry observed in biomolecules are (i) Point group symmetry which is further classified into cyclic, dihedral and cubic symmetry and (ii) translation symmetry and Quasi-symmetry

of hydrophobic residues, and their position helped in finding the key features like critical concentration of aggregation in the peptides [126].

β-hairpins: β-hairpins are short sequences, containing two short β sheets linked by a turn sequence. When the end amino acids in the β sheets do not interact with each other, β-hairpins ensures that the peptides stack in register with one other. β-hairpins also plays an important role in the amyloid self-assembly [127]. A C3-symmetric peptide conjugate, Trigonal-WTW, was synthesized based on the intramolecular tryptophan zipper (β-hairpin) forming peptide reported by Cochran et al. At a pH 11, the peptide self-assembled to form fibrous structures due to stacking interactions between the hydrophobic core [128]. A biological motif, peptide β sheet was rationally designed with sequences interacting through aromatic interactions formed macroscopic hydrogels with nano-scale order [129].

α - helix: First described by Pauling, Corey and Crick [130, 131], α – helical structures

are used as components of coiled-coils, in alternative to the usage of β-sheets for the formation of fibrous structures. With the aid of hydrogen bonding between backbone amides, and with a periodicity of 3.6 residues per turn, the α-helical peptides tend to stack on top of each other, to form extended columns. The extended structures are formed by the side chains of amino acids of the α-helical peptides, protruding outside from the helix to from interactions with other helices. Though it is challenging to produce α-helical structure in practice, owing to the longer length of amino acids required for making stable interactions, a few examples involving aromatic–aromatic interactions are also evident [132].

Non-natural Designs/Peptide derivatives

Non-natural peptides are designed based on the insights gleaned from natural proteins or they are entirely new designs based on the peptide derivatives. For example, surfactant-like peptides are inspired by the lipid bilayers [133], and aromatic peptides are derived from amyloidogenic sequences [95, 96]. Over the past few decades a number of peptide building blocks with short sequences such as cyclic peptides, dendritic peptides, amphiphilic peptides and aromatic peptides have been explored for creating functional nanostructures.

(i) Cyclic peptides: Cyclic peptides usually contains alternating L and D amino acids, where the building blocks stack upon each other to form a flat conformational structure. The final self-assembled structures are stabilized through H-bonding which are arranged perpendicular to the ring. In peptide crystallization, cyclic peptides are introduced to address the challenges of conformational flexibility in peptides. Cyclic peptides have distinct properties like precise diameter control and functionalization through amino acid sequences. A novel family of aromatic-bridged cystine cyclic peptides, with locked-in, well defined secondary structures, can act as a model for studying the biological reactions. The peptides also called cystinophanes had a general structure of cyclo(Ar-CONH-Cyst-NHCO$-)_n$ and cyclo (Ar-CONH-Xaa-Cyst-Xaa-NHCO$-$) (Ar = Ph or Pyr; Cyst = l-cystine dimethyl ester; n = 2, 3, 4, and Xaa = amino acid X). Crystallographic analysis revealed the near-parallel face-to-face orientation of the two phenyl rings in the cyclic peptides [134]. Another group of peptides called cyclodepsipeptides, with alternating repeats of aromatic and Ser units were synthesized and crystallized. The

molecules stacked on the top of each other through $\pi - \pi$ interactions between the aromatic groups like phenyl or pyridyl and H-bonding to form tubular structures [135].

(ii) Peptides with unnatural amino acids: Aib (aminoisobutyric acid), a non-proteinogenic alpha amino acid is known for inducing helix formation in peptide sequences. When the length of the amino acid becomes more, the problem of conformational flexibility arises. In such cases, Aib containing sequences are introduced to address this issue. To understand the importance of aromatic $\pi - \pi$ interactions in stabilizing helices and β-hairpins, three sets of peptides with phenylalanine at different positions were synthesized and crystallized. To restrict the conformation to remain as helix, Aib was also placed at different positions in the peptide sequences. Structural determination of the crystals, revealed that the peptide adopted helical conformations and the aromatic rings interacted through perpendicular, parallel-displaced, and inclined orientations [132]. Aib introduced between diphenylalanine (FBf) peptide to restrict the conformation of the peptide in α-helical region, formed nanocomb like structures [121].

(iii) Peptide Amphiphiles: Inspired by the association and structural integrity of the lipid membranes, amphiphilic peptide molecules with charged hydrophilic head groups and hydrophobic tails were designed. Among all the different types, aromatic peptide amphiphiles are considered to be a distinct class of building blocks as they require a minimalistic design strategy facilitated by the inclusion of a synthetic aromatic moiety. The aromatic moieties impart both amphiphilicity and structure to the directed self-assembly in the aromatic stacking interactions. Further, self-assembly is also influenced by the planarity and geometry, associated with the stacking interactions. The self –assembly of the aromatic amphiphiles through parallel, anti-parallel, and interlocked antiparallel stacking conformations are governed by the structural features of the four segments present in them. A typical aromatic amphiphiles is comprised of (i) an N-terminal aromatic component (ii) a linker segment (iii) Peptide sequence and (iv) a C-terminus. Self-assembly of the peptide amphiphiles are controlled by modifying the aromatic component and by changing the external conditions like pH, ion, temperature and kinetics [136].

(iv) Aromatic Short peptide derivatives: Aromatic nanostructures self-assembles through hydrogen bonding as well as π–π stacking of aromatic residues. Aromatic short

peptide derivatives were promising from a scientific point of view due to two main reasons, (i) Short dipeptide diphenylalanine, the core recognition motif of β amyloid sequence self-assembles to form nanotubes by means of π–π stacking of the phenyl rings [96]. (ii) The chemical coupling of a variety of short aromatic groups, like carbobenzyloxy, naphthalene, anthracene and fluorenylmethoxycarbonyl (Fmoc) derivatives self-assembled to form nano scale architectures, primarily directed by local electrostatics.

Diphenylalanine peptides and its derivatives: Investigation on the smallest recognition module or reduced minimal aggregate of amyloid protein, revealed that the stacking role of aromatic dipeptide diphenylalanine may play a key role in fibril formation [95]. The sequence which was identified as the core recognition motif for self-assembly, became the first reported dipeptide to self-assemble into extremely rigid [137], discrete, hollow nanotubes with high persistence lengths and were casted into nanowires [96]. Since then many studies have been carried out including the physicochemical characterizations of nanotubes, followed by the design and synthesis of various diphenylalanine derivatives. Under different conditions FF nanotubes self-assembles to form different nanostructures. They can be aligned vertically to form “nano-forest” or could be coated with magnetic nanoparticles and aligned horizontally in the presence of an external magnetic field [138]. Modulation of biological stability was achieved based on the incorporation of L and D- amino acid isomers in the peptide building blocks to make them stable against proteolytic degradation [96].

Many FF-based nanostructures such as nanotubes, nanoforests, spherical vesicles, nanofibrils, nanorods, and ordered molecular chains were formed under different conditions like vapor deposition, dilution and water-vapor-mediated self-assembly [139–141]. Different analogues of diphenylalanine peptides forming a variety of nanostructures are listed in Table [2]. The different nanostructures formed based on properties of the peptide assembly, finds applications in areas like bioimaging, biosensors, guest encapsulation, nanofabrication and drug delivery [22].

Other aromatic amino acid sequences: On chemical coupling of a variety of aromatic groups, like carbobenzyloxy, naphthalene, or fluorenylmethoxycarbonyl (Fmoc) to the N-terminus of some peptides aids the self-assembly by $\pi-\pi$ interactions and allows them to form nanostructures. The molecular basis for the formation of nanostructures from small peptide containing aromatic moieties, stems from the geometric restriction

Peptide	**Solvent**	**Nanostructures**
Diphenylglycine, Cysteine-diphenylalanine	HFIP-water	Nanospheres [97]
Fmoc-diphenylalanine	DMSO [142] HFIP-water [143]	Hydrogel
Fmoc-Phe–Phe-OH, Cbz-Phe–Phe-OH	HFIP-water	Fibrils [144]
(D-Phe-D-Phe)	Water	Nanotubes + Vesicles [145]
(L-Phe-D-Phe)	HFIP-water	Nanotubes [121]
Ac-Phe–Phe-NH2, NH2-Phe–Phe-NH2, Boc-Phe–Phe-OH, Cyclo-Phe–Phe-OH	HFIP-water	Nanotubes [144]
(Phe-Aib-Phe)	HFIP-water	Nanocombs [121]
di-para-fluoro-Phe	HFIP-water	Nanotubes [98]
di-pentafluoro-Phe	DMSO-water	Nanotubes [98]
di-para-iodo-Phe	DMSO-water	Nanotubes [98]
di-4-phenyl-Phe homo-dipeptide	HFIP-water	Square plates [98]

Table 2.2: Analogues of diphenylalanine and its structures

between the aromatic groups. Diphenylalanine has been replaced and substituted with functional groups like naphthalene and halogen atoms to impart certain properties like conductivity and rigidity/stiffness in them [98]. Other than FF based structures, a number of short linear peptides, like KLVFF [146], DFNK and DFNKF has been designed based on aromatic interactions which self-assembles into nanofibrillar structures [147].

(v) Amino- acid and Peptide based gelators: Gelation is a process to form molecular gels, by the designed peptide based gelators with well-defined nanostructures through weak interactions. On inducing molecular chirality, the gelators are endowed with

enhanced gelation capability which in turn bestows it with chiral functions such as chiral switch, sensing, and recognition. A few among the reported gelators are Fmoc–dipeptides, which are usually driven by hydrogen bonding and $\pi-\pi$ interactions. The π electrons in the aromatic fluorenyl rings plays a key role in the π stacking and it has been used as a driving force to self-assemble a series of Fmoc dipeptides into hydrogels. Ulijn et al. reported a series of Fmoc dipeptide forming hydrogels which can be used as biomimetic fibrous scaffolds for three-dimensional cell culture [136, 148, 149]. Non-covalent interactions responsible for the formation of hydrogelators enables the three-dimensional networks to respond to external stimuli. Enzyme regulated hydrogelation of a series of Fmoc peptides was reported and this property endows the hydrogels for potential applications in drug delivery, detecting the activity of enzymes, typing bacteria and screening for enzyme inhibitors [150]. A number of supramolecular hydrogelators from small molecules has been reported which are used for therapeutic applications [151]. Based on the hydrogelator principles a vast amount of work has been done on "self-delivery systems for therapeutic purposes," [152] among which, one of the hydrogelator has been approved by Food and Drug Administration (FDA) for clinical use [153]. Scientists have integrated the catalytic activity of enzymes to the regulate self-assembly of many aromatic peptide hydrogelators, to form supramolecular gels. Enzyme hydrogelation offers a new platform for developing many new biomaterials [150].

2.4.2.6 Nanostructures formed through aromatic $\pi-\pi$ interactions

Peptides have been recognized as very useful building blocks for creating various self-assembled nanostructures, through intermolecular aromatic $\pi-\pi$ stacking. The tailor-made modifications that can be introduced at the sequence level makes them ideal materials for engineering functionalities. Peptides can self-assemble into an array of nanostructures like nanotubes, nanospheres, hydrogels etc. depending upon its basic constituents and the environmental conditions.

(i) Nanotubes: Tube shaped proteins in nature, such as motor proteins, ion channels and aquaporins inspired scientists to design artificial nano tubular structures. Driven by the nature of the tubes with hollow cavity which can be functionalized based on the applications, many artificial nanotubes were fabricated from a variety of biomolecules. Among them peptide based self-assembled nanotubes through intermolecular interactions, has gained significant importance, and can be classified based on the building blocks.

Cyclic Peptide nanotubes: In 1974, De Santis and co-workers theoretically predicted that D- and L-amino acids could self-assemble to form nanotubes by stacking cyclic peptide monomers [154]. But the first engineered cyclic peptide nanotubes were developed by M. Ghadiri and coworkers in 1993 [155–157]. Ghadiri et. al first used the concept of alternating D- and L-amino acids in the context of a cyclic peptide to form a planar ring. The peptide formed extended β- sheet structure and stacked on top of each other, to form tubular structures of a desired diameter. In another interesting work from the same group, they modified the L and D amino acids of the cyclic peptide by incorporating a 1,4,5,8-naphthalenetetracarboxylic acid diimide (NDI) group to allow a charge transfer along the tubular system [157]. There are many other cyclic peptide sequences designed to self-assemble into nanostructures [158]. The diameter and function of the cyclic peptide nanotubes can be precisely controlled by tuning the length and sequence of the peptides. The surface properties of the nanotubes can be determined by the number and amino acid group in the side chain. These characteristic features make them distinctive from other self-assembled nanostructures.

Self-Assembled Peptide Nanotubes: Among peptide based self-assembled nanostructures, diphenylalanine, motif of the Alzheimer's β-amyloid peptide became the first reported dipeptide to self-assemble into nanotubes. In the self-assembly process, six FF units of the aromatic dipeptide comes together to form a cyclic hexamer. The cyclic hexamers stack themselves through hexagonal packing to produce narrow channels leading to the formation of sheets, and the sheets coils themselves to form nanoscale tubes with external hydrophobic walls. The nanotubular structures self-assembles on larger scales to form bundles are held together by the backbone hydrogen bonds and $\pi-\pi$ interactions between the side chain aromatic rings [159]. The molecular organization of the remarkably rigid peptide nanotubes studied through X-ray and electron diffraction studies revealed that aromatic stacking arrangement is critical for the arrangement of nanotubes as it serves as a glue between the hydrogen- bonded cylinders [138, 160]. This was further validated by the crystal structure reported by Gorbitz, where the hierarchical array of stacked diphenylalanine molecules in a surrounding water clusters tightly holds the hydrogen-bonded peptide main chains in nanotubes (NTs) [161]. Further, the dynamics of the nanotube assembly proving that the self-assembly process is a nucleation-dependent process was performed by Gazit et al. using nuclear magnetic resonance (NMR) spectroscopy. In the study, during nanotube formation, the migration

of diphenylalanine molecules out of their water solvation shells to form aggregates was reflected by a decrease in the integral of the diphenylalanine signal and a concomitant increase in the integral of the water signal [162].

The molecular organization of FF is compared to that of graphene and other organic polymers. Self-assembly pattern is similar to graphene as it forms a flat two-dimensional sheet stabilized by the interactions of aromatic ring side chains, which directs the order during the assembly by $\pi-\pi$ stacking. A model of FF nanotube assembly also suggests that self-assembled nanotubes are similar to fullerene and carbon nanotubes. The robustness and the stability of the peptide nanotubes has been tested under extreme physical and chemical conditions like boiling, autoclave treatment, and exposure to various organic solvents [163]. Alignment of the nanotubes in vertical and horizontal patterns are demonstrated by two different methods. By solvent evaporation on siliconized glass, vertically aligned nanoforests were formed by axial unidirectional growth of a dense array of dipeptide nanotubes. Whereas, the horizontal alignment of the tubes was done by coating the nanotubes with a ferrofluid and the application of an external magnetic field. A seven residue peptide CH_3CO-KLVFFAE-NH_2, the core segment of Aβ peptide, with a capped N- and C-termini, self assembles into parallel β-sheet and forms micron-long highly homogeneous hollow tubes at pH 2. By using "salting out" technique Lynn and coworkers directed the same peptide from homogeneous nanotubes to macroscale parallel arrays [164, 165]. Modification of FF nanotubes with Boc, fluorine and amine groups also resulted in tubular nanostructures [98]. On replacing the phenyl group with naphthalene, reported as a promising molecular conductor, di-D-2-Nal dipeptides formed tubular structures. In order to study the role of electrostatic interactions in the formation of tubular structures, two different peptide sequences with N and C terminal modifications (Ac-Phe–Phe-NH_2 & NH_2-Phe–Phe-NH_2) were analyzed. Both the sequences self-assembled to form nanotube like structures further validating the hypothesis of the role of aromatic $\pi-\pi$ interactions in amyloid formation [144].

(ii) Nanofibers: Nanofibers are fibrillar nanostructures with large aspect ratios and specific surface area. Due to such structural properties, nanomaterials with fibrillar structures finds applications in various fields such as biomedicine, sensors, electronic nano- devices, and catalysis. Nanofibers formed by different types of peptides through aromatic $\pi-\pi$ interactions are discussed. Nanofibril formation were initially reported in various analogues of the amyloid forming sequences studied for understanding the

mechanism of amyloid formation [147]. From the shortest FF sequence derived from Aβ peptide, a number of variations and analogues were synthesized, which formed nanofibers of various dimensions. The N-terminus of diphenylalanine upon modified with aromatic groups such as Fmoc and CbZ resulted in nanofibrils, which are more similar to amyloid fibrils in their morphology [98]. Diphenylalanine replaced by naphthalene group, (D-1-Nal)-(D-1-Nal), under conditions similar to that of diphenylalanine, formed fibrils of approximately 10 nm in diameter [98]. In addition to the sequences, varying the experimental conditions like changing the solvent system, pH etc. also resulted in fibrillary structures. By introducing acetonitrile as a co-solvent, a structural transition of self-assembled diphenylalanine peptide from microtubes to uniform peptide nanofibers was observed [166]. In a similar study, a temperature induced and substrate assisted transition from an organogel to uniform crystalline nanowires was also demonstrated [167].

(iii) Hydrogels: Peptide based hydrogels formed from both natural and synthetic hydrogelators, are an interesting class of materials, as they find applications in tissue engineering and regeneration. Peptides can be decorated or tailored with the required functional group for promoting cell adhesion and growth. A β-sheet peptide, designed based on a sequence related to transmembrane domain of the IsK protein self-assembles in methanol through aromatic interactions to form hydrogel with polymeric β-sheet tapes [129]. Among the aromatic peptides, diphenylalanine is the smallest peptide gelators that self-assembles into long organic fibrils in organic solvent systems and entangles further to from gels [168]. On addition of aromatic groups carbobenzyloxy naphthalene,or fluorenyl-methoxycarbonyl (Fmoc) to the N-terminus of some peptides, at preparative conditions forms stable hydrogels [27, 143, 169–171]. The results presents the role of different aromatic moieties in controlling the stacking effect. Same diphenylalanine peptide protected by different aromatic stacking ligands, self-assemble into nanofibrous hydrogels of different dimensions via interlocked β-sheets/π-stacks. Effect of variation in the stacking group, has reflected in the curvature, branching and diameter, of the resulting fibrous components [170]. A peptide Ac-C$(FKFE)_2$CG-NH_2 sequence cyclized through disulfide bonding of the flanking cysteine residues, transformed into preferred β-sheet conformation and self-assembled into fibrillar structures. Increasing the peptide concentration, it formed rigid viscoelastic hydrogels [170, 172].

(iv) Nanospheres/vesicles: Nanovesicles are potential candidates for the delivery of drugs, biomolecules, and other chemical agents. Two sets of amphiphilic dipeptides α,β-dehydrophenylalanine (ΔPhe), H-Glu-ΔPhe-OH and H-Lys-ΔPhe-OH self-assembled into nanovesicles. The structures which are resistant to proteinase K was shown encapsulating small drug molecules such as riboflavin, vitamin B_{12}, bioactive peptides, and small protein molecules [173].

Many studies have been done on developing smart vesicular systems which responses to external stimulus like pH, temperature, and enzymatic conditions. Diphenylalanine nanotubes diluted at pH 7, transformed into spherical vesicular structures [140]. In another experiment to delineate the role of aromatic residues, a systematic replacement and shuffling of FF sequences were attempted with cyclohexylalanine and proline yielded nanovesicular structures [174]. For example, on introducing thiol group in diphenylalanine (CFF), it changes the nanoassembly from nanotubes to nanospheres [97]. An aromatic peptide diphenylglycine, with molecular properties similar to that of diphenylalanine, but with a rigid molecular structure due to the lack of rotation around C−C bond and steric hindrance, self assembles to form nanospheres [97]. When diphenylalanine modified with nitro and phenyl group- di-para-nitro-Phe peptide, at a higher concentration of 10 mg ml^{-1} form spherical structures [98].

2.4.2.7 Factors controlling the formation of nanoassemblies

Self-assembly process gives the flexibility to fabricate and develop many functional materials with the desired tunable properties. But the ability to control and manipulate the self-assembly processes is an ongoing endeavor in biotechnology. As soon as the self-assembling systems are placed in the medium for aggregation, assembly is initiated. Hence, it becomes difficult to control the nucleation and growth. The key strategy to construct any complex assembly is to program the assembly of the individual building block at a location on the substrate or device geometry. Reconfiguration of the self-assembly process can be done by triggering the assembly disassembly command. It can be achieved in laboratory based conditions using triggers that can be any external stimuli such as pH, ionic strength, temperature, electric/ magnetic fields, and photon. In response to the external stimulus, conformation and recognition function of the building

blocks is modified leading to structural variations or physical change. Control in the recognition patterns of the materials with respect to the external stimulus is essential for the fabrication of functional nanostructures with enhanced complexities and fewer defects. Technological applications are envisioned for such smart responsive materials and flexible sensor systems. Many significant attempts are made in developing stimulus responsive nanomaterials that assemble and disassemble on cue and few such methods are discussed in the following sub sections.

(i) Ionic strength/pH: Few amino acids have charged functional groups in the side chains. pH switch is one of the simplest method to control the self-assembly. The ionic strength of the solution is varied, which in turn masks the effect of charges in the amino acids. Few Fmoc-based hydrogels are pH responsive, and forms different nanostructures at different pH conditions [175–177].

(ii) Enzymes: Enzyme assisted self-assembly is an emerging concept to use the catalytic activity of the enzymes in the bottom-up fabrication of nano-materials. In biological systems, usually enzyme assisted reactions are tightly regulated by spatially confined molecular mechanisms. In an effort to enhance the control over self-assembly in the nanofabrication process, researchers are trying to mimic the biological approach. Enzymatic reactions dictate the self-assembly process are achieving it by either enhancing the self-assembly by catalyzing the synthesis, or by removing the blocking group from a molecule to allow assembly. The degree of specificity of the enzyme catalyzed reactions to the substrate ranges from highly specific to non-specific reactions. The range of specificity towards the substrate can be utilized in reactions with different types of natural and unnatural molecules. A number of interesting smart materials created through the enzyme controlled self-assembly can be used in applications such as drug delivery, biomineralization and biosensing [150, 178].

One such example of an enzyme assisted self-assembly is the use of proteases to selectively trigger the self-assembly of Fmoc-FF to form hydrogels via reversed hydrolysis. The reversible nature of the hydrogels, prevents the formation of kinetic aggregates and paves way for the formation of a thermodynamically stable structure with fewer defects [27]. A kinase/phosphatase switch used to control the sol-gel transition was demonstrated in a hydrogelator Nap−FFGEY. On addition of kinase in the presence of ATP, makes the peptide more hydrophilic (Nap−FFGEY−$P(O)(OH)_2$) and induces

a gel-sol phase transition, whereas, on treating the same solution with phosphatase restores the hydrogel structure. Such biomimetic enzyme assisted approaches may help in regulating and constructing new biomaterials [179]. A number of Fmoc based enzyme assisted self-assembled complex nanostructures have been reported which otherwise would have resulted in kinetically trapped misfolded aggregates [180].

(iii) Solvent System and Concentration: Solvent effects has a profound impact on the process of self-assembly, as fine-tuning the solubility parameters give a control on the nucleation process. Solvent has different functions such as (i) participants in the H-bonded network and (ii) as space fillers with no interactions between solvent and solute. Other than the conventional method, peptide nanotubes were synthesized by heating and cooling D-Phe-D-Phe in water. On diluting the nanotube mixture with water along with the nanotubes vesicles was also observed suggesting concentration as a key factor in nanoassembly formation [145].

(iv) Magnetic field: Magnetic field can be used as a tool to induce orientation in anisotropically shaped macromolecular assemblies. The physical torque that originates in polypeptides or proteins is due to the diamagnetism of the oriented aromatic groups [181] and planar peptide bonds [182, 183]. In protein, the secondary structures involving α-helices will orient with the helices parallel to the magnetic field, whereas in β-pleated sheets the orientation of aromatic side chains decides the orientation of the structure. Magnetic field has been also been used to grow highly oriented amyloid fibrils for X-ray diffraction [184]. In nanotechnology, much efforts have been invested in controlling the spatial organization of objects at the nanoscale. In one such attempt, horizontal alignment of the peptide nanotubes was achieved by non-covalent coating of the nanotubes using a ferrofluid. A magnetic field of 0.5 T was used to align the tubes to the direction of the magnetic field [138]. In an another experiment of magneto-alignment, Richard et al. demonstrated the alignment of nanotubes without any coating at a magnetic field of 12 T. The alignment with respect to the magnetic field was attributed to the effect of magnetic torque associated with the diamagnetic anisotropy of the aromatic phenyl rings involved in the $\pi-\pi$ interactions [185].

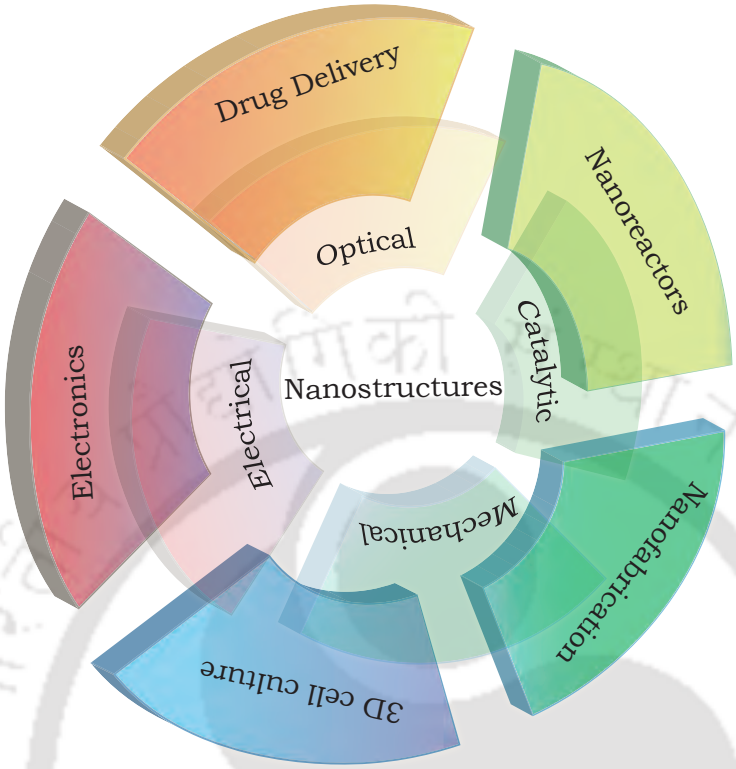

Figure 2.7: Physical Properties and respective technology platforms developed from peptide nano-assemblies

2.4.2.8 Physical Properties of Nano-assemblies

Self-assembling peptides are a valuable asset due to their ability to assemble into well-ordered nanostructured biomaterials, which can be chemically or biologically functionalized, and display a range of physical properties.

Electrical Properties

Most of the peptide based conducting materials are aromatic peptides, self-assembled by aromatic stacking and charge transfer occurs through $\pi - \pi$ interactions. One of the most intriguing applications is in organic electronics. Electrical measurements of a peptide monomer GFPRFAGFP forming films and its self-assembled nano fibers has been designed. The electrical conductance of thin films formed by the peptides has significantly improved once it self-assembled to fibers. The extended stacking of aromatic residues providing $\pi - \pi$ conjugation along the fibers is considered to play an important role in the

conductivity of the self-assembled peptides [186]. Conductive protein fibers in bacterial systems, inspired the design of peptide sequences, that can self-assemble into conductive nanostructures. The most commonly studied pilus system, contains π-stacking amino acid side chains responsible for the long-range conductivity [187].

Optical Properties

The packing of the molecules during self-assembly plays an important role in determining the optical properties of the self-assembled nanostructures. FF nanotubes and Boc-FF nanospheres exhibited optical properties similar to that of zero dimensional quantum dots. FF peptides when cyclized and vertically aligned using vapor deposition process generated 2D quantum-wells. In addition, to the above properties, Fmoc –FF self-assembled into gel like architectures, displayed strong photoluminescence in the blue region along with UV absorbance of the exciton [188].

Park et. al also reported a novel photoluminescent peptide-nanotube materials by incorporating photosensitizers and/or lanthanide ions, such as terbium (Tb) and europium (Eu), into the FF nanotubes through a self-assembly process. FF nanotubes acted as efficient host matrix for different luminescent complexes developed colors based on the complexes [189].

Mechanical Properties

Mechanical characterization of individual insulin amyloid fibrils has shown that fibrils has strength values (0.6 ± 0.4 GPa) comparable to steel (0.6–1.8 GPa), and mechanical stiffness (3.3 ± 0.4 GPa) comparable to silk (1–10 GPa). In light of the results, the analysis of the mechanical properties can be seen in two different perspectives. The intramolecular interactions responsible for the strength and stiffness of the fibrils explains (i) why it is extremely difficult for the mechanisms to degrade the amyloid fibrils and (ii) the possibility of using fibrils as a biomaterial for various applications [190]. Self-assembly of the short aromatic dipeptide driven by the aromatic interactions resulted in one of the most rigid organic nanotubes, with a Young's modulus of 19 GPa [137]. The physical strength of the diphenylalanine nanotubes makes them attractive building blocks for biocompatible devices. The diphenylalanine nanotubes were known for its stiffness and nanostructures made from dinapthylalanine peptides display a greater flexibility. A set of experiments where the two peptides mixed in different ratios yielded nanostructures with

different morphologies. The mechanical mapping of the nanostructures from different propositions revealed that as the percentage of dinapthylalanine peptides increases, a relative reduction in the stiffness was observed, suggesting the generation of materials with variable stiffness using individual concentration as a variable [191].

2.4.2.9 Applications

The scope of applications of the peptide nanoassemblies is diverse considering the possibility of its functionalization in comparison to carbon and other inorganic nanostructures.

Biological Applications

(i) Implications of the π-stacking hypothesis for the control of amyloid formations: A sharp increase in the occurrence of amyloid diseases and the increased reported instances of protein misfolding diseases, is urging scientists to explore new ways to control the amyloid formation. Physical blockage of the self-assembly process by known aromatic drugs is one way to clinically control the amyloid formation. Considering the role of π-stacking in amyloid formation, it was suggested that any drug that can block π-stacking interactions may be a potential candidate for controlling the amyloid diseases. A few molecules containing aromatic residues, Ro 65–8815/001 [192], and 3-p-toluoyl-2-(4'-(3-diethylaminopropoxy)- phenyl]-benzofuran [193] have shown effectiveness in controlling the Aβ amyloid formation. Congo red, a specific amyloid binding dye containing aromatic elements also inhibits amyloid fibril formation in Aβ [194]. An interesting observation is, Congo red and the aromatic drug Ro 65–8815/001 binds at the same site of Aβ. It was also shown that two anticancerous drugs with polyaromatic rings, 4'-iodo-4'-deoxydoxorubic and the antibiotic tetracycline inhibits amyloid formation. The anti-cancer drug 4-iodo-4-deoxydoxorubicin, like Congo red, is a generic anti-amyloid agent and inhibits amyloid formation by five unrelated proteins [195]. But the lack of specificity in the drug molecules and their side effects demanded other direct approaches like the usage of short aromatic 'molecular recognition elements'. Various short peptide analogs containing FF motif inhibits Aβ amyloid formation [110–112]. Aromatic recognition elements of amyloid forming proteins, can be conjugated to breakers of the amyloid self-assembly process. The breakers can be (i) charged amino acids to electrostatically block the Aβ self-assembly, (ii) bulky moieties that will sterically block molecular interactions or (iii) β-breaker amino acids such as proline, glutamic acid, or aspartic

acid, to affect the structure of the stacked assembly. Above mentioned approaches were successfully implemented to arrest the amyloid fibril formation by the Aβ peptide.

(ii) Drug Delivery: Microtubes of FF were used as potential drug delivery vehicles. In an experiment by Silva et. al in 2013, Rhodamine was conjugated to the peptide arrays. Using microscopy and X-ray studies it was revealed that cargo was either uniformly distributed at the hydrophobic surface or homogeneously embedded at the polar sites of the matrix. The drug was released at a constant rate from the FF-MTs through first-order kinetics, demonstrating the peptide arrays as potential drug carriers [159].

(iii) Cell culture/Tissue Engineering: The design of self-assembled peptide-based structures for three-dimensional cell culture and tissue repair has been a key objective in biomaterials science for decades. Fmoc-modified di and tri peptides forming highly ordered hydrogels through H-bonding and $\pi-\pi$ interactions has been used for cell proliferation of chondrocytes in three dimensions [170]. Hydrogels formed through the co-assembly of two Fmoc containing peptides Fmoc-FF and Fmoc-RGD, acted as scaffolds for the growth of cells. Dermal fibroblasts when combined with the hydrogels formed dense fibrous networks through the secretion of extracellular matrix from cells [196].

In another experiment, three diphenylalanine analogues with different aromatic ligands, Fmoc- Phe-Phe-OH, Nap (naphthalene)-Phe-Phe-OH and Cbz (benzyloxycarbonyl)-Phe-Phe-OH formed fibrous architectures with varying dimensions. The varying curvature of the fibrous dimensions is attributed to the difference in the protecting group. The fibrillar nature resembled the extracellular matrix and the hydrogels supported chondrocyte cell culture in both two and three dimensions [170].

Non-Biological Applications

(i) Electronics: Nanowires: Nanotubes or fibres can be used as templates for synthesizing metal nanowires. Gazit et al. used an aromatic system FF as a template to fabricate silver nanowires, and the peptide was degraded using proteinase K to form fine nanowires of 20 nm in diameter [96].

Ultracapacitors: The three dimensional alignment of FF peptides as vertical forests was fabricated by solvent evaporation [138] and vapor deposition techniques. For the application FF systems as ultracapacitors, peptide nanotubes were vertically assembled

on carbon electrodes, which showed double-layer capacitance when compared to the same configuration of carbon nanotubes [139].

(ii) Sensors: A self-assembled peptide functionalized with nanoparticles can be used in detecting the concentration of enzyme protease. A tripeptide was designed with an Fmoc-group, which aggregates through π-stacking interactions in the absence of the enzyme. On addition of the enzyme, it cleaves the Fmoc group from the particle and reveals the amine group resulting in dispersion via electrostatic repulsion. Due to the dispersion of nanoparticles, a visible color shift occurs from blue to red. The approach is very simple and sensitive to detect the concentrations of the enzyme and can be tailored for other protease enzymes [197]. Integration of peptides with optical probes, is one of the most popular systems in biomolecular sensor applications for fabricating miniature biosensors. A new peptide based amperometric biosensor has been designed and fabricated by integrating peptide nanotubes with electrodes to form composite electrodes. The biocomposite electrode with conductive peptide nanotubes exhibited excellent sensitivity in determining glucose and ethanol by monitoring the electrocatalytic oxidation of enzymatically liberated hydrogen peroxide and Nicotinamide adenine dinucleotide (NADH) [198].

(iii) Nanoreactors: Nanoreactors, designed by the strategies employed by living cells, are associated with confining a reaction environment, by hosting or encapsulating guest materials. They are generated by either positioning the required catalysts on the surface of the supramolecular architectures or by confining them inside closed structures. The amino acids and their spatial arrangement dictated by the tertiary structure plays an important role in the functionality of the biomolecular nanoreactors. Hence to design nanoreactors with high level complexity, the choice of molecular candidate is an important parameter. The biomimetic approaches, which can be done at low temperatures yields crystals with less defects in comparison to the established high temperature procedures in materials science. Pd^0 nanoparticles grown on the nanofibers using a multistep reduction technology, was used for mild and efficient Suzuki–Miyaura coupling reactions in aqueous media at room temperature without additives [199].

(iv) As scaffolds or templates: Though most of the self-assembled nanostructures are non-conducting, as they can be functionalized through alterations at the sequence

level qualify them as templates for the fabrication of components in nano-circuitry. Histidine rich peptides are well known for their functional affinity towards metal ligands. In an experiment, assembled histidine nanotubes were coated with Cu nanocrystals for enhancing the electronic properties of the nanotubes. The size of the Cu crystals immobilized on the nanotubes is controlled by the conformation of the peptide nanotubes, which in turn is dictated by the pH conditions. Changes in the crystalline structure leads to significant changes in the electronic properties of the structure [200]. Peptide nanotubes were used as scaffolds to fabricate a metal–insulator–metal, trilayered, "Teslaian" coaxial nanocables. The triaxial silver–peptide–gold nanowires were fabricated by linking FF peptides to linker peptides capable of binding gold nanoparticles, and then reducing silver nitrate in the hollow pore of the peptide nanotubes [162].

2.5 Conclusion

The cost in the production and change in the functionalities in non-biological environment are few among the important challenges in the application of peptides in nanotechnology. But with the advantages of easy reproducibility, and versatility in tailoring the chemical moieties as per the required application, makes them stand apart in comparison to other nanomaterials. Structures formed through self-assembly are considered to be the major tools for the future of nanotechnological applications. A wide number of organic, peptide and composite materials have been explored for functional nanostructures that can be utilized in various applications. There are many ways in controlling the formation of nanoassemblies. Aromatic molecules interacting through aromatic $\pi - \pi$ stacking is one among the most promising basic building unit for the design and construction of such functional nano-assemblies.

CHAPTER 3

RESEARCH DESIGN AND THESIS OBJECTIVES

Aromatic $\pi - \pi$ interactions known as π-stacking involves interactions of aromatic rings between themselves. Among all the aromatic systems reported, benzene dimer is considered to be the prototypical system for the study of $\pi - \pi$ stacking. As per the literature, in the gas phase, the dimer is experimentally bound by 8–12 kJ/mol with a separation of 4.96 Å between the centers of mass for the T-shaped dimer [11]. Though the small binding energy makes the benzene dimer difficult to study experimentally, the two most stable conformations reported are the parallel displaced and T-shaped interactions, which are isoenergetic and represent energy minima, in the conformational free energy landscape.

The relative binding energies of the benzene dimer in the two stable geometric configurations are explained by a balance of quadrupole/quadrupole and London dispersion forces. Benzene has a strong quadrupole moment due to local C-H dipole in the 6 carbon atoms of the benzene ring [201]. It creates a positive charge and corresponding negative charge is created by an electron cloud above and below the ring. Among the favorable interactions in this system, parallel displaced configuration reduces the repulsive interac-

tions between the electron cloud and is stabilized; whereas, in the T-shaped configuration an environment for favorable quadrupole/quadrupole interactions exists, as the positive quadrupole of one benzene ring interacts with the negative quadrupole of the other. And also as the benzene rings are farthest apart with a distance of 4.96Å, the favorable quadrupole/quadrupole interactions evidently compensate for diminished dispersion forces.

Most discussions of π-stacking interactions are cited back to a seminal work published in 1990 by Hunter (Hunter–Sanders model) [12]. The model explained a simple conceptual framework for understanding the nature of π-stacking interactions between aromatic rings, as well as the impact of substituents and hetero-atoms on the π systems. In the model proposed, each aromatic ring was treated as a local quadrupole comprising the positively charged nucleus and a pair of negative charges located at a distance above and below the molecular plane. Later, in a subsequent work published by Hunter and co-workers [28], the simpler view of stacking interactions with the distributed quadrupoles was replaced with the term "π-electron system."

Pi stacking systems are important building blocks in the design of peptide and small organic molecules as it dominates most of the supramolecular assembly and recognition process. External perturbations are believed to influence the pi stacking interactions through their impact on the π-electron density of the aromatic ring. Self-assembling peptide and organic systems containing quadrupole and dipole ring systems are chosen as the model systems for our experiments.

Self-assembly, a spontaneous process, is modular in nature and has its own advantages in controlling the final entity. Self-assemblies in biological systems leading to three-dimensional bio-nanomachines called proteins are built with the one-dimensional information available in DNA. Though it is a spontaneous process, where no further input of information is required, the final structures cannot be directed as it happens in macroscopic engineering. Fabrication at the nanoscale is a process at which the atoms are placed specifically at its designed plane and space. Here we are trying to direct the fabrication process by i) Incorporating the concept of three different design elements in the basic units, where the basic building blocks are sequences of amino acids with different symmetry elements ii) Exploring the susceptibility of external fields namely electric fields, and magnetic fields in organic molecules with quadrupole and dipole aromatic ring currents and iii) taking advantage of the properties exhibited by these nano-assemblies and harnessing them in fabricating stimulus responsive nano structures.

The objectives of this thesis may be summarized as follows:

1. To investigate how symmetry elements tune up nano-molecular assemblies?

2. To investigate how perturbation of local electrostatics implemented by altering chain stereochemistry directs nano-level architecture?

3. Design, synthesis and characterization of trityl based stimulus responsive organic nano-assemblies.

4. Generation of hybrid organic–inorganic nano-adsorbents for chromium sequestration.

5. Synthesis and physical characterization of Di-Histidine based stimulus responsive nanostructures.

CHAPTER 4

SYMMETRY-DIRECTED SELF-ORGANIZATION IN PEPTIDE NANO ASSEMBLIES THROUGH AROMATIC $\pi - \pi$ INTERACTIONS

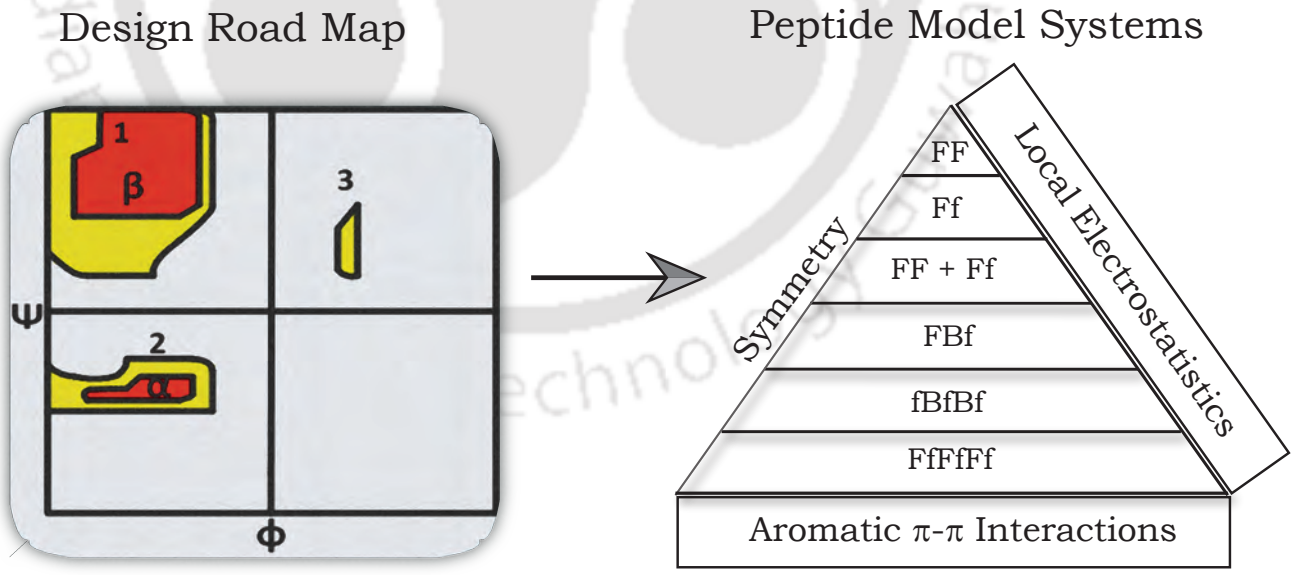

An article based on this chapter is published in *J. Phys. Chem. B*, vol. **121**(2), year 2017, pages 404-411; title: "Symmetry-Directed Self-Organization in Peptide Nanoassemblies through Aromatic $\pi - \pi$ Interactions"; authors Sajitha Sasidharan, Prakash Kishore Hazam and Vibin Ramakrishnan. Selected contents are reproduced with permission ©American Chemical Society 2017.

4.1 Summary

Almost all biological systems are assemblies of one or more biomolecules from nano- to macrodimensions. Unlike inorganic molecules, peptide systems attune with the conceptual framework of aggregation models when forming nanoassemblies. Three significant recent theoretical models have indicated that nucleation, end-to-end association, and geometry of growth are determined primarily by the size and electrostatics of the individual basic building blocks. In this study, we tested six model systems, differentially modulating the prominence of three design variables, namely, aromatic $\pi-\pi$ interactions, local electrostatics, and overall symmetry of the basic building unit. Our results indicate that the crucial design elements in a peptide-based nanoassembly are (a) a stable extended $\pi-\pi$ interaction network, (b) size, and (c) overall symmetry of the basic building blocks. The six model systems represent all of the design variables in the best manner possible, considering the complexity of a biomolecule. The results provide important directives in deciding the morphology and crystallinity of peptide nanoassemblies.

4.2 Introduction

Molecular self-assembly, a ubiquitous phenomenon in the nature, has always inspired materials scientists in terms of its design principles. With the complex operating mechanism at the nanoscale, the bionanomachines are self-sufficient working systems with utmost precision. Almost all biological systems are natural association of fundamental biomolecular units from nano- to macrodimensions, facilitated through nonbonding interactions. The robustness and efficient functioning of these assembled architectures are already well established. Understanding the algorithm that connects the physicochemical characteristics of the basic building blocks to form stable nano- and micro level assemblies is an ongoing endeavour in bionanotechnology, while considering the possibility of exploring such biomolecules as fundamental units. Although bioinspired design is a topic of modern-day curriculum, pioneering work on this topic is the book "On Growth and Form" by D'Arcy Wentworth Thompson, written almost 100 years ago, which attempted to quantitatively assess structural patterns and formations in biological systems [4].

Self-organization is envisaged as a spontaneous process that involves integrating local interactions between smaller subunits of an initially disordered system to develop

an ordered or a recurring pattern. A classic case of self-organization is folding and aggregation of protein chains to functional and dysfunctional forms, respectively [1]. Helmholtz in one of his recorded lectures makes an observation that "the forces so far as they cause chemical and mechanical influence in a living system, must be quite the same character as inorganic forces" [4]. Uncertainty and lack of understanding in ascertaining the long-term physiological effects of nanomaterials of inorganic origin [16] are prompting researchers to consider materials of biological origin, such as nucleic acids and proteins, as basic building units.

Protein or peptide molecules are heteropolymers made of 20 amino acids of L-stereochemistry. The planarity of the peptide bond and the L-stereochemistry, limits the conformational possibilities and sterically restricts the individual amino acids forming a protein chain. This results in a peculiar situation, in which only 21% of the total ϕ, ψ space of the Ramachandran map can be accessed for the protein main chain [202]. Even then, natural proteins have an enormous number of variations in their functional space and about 1500 variations in fold space [203]. Protein molecules are long polymeric chains folded into functional structures, sometimes even extending beyond 1000 amino acids whereas peptides, their smaller units are generally non-functional. The smallest polymer unit is a dipeptide, with two amino acids joined together through a peptide bond. However, assembly of individual peptides to form potentially functional units was a distinct possibility, although unrealized until Ghadiri first engineered peptides at the nanoscale to from cyclic peptide nanotubes. Ghadiri et al. introduced the concept of locking conformational basins by incorporating D amino acids, in the context of a cyclic peptide to form a planar ring that self-assembles on top of the other to form tubular structures [155, 204]. Several other work followed, where a cyclic peptide Lanreotide growth hormone inhibitor self-assembled into tubular structures [205] and charged peptide building blocks assembled to form fibrillar structures [206].

A significant observation involving supramolecular self-assembly of amino acids like leucine, phenylalanine, and their combinations was reported later by Gorbitz [161]. Gazit, Rosenman, and co-workers made tremendous advancements in the following years by demonstrating multivarious applications for diphenylalanine (FF) nanotubes [96, 207]. Design of FF nanoassemblies to generate nanotubes, nanowires, quantum dots, and nanospheres followed, thus establishing an important discipline of peptide nanoassembly (PNA) in the advancement of nanotechnology [188]. Although a number of amino acids and their combinations were possible in principle, FF nanotubes emerged as the most

sought after model system due to its structural simplicity and robustness in assembly formation [96, 163]. Attempts to alter the basic model systems, like combination of phenylalanine (F) with tryptophan (W) [96, 207], using tripeptides (FFF) [208], and so forth, were made, resulting in an assembly pattern that was morphologically different from that of FF nanotubes. Assembly experiments with a stereochemical variant ((D)Phe-(D)Phe) resulted in a structure of opposite handedness [96]. Also, a recent work by Joshi and co-workers demonstrated the hierarchical assembly of such conformationally rigid monomeric units forms robust nano- and microscale networks [209]. Apart from the basic building blocks, fabrication conditions, also plays a crucial role in assembly formation, as demonstrated by Li and co-workers in a recent report [210]. The success in constructing supramolecular structures is dependent on the noncovalent interactions used to bind the molecules into a stable and structurally well-defined aggregates. Earlier studies have provided ample evidence that FF nanoassembly is mediated through quadrupolar interactions involving phenyl embraces self-arranged in parallel displaced and T-shaped configurations for maximum stability [11]. Apart from electrostatics, another important variable for any assembly is the symmetry of the constituent basic units. Asymmetry in a basic unit prohibits epitaxial growth, forming a stable macromolecular assembly [211].

In this study, we tested six model systems, with varying symmetry elements differentially modulating the prominence of the other two design variables, namely, aromatic $\pi-\pi$ interactions and end-to-end local electrostatics of the basic building units, while designing nanolevel assemblies of peptides. Our results indicate the contributions of extended $\pi-\pi$ interactions and oppositely charged end groups in directing peptide nanoassemblies. Our results further suggest that the size and overall symmetry of the basic building blocks also have an important role in deciding the morphology and crystallinity of nanostructures.

4.3 Materials and Methods

4.3.1 Materials

FF peptides were purchased from Sigma Aldrich Pvt. Ltd. Designed Ff, FBf, fBfBf, and FfFfFf peptides were purchased from Mimotopes Pvt. Ltd. (Australia) and used as received. The other chemical 1,1,1,3,3,3-hexafluoro-2-propanol was purchased from Sigma- Aldrich. Milli-Q water (18 MΩ cm) was used for all the experiments.

4.3.2 Preparation of Peptide Samples

FF and Ff stock solutions were prepared by dissolving the peptides in 1,1,1,3,3,3-hexafluoro-2-propanol (Sigma Aldrich) at a concentration of 100 mg/mL. FfFfFf and fBfBf were dissolved at a concentration of 50 mg/mL and FBf at a concentration of 25 mg/mL. Stock solutions of all the peptide samples were further diluted in Milli-Q water.

4.3.3 Field-Emission Scanning Electron Microscopy(FE-SEM)

A working concentration of 0.5 mg/mL was used for FE-SEM analysis. Analysis were performed using Nova Nanosem NPE206 at 15 kV. Peptide samples (20 μL) that were one day old were loaded on a silica wafer for analysis and air dried. Samples were coated with chromium for enhancing the conductivity.

4.3.4 Atomic Force Microscopy (AFM)

AFM images were generated using an Agilent Model 5500 series instrument. Peptide samples (20 μL) that were one-day old and with a working concentration of 0.5 mg/mL were loaded onto a silica wafer for analysis. Air-dried samples were analyzed using the semi contact imaging mode. The obtained data were processed and analyzed using WSxM 5.0 Develop 7.0 software [212].

4.3.5 Transmission Electron Microscopy (TEM)

A one-day old peptide solution (10 μL) of concentration of 2 mg/mL was loaded onto a carbon300 mesh copper grid covered with a strong carbon film. Negative staining was performed by adding 10 μL of 2% uranyl acetate in water. After 2 min, the excess fluid was removed from the grid and the samples were dried at room temperature. Negatively stained samples were viewed on a JEOL transmission electron microscope (model: JEM 2100) operating at 200 kV.

4.3.6 X-ray Diffraction (XRD)

Stock solution of FfFfFf peptides in HFIP was prepared at a concentration of 50 mg/ml and it was diluted in dd.H_2O to a final concentration of 2 mg/mL. Powder XRD characterization was carried out on Rigaku TTRAX III with a power of 18 kW. The assemblies

dried on the glass slide were subjected to Cu/Kα-1 X-ray radiation with a wavelength of k=1.54056 Å. The diffraction patterns were recorded over 2 theta values in the range of $3-55^{\circ}$ with an increment of 0.02 degrees.

4.4 Results and Discussion

The de novo designs of the six model molecular systems used in this study were based on three criteria: aromatic $\pi-\pi$ interactions, local electrostatics, and the symmetry of the basic building blocks. We have designed these systems by placing amino acids in specific allowed basins in the Ramachandran diagram such that they are conformationally locked, assuming a singular structure, and may associate further to form an assembled architecture. This was a primary requirement while designing such model systems because peptides are otherwise free to assume any conformation on the basis of the reaction conditions while assembling themselves into a supramolecule. However, the specific role that the solvent (water) plays in such assembly formation is yet to be fully understood. We have broadly defined the conformational possibilities of the phenylalanine (F) residue in FF (Figure 4.1), adopting any three ϕ, ψ basins. First, in a β basin extending up to the polyproline II helix (PPII) region; second, in a right-handed α-helical basin; and third, in a rare left-handed (LH) α-helical basin (Figure 4.1 (b)). Two diphenylalanine (FF) monomeric units (Figure 4.1 (a)) can have roughly nine geometric variant combinations with each phenylalanine residue adopting any of the three conformational basins (Figure 4.1 (c)). We modeled all geometrical possibilities and calculated the distance between the geometric centers of phenylalanine benzene rings (Figure 4.1 (f)) (Table 4.1). The equilibrium distance for an aromatic $\pi-\pi$ interaction is 4.96 Å, where it has a maximum energetic advantage of 3−4 kcal/mol. However, the distance for favorable quadrupolar interactions involving benzene rings ranges from 4.04 to 6.0 Å [11]. Two (ϕ, ψ) basin combinations of FF fall within this range, and of these two, (13) and (21) combinations were at an optimal distance for a possible aromatic $\pi-\pi$ interaction (Figure 4.1 c, f). In basin combination (21), the two benzene rings of FF are approximately orthogonal in their orientation, whereas in (13), they are parallel and at an optimum position for T-shaped geometry (Figure 4.2). Basin 3 is a LH α-helical region and is not a preferred basin for a phenylalanine residue as per the statistics obtained from protein databases [213].

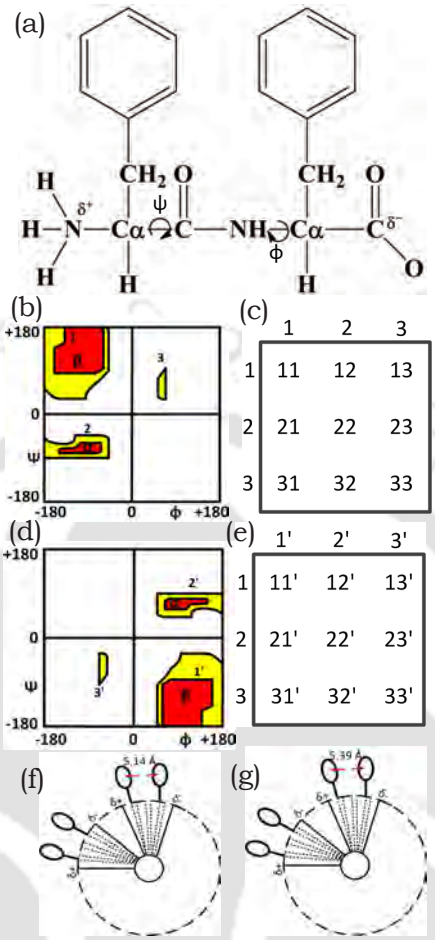

Figure 4.1: Chemical structure of an FF molecule (a). Allowed basins 1–3 on a Ramachandran map (b) and their respective combinations (c) for FF. (d) Allowed region for D-Phe(f) in the Ramachandran diagram and (e) combination of L-Phe(F) and D-Phe(f) basins. (f, g) Distance between the geometric centers of benzene rings in two phenylalanine residues of FF and Ff.

Interestingly, the (13) basin combination (Figure 4.3 (a)) is specifically the geometry that is observed in the crystal structure data of FF nanotubes solved by Gorbitz (CCDC 16340) [161]. The second and probably the only other possibility for designing two phenylalanine residues in the same (13) basin configuration is by using D-phenylalanine (abbreviated as D-Phe or f) as the second residue, and this combination, “Ff”, is our second model system. This Ff dipeptide will have a basin combination of (12’), in which basin 3 of L-Phe (F) is replaced by the 2’ basin of D-Phe (f) (Figure 4.1d,f).

This molecular model also has comparable distances between the geometric centers of its benzene rings, of 5.39 Å (Figures 4.1 (g) and Figures 4.3 (b)) (Table 4.1). Our third

FF		Ff	
Basin combinations	**Distance(Å)**	**Basin combinations**	**Distance(Å)**
11	6.79	$11'$	6.57
12	8.81	$12'$	8.82
13	5.15	$13'$	5.40
21	5.14	$21'$	5.59
22	2.67	$22'$	2.60
23	6.48	$23'$	6.14
31	3.22	$31'$	8.77
32	7.18	$32'$	6.83
33	8.37	$33'$	3.39

Table 4.1: Distance calculation between the geometric centers of phenylalanine benzene rings in FF and Ff

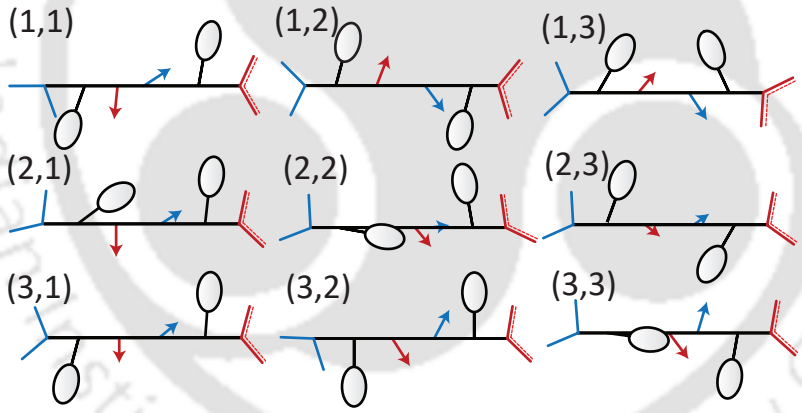

Figure 4.2: Spatial orientations of all the combinations of FF. Oval-shaped cartoon representation indicates benzene ring. Red and blue colored arrows indicates C=O and N-H dipole.

model system is an equimolar mixture of both FF and Ff (Figures 4.3 a and c), to assess whether they form any nanolevel assembly. To test the specific role of intramolecular interactions between benzene rings in determining the nanolevel architecture, FBf was designed such that α-amino isobutyric acid (Aib or B) separates two phenylalanine residues (Figures 4.3 (d)). The advantage of having Aib is that it restricts the conformational flexibility of the tripeptide to only the α-helical conformation due to steric effects and hence the tripeptide is structurally locked. The exclusive right-handed α-

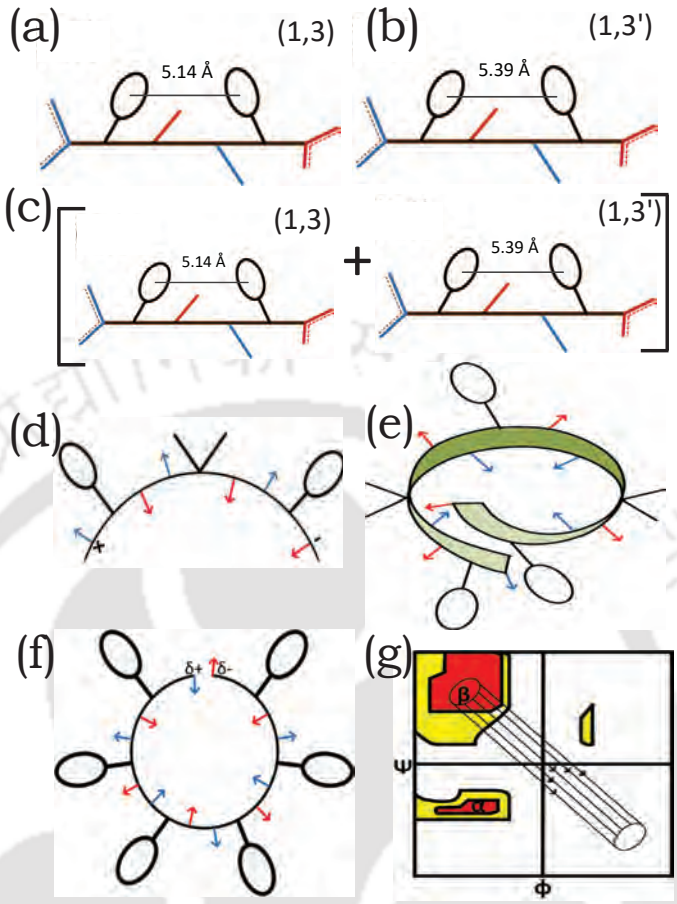

Figure 4.3: Spatial orientations of combinations of diphenylalanine sidechain orientations that are chosen as model systems 1–3 in this study (a–c). All combinations are shown in Figure S2. The oval cartoon representations indicate benzene rings. The red and blue lines indicate CO and NH dipoles. Peptide models 4 and 5, with their conformations restricted by incorporating Aib in the sequence, FBf (d) and fBfBf (e). FfFfFf peptide based on the design clues from gramicidin and Ghadiri's nanotubes (f). Gramicidin-like β- helical structures result when the backbone ϕ, ψ angle alternates between L and D β basins of the Ramachandran diagram (g).

helical basin preference of Aib separates the two phenyl rings from interacting distance (Table 4.2).

It is logical to assume that the geometry of the assemblies is a derivative of the individual geometry or symmetry of the basic constituents, and this is especially obvious in inorganic systems. Earlier schools of thought, according to which nature's creations are not excluded from the laws of geometry [2], and correlation studies between biological forms and mechanical phenomena support this logic [4]. Some observations on biomolecular interactions also give confidence to test the role of individual symmetries of peptidic

FBf		**fBfBf**	
Basin combinations	**Distance**(Å)	**Basin combinations**	**Distance**(Å)
$21'$	7.80	F1-F2	11.08
$22'$	7.08	F1-F3	7.07
$23'$	8.14	F2-F3	11.08

Table 4.2: Distance calculation between the geometric centers of phenylalanine benzene rings in FBf and fBfBf

systems in defining the nanoarchitecture [211]. A fifth model, fBfBf, was designed (Figure 4.3 (e)), which is considerably asymmetric in all three planes (Figure 4.4). This will also have a restricted right-handed helical conformation (Figure 4.3 (e)), having an asymmetric spatial orientation. If we assume that the distances along all three directions are vertices of a triangle, we get an asymmetric structure with three faces, having three different size proportions(Figure 4.4 (d)), thus limiting the possibility of an assembled architecture. The preference of short peptides and "disordered" segments to assume a polyproline II conformation has already been established by various groups using polyalanines as model systems. Solvation effects and interatomic electrostatic interactions within a peptide were proposed to be the driving forces for this preference [214]. We have shown by molecular dynamics simulations the existence of specific folds, such as helices and hairpins, in an octa-alanine conformational ensemble [215]. We have further shown that the countervailing local and global electrostatic interactions may be attributed to the complex conformational folding behavior of peptide sequences, which is distinctly different from that in other heteropolymers [216]. Recent protein aggregation models by research groups of Fodera, Fink, Gloss, and Donald predict the formation of multifractal structures, with the geometry of growth primarily directed by electrostatic interactions [217–221].

Peptide systems 1–5 have unfavorable intramolecular local electrostatics, which are compensated by favorable interpeptide interactions through partially charged end groups. The sixth molecular model system is an exception to this, with intrapeptide as well as interpeptide interactions in a favorable orientation (Figure 4.3 (f)). The FfFfFf peptide segment, with alternating L and D chiral phenylalanine residues, resembles the nanotubes reported earlier by Ghadiri (Figure 4.3 (g)) [155, 204]. The most optimized structure among $3^6 = 729$ total conformational possibilities feasible for this sequence is

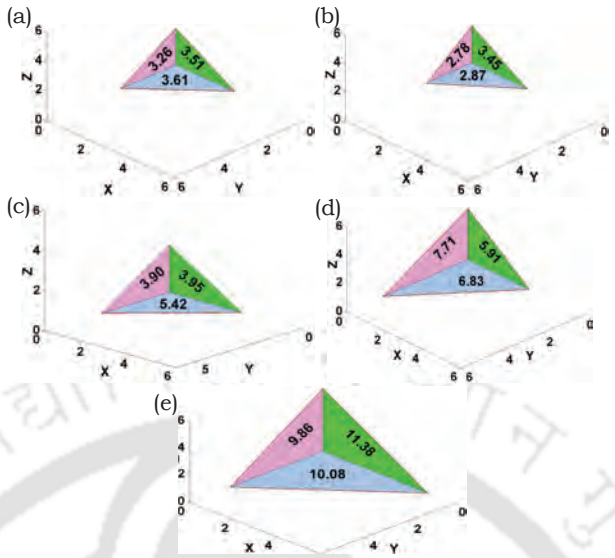

Figure 4.4: Approximate projections of the three-dimensional spatial arrangements of five model systems. The radii of gyration along X, Y, and Z are assumed to be the vertices of a triangle, to present a qualitative impression of the topology of the system. Comparative analysis of the area (in Å2) of each triangle will provide a qualitative impression of the extent of symmetry in the distribution of constituent atoms in space.

shown in Figure 4.3 (f), yet other conformations are not sterically prohibited in FfFfFf, unlike that in the other five structurally locked model systems (Table 4.3). This peptide is designed to investigate whether a stable architecture is feasible with the assembly of structurally unlocked basic units satisfying quadrupolar interactions between the benzene rings of phenylalanine residues alone. The topologies of the two benzene rings facilitating intramolecular $\pi - \pi$ interactions are optimum in the FF dipeptide nanotube crystal structure data by Gorbitz [161]. In the crystal structure reported, the first phenylalanine residue is in the β basin and the second one is in the LH α-helical basin, thus conforming to the critical distance requirement for optimal T-shaped phenyl embraces, mediated through quadrupolar interactions. The end residues of FF are at least partially positively and negatively charged. This facilitates end-to-end propagation of the basic FF units. Apart from this, two phenyl rings protrude out of the main chain Cα atom, with a β carbon (CH_2) in between. The chi1 and chi2 side-chain dihedral angles can facilitate optimal $\pi - \pi$ interactions. Overall, the local electrostatics of opposite polarities at the ends, symmetrical positioning of two phenyl rings, and optimum inter-ring distance between phenyl groups facilitate the formation of an assembled architecture mediated

Basin combinations	**Distance**(Å)
F1-F2	5.76
F1-F3	9.21
F2-F3	8.36
F1-F4	12.80
F1-F5	9.58
F1-F6	8.97

Table 4.3: Distance calculation between the geometric centers of phenylalanine benzene rings in FfFfFf

through favorable electrostatics. However, location of the second F unit in the not-so favorable LH α-helical region appears to be a necessity for FF nanotube formation. The designed Ff dipeptide, with the second phenylalanine (f) in the 2' basin, forming the (12') configuration (Figure 4.1 d, e), was hypothesized to have an almost identical nanotubular structure to that of FF. This experiment worked remarkably well with Ff, forming nanotubes of comparable dimensions to those of FF nanotubes, observed from FESEM, AFM, and TEM experiments (Figure 4.5). The melting points of FF and Ff were also comparable, that is, 592 and 551 K for FF and Ff, respectively. This prompted us to check the assembly of an equimolar mixture of FF and Ff as the third composition, but no significant assembled architecture was observed (Figure 4.6), an observation similar to that from an earlier report on napthalene-conjugated dipeptides by Yang et al [222].

The configuration of the phenyl embraces was modified by adding Aib as the middle residue between F and f. Location exclusively in the RH α-helical basin is the hallmark of Aib. Aib also forces the neighboring residues to adopt an RH α-helical conformation, restricting intramolecular $\pi - \pi$ interactions. This changed the assembly from nanotubes to nanocombs (Figure 4.7 (a)). The same constraint was further extended by designing an asymmetrical fBfBf peptide (Figure 4.4 (d)). The hypothesis that asymmetry in the basic unit may have prohibitory effects on a nanolevel assembly also worked remarkably well, with the fBfBf model system not showing any consistent pattern in its nanoassembly (Figure 4.7 (b)). The sixth and final model system, FfFfFf, as a basic building block can form a channel-forming helical conformation much like that seen in gramicidin [223] or Ghadiri's nanotubes [155, 204]. However, individual residues of the FfFfFf molecule

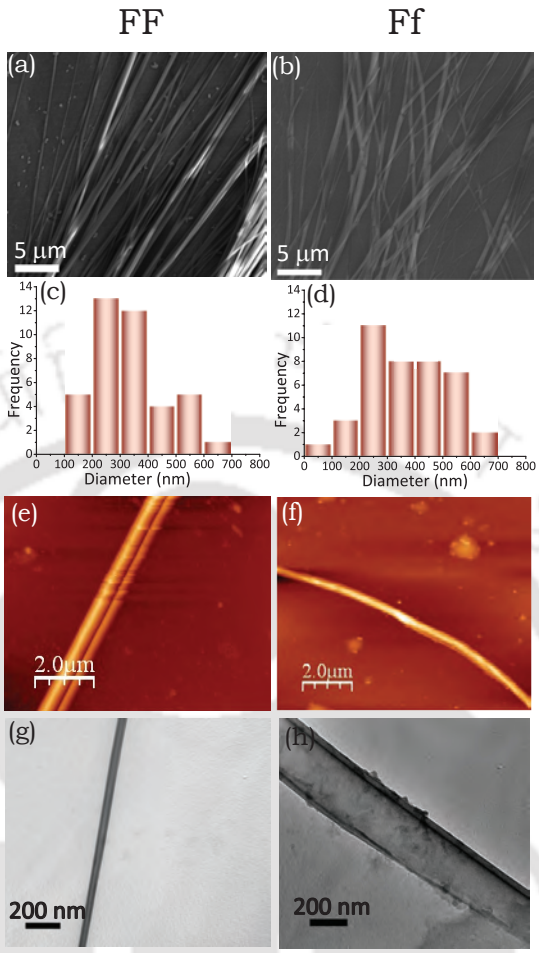

Figure 4.5: Micrographs of the nanotubes formed by the first two model systems of diphenylalanine peptides (FF and Ff): FESEM images (a-b) and the statistical distribution (c-d) of the diameter of the nanotubes formed by the model systems. AFM micrograph (e-f) showing individual nanotubes and TEM images (g-h) of the negatively stained nanotubes of FF and Ff.

can sample any three allowed basins and, in principle, can form $3^6 = 729$ conformational variants. Nevertheless, its nanoassembly is consistent, forming noncrystalline amorphous stable nanofibers (Figure 4.7 (c) , Figure 4.8). Epitaxial growth of individual building blocks that have fewer degrees of freedom is the key to designing molecular architectures at a nanolevel. Symmetry and electrostatics expectedly play a crucial role in such assembly buildups. The (13) and (12′) basin combinations of FF and Ff present almost the same electrostatics, symmetry, and geometry of phenyl embraces.

Consequently, FF and Ff resulted in almost identical assembled architectures (Figure 4.5). From a design perspective, this experiment confirms that the nano assembly is indeed a function of the symmetry and electrostatics of the fundamental units, even in

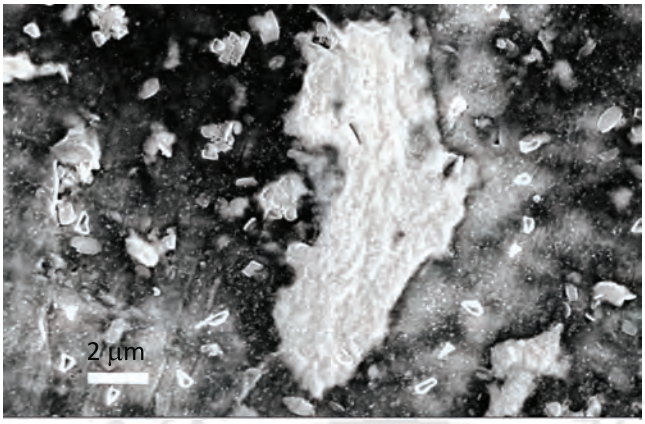

Figure 4.6: FESEM analysis confirming that no significant nanolevel architecture was formed from the equimolar mixture of FF and Ff.

the case of peptide systems, in which conformational flexibility and its effect are much more pronounced compared to those in inorganic systems. A difference of 41 K in the melting point between FF and Ff was observed, and this difference may be attributed to the observation that Ff is comparatively less symmetric than FF (Figure 4.4 a,b). Although this asymmetry is not significant enough to prohibit assembly, it may affect the overall stability of a well-packed structure. However, the effect of asymmetry is very well evident in fBfBf, with no pronounced assembly formation observed on microscopy (Figure 4.7(b)). A change in the chemical constitution along with the lack of intramolecular $\pi - \pi$ interactions between two benzene rings of adjacent phenylalanine residues prohibited nanotube formation of conformationally locked FBf basic units; however, they adopted a nanocomb-like architecture (Figure 4.7(a)) by intermolecular association. The amorphous but stable nanofibers formed by FfFfFf (Figure 4.7(c)) may be attributed to favorable local electrostatics and intramolecular $\pi - \pi$ interactions between phenylalanine residues and adjacently positioned side chains. Recent coarse grained molecular dynamics (MD) simulation results by Schatz and co-workers attribute nanofiber formation of such short peptide amphiphiles to the micellar and van der Waals interactions at various stages of assembly formation [224]. Intermolecular phenyl embraces can also form stable assemblies, as evidenced from FBf and fBfBf, but they are relatively less stable compared to FF nanotubes, an observation based on the beam damage caused by the TEM experiment. From the experimental results, it was found that the most important design element in a peptide-based nanoassembly is a stable extended $\pi - \pi$ interaction network. In the case of the FF assembly, the two phenyl rings are placed at optimal

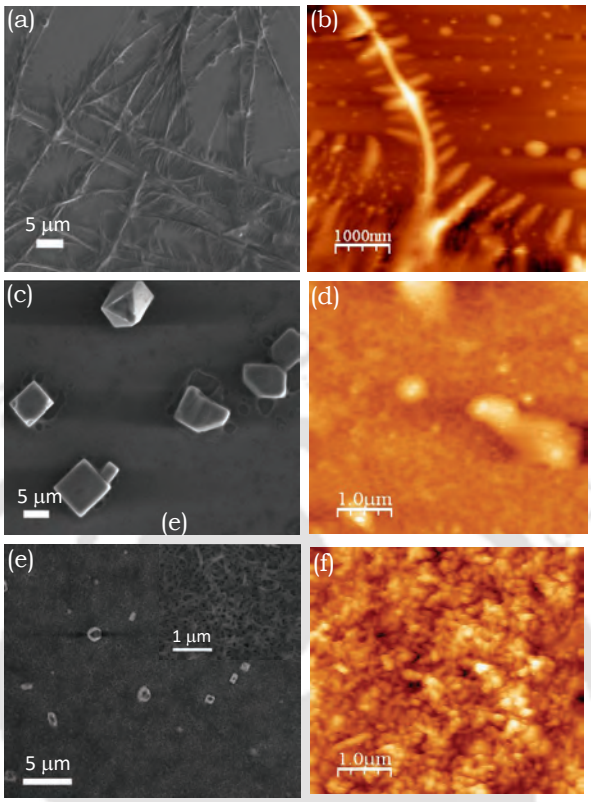

Figure 4.7: FESEM and AFM images of (a-b) nanocombs formed by FBf, (c-d) random nanoassemblies formed by fBfBf, and (e-f) nanofibers formed by FfFfFf.

distances for maximum stability. The opposite polarities of the two ends facilitate the intermolecular extended network formation necessary to assume a tube-like structure. The ϕ dihedral angle range from -150 to -90 in basin 1 of the first residue ensures that nanotubes with a wide variety of diameters are possible. The diameter of the nanotube decreases as the ϕ angle becomes closer to the PPII basin. This explains the wide range of FF nanotube diameters reported by Gazit and co-workers, ranging from 20 to 300 nm [96]. The basic configurations of the two phenyl rings in FF and Ff are the same and so are their nanolevel assemblies. It was found that quadrupolar interactions between the phenyl rings within and between FF molecules play a key role in their assembly. Hence, FBf was designed such that both phenyl rings are 7.08 Å apart in a sterically locked conformation, with all amino acids locating in RH α-basins (Table 4.2). The polar ends are relatively symmetric in their positioning. In this structure, it helps the molecule to form a comb-like architecture; although intramolecular phenyl embraces are absent,

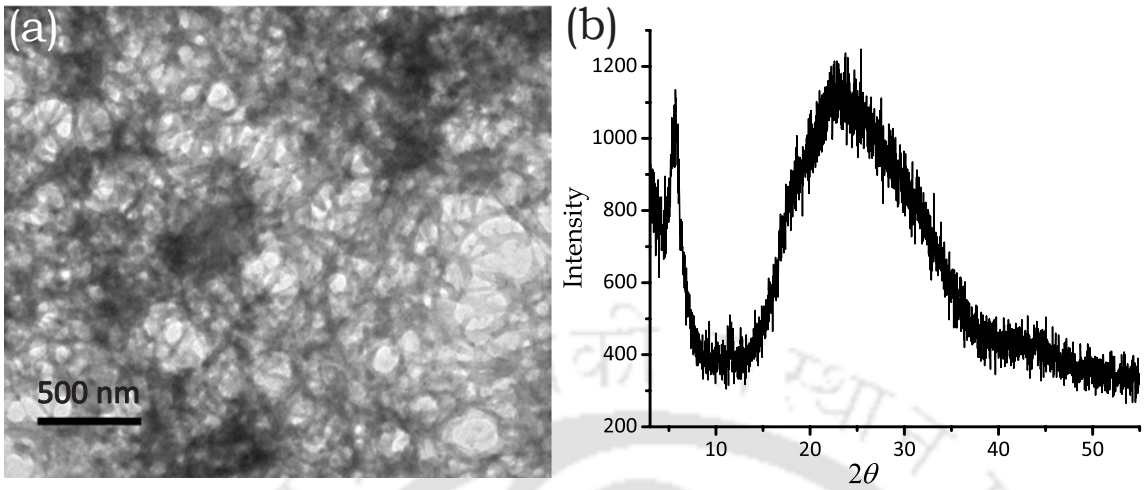

Figure 4.8: FESEM analysis of nanofibers formed by FfFfFf peptides and the X-ray Powder diffractogram of the nanofibers, indicating the amorphous nature of the assembly.

intermolecular interactions are still possible. No significant nanolevel assembly was observed in the case of fBfBf. Understandably, molecules with inherent asymmetry cannot undergo symmetric assembly.

In the present work, we tried to optimize inter- and intramolecular quadrupolar interactions between phenyl rings, as in FfFfFf, to obtain some design directives that can be employed while designing PNAs. FF is the core recognition motif of the β-amyloid peptide in Alzheimer's disease. Therefore, the mechanism of self-assembly of phenylalanine-based systems may be more similar to that in peptide/protein aggregation models than that in inorganic systems [225]. A recent study by Donald and co-workers has presented a convincing model for protein aggregation, arguing that the geometry of growth is principally determined by the electrostatic interactions between basic units [221]. Donald and coworkers argue that peptidic systems containing polar groups unevenly distributed on the molecular surface will generate multipole moments affecting interpeptide association. Consistent with this argument, our systems (except FF and Ff) have similar molecular structures and therefore have almost similar assembled architectures. FF and Ff, although stereochemically different, have identical charge distributions when they assume identical basins in the Ramachandran map, resulting in a nanotube-like morphology. Knowles and co-workers in a recent work highlight the role of filamentous structures undergoing nucleation and end-to-end association in the dynamic behavior of growth of linear protein assemblies. Adapting this framework, it can be assumed that par-

tially charged end groups have a directive influence on nucleation and association [226]. Such elongated systems can further self-catalyze to form extended architectures, a phenomenon predicted by Fodera and coworkers in a recently published two-dimensional model for aggregation [227]. As stated earlier, three design elements were tested, namely, benzene quadrupolar interactions, peptide backbone electrostatic interactions, and overall symmetry, for indicative results so that researchers involved in the creation of a peptide-based nanoassembled architecture will get a supportive design guideline. The sample set chosen and the results are sufficient to provide clear directives, although a more detailed study would further enrich this line of inquiry. Although modular design attempts with peptides have been reported earlier, this is probably the first attempt to modulate nanoassembly from molecular size and symmetry[228]. It will also complement the mechanistic investigations on the driving forces involved in protein and peptide aggregation.

Peptide Sequence	**Morphology of the nanoassemblies**	**Crystallinity**
FF	Nanotube	Crystalline
Ff	Nanotube	Crystalline
FF + Ff	No significant nanoassemblies	Unknown
FBf	Nanocomb	Amorphous
fBfBf	No pronounced assembly formation	Unknown
FfFfFf	Nanofibres	Amorphous

Table 4.4: Summarization of the effect of three design variables in the morphology and crystallinity of the six peptide model systems

4.5 Conclusions

Organic and bioorganic molecules have variables like non-bonded interactions, stereochemistry, and symmetry that play a large role in the stability and morphology of the formed assemblies. These factors are often detrimental in directing their assembled architecture and consequently their function. In this chapter, indicative information was obtained on the relative prominence of symmetry, $\pi - \pi$ interactions, and overall size through six model molecular systems (Table 4.4). From the results, it is inferred

that their individual symmetries mainly decide the morphology and stability of these electrostatic interaction-mediated assemblies. Smaller molecules with a larger number of symmetry elements tend to form more ordered crystalline assemblies, whereas larger molecules, especially asymmetric ones, are more prone to be amorphous. From these experiments, it is clear that the overall size, symmetry, and charge distribution of the fundamental units dictate the topology of the PNA. However, a comprehensive mechanistic picture, especially the role of water in modulating assembly formation, is yet to be obtained and may require elaborate investigations.

CHAPTER 5

SINGLE CRYSTAL ORGANIC NANOFLOWERS

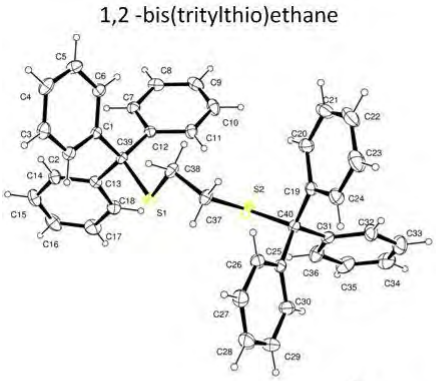

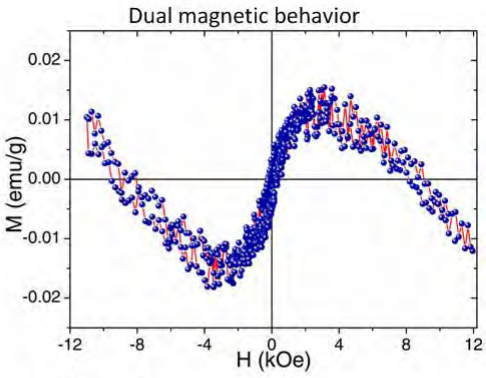

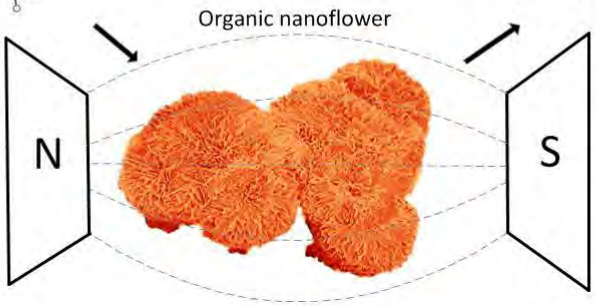

5.1 Summary

Nanoflowers, reported so far were mostly constituted of inorganic elements and have shown a lot of promise due to their thin and open edges [229]. We report synthesis and crystallization of a new triphenyl methyl derivative, 1, 2-bis(tritylthio)ethane and its nano-level assembly forming a rare organic nano-flower. The reported 1, 2-bis(tritylthio)ethane, forming plate and organic-flower like morphologies at nano-level is the first organic crystal to exhibit an inherent dual magnetic behavior at 300 K and 2 K. Apart from its fundamental importance in providing a new direction to the conceptual understanding of 'organic magnetism', the molecule also exhibited conductivity and capacitance in electrical measurements. Organic molecules with such properties can be important lead for possible applications in spintronics, nano electronics and memory storage devices [230].

5.2 Introduction

Structural and functional adaptability of organic molecules have always been a source of inspiration to explore the possibility of designing stable, well-defined molecular architectures important for the development of newer technologies. Among different nanoarchitectures, nano-flowers due to their thin and open edges have shown immense promise and were fabricated for various important applications such as catalysis, biosensors and optoelectronic devices [229]. The data reported on nano-flowers are either inorganic [229] or hybrid materials [231, 232]. Carbon, elemental metals and compounds of metals with fifth and sixth group elements were the principal constituents of such assemblies. Single crystal organic nanoflowers have not been discovered so far to the best of our knowledge, though assemblies of single crystal inorganic nanoflowers [233], organic nanoflowers [234, 235], hybrid organic-inorganic nanoflowers using copper (II) ions [231, 236], diphenylalanine [237], N,N'-diphenyl-N,N'-bis(1-naphthyl)-1,1'-biphenyl-4,4'-diamine (NPB) [238] and DNA based nano-flowers have been reported recently [239–241]. Although, extensive studies have been done on trityl based molecules and their applications, trityl group forming nanoassemblies and their application has not been reported yet. Through this work, we report synthesis and crystallization of a pure organic molecule and its assembly to a stable crystalline organic nanoflower. Crystal structure at nano and micro level indicates that interaction between aromatic systems is the principal

factor governing molecular recognition and assembly. Crystals at room temperature (300 K), exhibit ferromagnetism at lower magnetic field and diamagnetism at higher fields; an inherent dual magnetic property not reported so far in organic materials. Ferromagnetic behavior was consistent at low temperature (2 K) measurements at lower magnetic fields, but a transition from ferromagnetism to paramagnetism was observed at higher fields.

5.3 Materials and Methods

5.3.1 Materials

All the chemicals and solvents used for experiments are of reagent grade. Amino acid Fmoc-His(trt)-OH and solvents Trifluoroacetic acid, Thioanisole, and 1,2-ethanedithiol were purchased from Sigma-Aldrich. Diethyl ether and m-cresol were purchased from Merck.

5.3.2 Synthesis and Crystallization of 1,2-bis(tritylthio)ethane

The compound was synthesized by treating trityl group released from the side chain of Fmoc-His(trt)-OH with 1,2-ethane dithiol, m-cresol and Thioansiole in the presence of trifluoroacteic acid(1:2:2:20). Crystallization and purification were done using diethyl ether as a solvent. Melting points were recorded on a Stuart smp30 melting point apparatus.

5.3.3 Characterization

NMR Analysis

^{1}H NMR was recorded on a Bruker 600 MHz NMR spectrometer. NMR spectra were recorded in deuterated chloroform ($CDCl_3$), and the chemical shifts were reported relative to TMS (δ=0 ppm) as an internal reference. Spin multiplicity was abbreviated as follows: s = singlet, d = doublet and t = triplet. ^{1}H NMR (600 MHz, $CDCl_3$) δ (ppm): 7.32–7.31 (d, 12 H), 7.25–7.22 (t, 12 H), 7.20–7.17 (t, 6 H), 2.1 (s, 4 H).

X-ray Diffraction

Single crystal XRD measurement of the plate-like crystal was done on a Bruker APEX-II CCD diffractometer with graphite-monochromatized (MoKα = 0.71073 Å) radiation at room temperature [296(2) K]. The X-ray data collection was monitored by SMART program (Bruker, 2003) [242]. Powder XRD data measurements were made using a high power (18 kW) Rigaku TTRAX III X-Ray Diffractometer. The powdered crystals were subjected to X-ray radiation of Cu/Kα with a wavelength of 1.54056 Å. The diffraction patterns were recorded over 2 theta values ranging from 5 to 55° in increments of 0.02 degrees.

Electron Microscopic Characterization

Ethyl ether was added to the plate-like crystals and vortexed to yield flower-like morphologies. 20 μl of the sample was loaded for Field-Emission Scanning Electron Microscope (FESEM) analysis, and the morphology of nano-assemblies was analyzed using Zeiss (Model: Sigma) Field-Emission Scanning Electron Microscope at 3 kV. Samples were coated with gold for enhancing the conductivity. 10 μl of the vortexed sample was placed on the 300 mesh copper grid covered with strong carbon film; SAED and Transmission Electron Microscopic (TEM) analysis of the sample was performed on JEOL transmission electron microscope, Model: JEM 2100, operating at 200 kV. 10 μl of the hybrid material vortexed with the chromium solution was loaded on the carbon coated grid for analysis. FE-TEM analysis and STEM-EDS mapping were done using JEOL JEM 2100 F.

Raman Spectroscopy

Sample containing both sheet and flower like morphologies was drop casted on a glass slide. An optical microscope of 100X objective lens was used to focus the laser on the crystal structures. Raman spectra of the samples were recorded at room temperature using Horiba JobinVyon, Laser Micro Raman System with a laser excitation wavelength of 514 nm.

Magnetic Measurements

Vibrating Sample Magnetometer: Magnetic properties of 1,2-bis(tritylthio)ethane assemblies, were examined using two different Vibrating Sample Magnetometers of the same model, LakeShore Model 7410 with maximum applied field of 12 kOe. The saturation magnetization (M_S) and coercivity (H_C) values have been extracted from the magnetic hysteresis (M-H) loop measurements using IDEAS VSM software.

SQUID magnetometer: The magnetization (M) measurements at around 2 K has been performed using a superconducting quantum interference device (SQUID) magnetometer (Quantum Design MPMS XL, 7 T, U.S.A) with maximum applied field of 70 kOe.

Conductivity Measurements

Sample preparation for conductivity measurements: 1, 2-bis(tritylthio)ethane was dissolved in diethyl ether at a concentration of 1 mg/ml.

Conductance measurements were performed with two-terminal sensor devices. The device containing the main electrode was fabricated on the glass substrate. The glass substrates were initially cleaned in piranha solution (3:1 H_2SO_4:H_2O_2) followed by repeated washing in deionized water and then dried under vacuum at 100 ºC. By masking technique, aluminum electrodes of 150 nm thickness were deposited on the dried glass substrate by thermal evaporation under high vacuum < 10^{-6} mbar to make a blank channel with 30 µm length (L) and 1500 µm width (W). From the sample, 20 μl was drop casted on the channel between the electrodes. The sample was dried under room temperature and the electrical measurements were carried out under ambient conditions using a Keithley 4200-SCS semiconductor parameter analyzer. And the measurements of other parameters were performed using hioki im3590 chemical impedance analyzer.

5.4 Results and Discussion

The molecule we report here is 1, 2-bis(tritylthio)ethane (Figure 5.1a). Triphenylmethyl (trityl) group is a stable radical first reported by M. Gomberg in 1900 [39]. Tritylcations with a positive charge on the α-Carbon atom is one of the most versatile and stable molecule widely used in biomedical applications such as neurotransmission measurements, oligonucleotide arrays (DNA chips) and as organic dyes [243]. Three aromatic rings stabilize the positive charge on α-Carbon atom by resonance effect. The acid labile

nature of trityl group is utilized in serving as a class of protective group widely used in nucleoside, oligonucleotide, peptide and carbohydrate chemistry [243]. We first observed crystallization of 1, 2-bis(tritylthio)ethane while synthesizing small peptides on a solid support.

Solid phase peptide synthesis involves sequential coupling of individual amino-acids, with alternate cycles of de-protection and coupling [244]. After completion of synthesis, in Fmoc protocol, acidic reagents like trifluoroacetic acid (TFA) are used to cleave the alkoxy benzene ester group at the linker. Often scavengers like 1, 2-ethanedithiol (EDT)

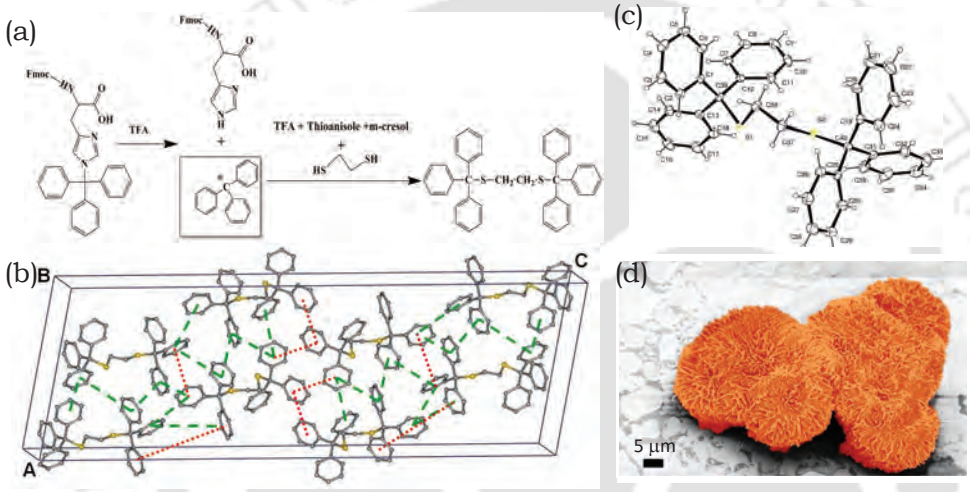

Figure 5.1: Synthesis, crystallization and nano-assembly of 1, 2-bis(tritylthio)ethane. (a) Scheme illustrating the reaction conditions for the synthesis and crystallization of 1, 2-bis(tritylthio)ethane. (b) ORTEP diagram of 1,2-bis(tritylthio)ethane. (c) The schematic unit cell of 1, 2-bis(tritylthio)ethane, showing the type of interactions in phenyl embraces (The green dashed line indicates T-shaped edge-to-face interaction, and the red dotted line indicates parallel displaced orientation). (d) False-colored FE-SEM image showing flower like assembly.

and thioanisole are used to capture the carbocations formed by the cleavage of trityl groups, from side-chain substituents. We first observed formation of 1,2-bis(tritylthio)-ethane in one such deprotection reaction. 1, 2-bis(tritylthio)ethane was spontaneously formed by treating trityl group released from the side chain of trityl protected amino acid, with EDT, m-cresol and thioansiole in the presence of TFA (Figure 5.1a).

Solid state structure of 1, 2-bis(tritylthio)ethane was determined by X-ray crystallography. Single crystal X-ray diffraction (S-XRD) (Mo Kα, $\lambda = 0.71073$ Å) analysis details of the obtained crystals were deposited in Cambridge crystallographic database (CCDC deposition number 1412852). The molecule crystallizes in the monoclinic system, with a

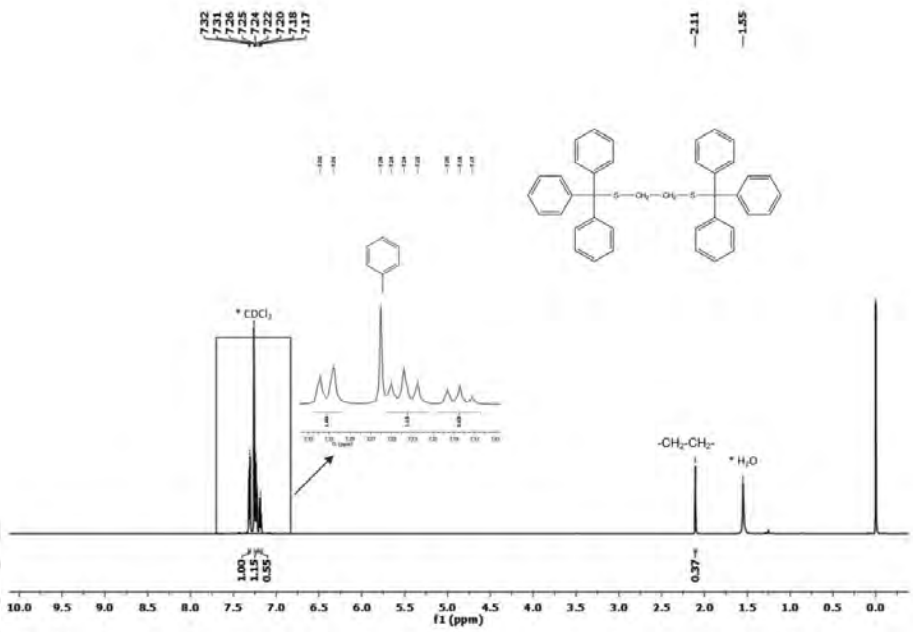

Figure 5.2: ^{1}H NMR of 1, 2-bis(tritylthio)ethane ($CDCl_3$, 600MHz)

C2/c space group in a unit cell consisting of 8 molecules. A unit cell containing fragment of crystal structure is presented in Figure 5.1c, and the complete details are shown in Table 5.1. The melting point of the crystals was found to be in the range of 180–185 °C. The purity of synthesized crystals was verified using proton NMR (Figure 5.2). The morphologies and microstructures of 1, 2-bis(tritylthio)ethane crystals formed in diethyl ether were examined using Field Emission - Scanning Electron Microscope (FE-SEM). FE-SEM analysis shows plate-like morphologies (Fig. 5.3a) of varying width in nm-μm range, collectively aligned in almost regular petal-like orientation as in a typical nanoflower (Figs 5.1d, 5.3b).

Detailed examination of a single nanoflower shows that they are composed of plate-like and curled thin petals, with smooth surfaces usually observed in a natural flower (Figure 5.4). Morphology evolution of similar kind as a result of collective and cooperative alignment of nanorods [245, 246], nanoblades [247] and nanosheets [249, 280] has already been reported by various groups with inorganic materials.

We verified the chemical composition of both the morphologies, by recording their respective Raman spectra (400-3200 cm^{-1}, Figure 5.5). Raman spectra of both plate and flower like morphologies and the obtained peaks are assigned to various functional groups present in the compound (Table 5.2). The vibration peaks at 618.96 and 677.62 cm^{-1} can

Identification code	1,2-bis(tritylthio)ethane
Empirical formula	C_{40} H_{34} S_2
Formula weight	578.79
Temperature	296(2) K
Wavelength	0.71073 Å
Crystal system, space group	Monoclinic, C2/c
Unit cell dimensions	a = 16.9966(4) Å alpha = 90 deg. b = 7.3711(2) Å beta = 99.0830(10) deg. c = 50.3919(11) Å gamma = 90 deg.
Volume	6234.1(3) $Å^3$
Z, Calculated density	8, 1.233 Mg/m^3
Absorption coefficient	0.198 mm^{-1}
F(000)	2448
Crystal size	0.25 x 0.15 x 0.15 mm
Theta range for data collection	0.82 to 25.00 deg.
Limiting indices	-18<=h<=18, -7<=k<=7, -53<=l<=53
Reflections collected / unique	3064.46
Completeness to theta = 25.00	99.8 %
Absorption correction	Semi-empirical from equivalents
Max. and min. transmission	0.9709 and 0.9521
Refinement method	Full-matrix least-squares on F^2
Data / restraints / parameters	3967 / 0 / 379
Goodness-of-fit on F^2	1.155
Final R indices [I>2sigma (I)]	R1 = 0.0359, wR2 = 0.0916
R indices (all data)	R1 = 0.0494, wR2 = 0.1089
Largest diff. peak and hole	0.202 and -0.226 $e.Å^{-3}$

Table 5.1: Crystal data and structure refinement for 1,2-bis(tritylthio)ethane

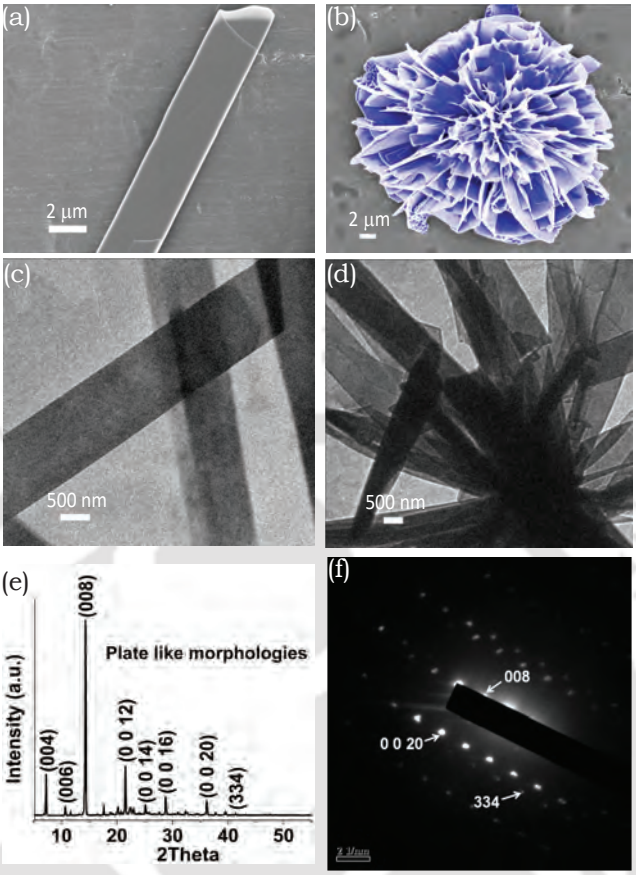

Figure 5.3: Morphological and structural characterization of 1, 2-bis(tritylthio)ethane assemblies. (a,b) FE-SEM images of different structural morphologies formed by 1, 2-bis(tritylthio)ethane; (a) plate-like assemblies and (b) nanoflower (False coloured in blue). (c,d) TEM images showing (d) nanoflowers made from (c) individual plate-like morphologies. (e) P-XRD of plate-like structures. (f) SAED pattern of the flower with a diffraction spot indexed as (008), verify the constitution and single crystalline nature of the flower at nano-level.

be assigned to C-S and C-S-C stretching. Wag vibrations in the CH_2 groups occurs due to the coupling between two adjacent rocking CH_2 groups, where the region 1295-1063 cm^{-1} represents CH_2 twisting and 1174-724 cm^{-1} represents CH_2 rocking vibrations. The in-plane C-H bending of aromatic rings occurs at 1003.11 and 1034.69 cm^{-1} and C-C aromatic ring chain vibrations occurs at 1579.86 and 1595.65 cm^{-1}. The stretching vibrations of CH bonds in the aromatic ring appears at 3064.6 cm^{-1}. Transmission electron microscopic (TEM) (Figure 5.3c, d) analysis further supports the results from FE-SEM and Raman, indicating the assembly of nano-plates to nanoflowers. S-XRD and Powder X-ray diffraction(P-XRD) (Figure 5.3e) ensured the crystallinity of the plate

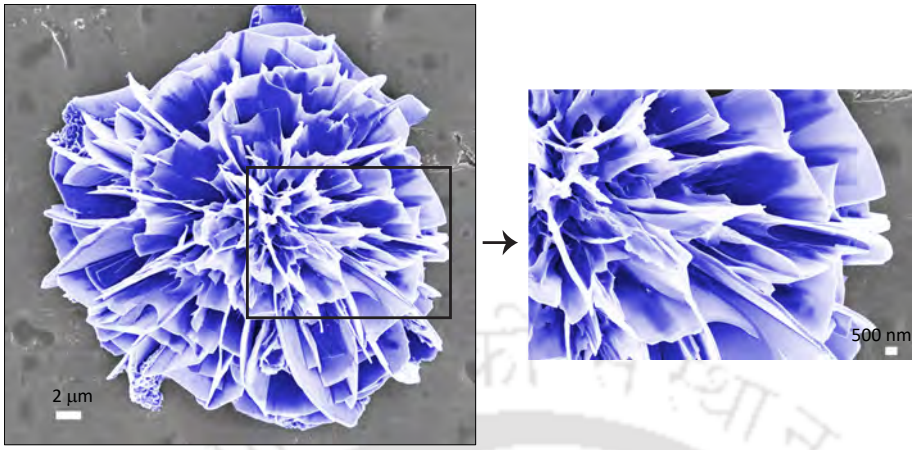

Figure 5.4: Detailed analysis of nanoflower like morphologies showing curled and plate like petals.

like morphologies, while the Selected Area Electron Diffraction (SAED) pattern (Figure 5.3f) clearly indicate the single crystalline nature of the flower-like assembly even at the nano-scale. In addition to this, the indexed peak (008) in the SAED pattern of the single crystalline nano- flower (Figure 5.3f) corresponding to the major crystalline phase in the P-XRD of plate-like structures (Figure 5.3e) verify that the observed nanoflower is an assembly of individual petals with plate like morphology. The weak planes in the SAED pattern correspond to the secondary crystalline structures in the nanoflower.Comparison of the experimental powder X-ray diffraction pattern with simulated PXRD pattern of the single crystal has also been performed. As shown in Figure 5.6, Bragg's peak positions of the experimental XRD are in good agreement with the simulated pattern.

Multiple phenyl embraces is an important feature of molecules containing the fragment XPhy (X is any tetrahedral atom and y = 2,3,4) while they engage each other through a supramolecular interaction network. 1, 2-bis(tritylthio)ethane molecule has six phenyl rings, which can form multiple phenyl embraces (MPE). Such orthogonal (edge-to-face, or T-shaped) and parallel (offset face-to-face or parallel displaced, PD) phenyl embraces were earlier identified in crystals [13]. Phenyl embraces, both T-shaped and PD in 1, 2-bis(tritylthio)ethane crystal structure is shown in Figure 5.1b. The green dashed-line indicates T-shaped edge-to-face interaction and red dotted line indicates parallel displaced orientation. The entire assembly is a result of well-organized repetitive patterning of T-shaped and PD interactions. Such face-to-face or edge-to-face quadrupole stacking between benzyl side-chain groups account for molecular recognition process in

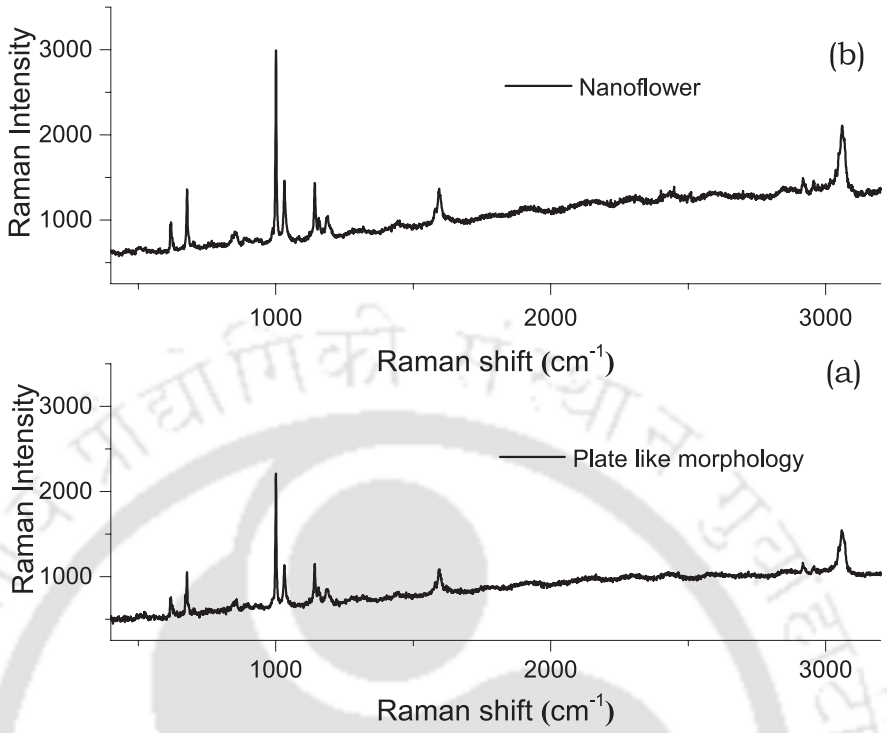

Figure 5.5: Characteristic Raman spectra of (a) Plate like morphologies, (b) nanoflower like morphologies.

S.No	Sample Peaks (cm^{-1})	Peak Assignment
1	618.878 – 685.272	C- S stretch [250]
2	1003.11, 1034.69, 1579.86, 1595.65	Benzene ring [251]
3	1160.32 – 1195.46	CH_2 wag and twist
4	3064.46	CH stretch in aromatic compounds

Table 5.2: Raman peak assignment for 1,2-bis(tritylthio)ethane

various fibrillar and nanotubes formation involving dipeptides with aromatic sidechains reported [96, 98].The nano-level assembly forming plate-like structures and their co-assembly forming nanoflowers may also be attributed to attractive interactions between aromatic systems. The distance between a typical T-shaped phenyl embraces are 4.06 and 7.08 Å respectively between the closest and farthest carbon atoms. This is in good agreement with the earlier reported distance range and energy estimates in the case of Benzene dimer [11].

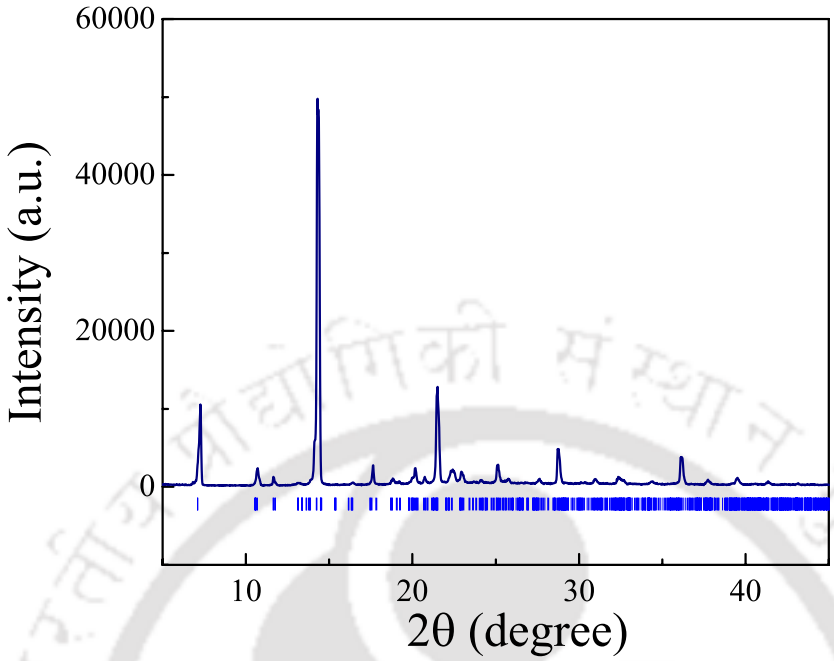

Figure 5.6: A comparison of the experimental powder X-ray diffraction pattern and simulated P-XRD pattern., where the simulated pattern is represented by blue color vertical straight lines

Heisenberg's theory of ferromagnetism ruled out carbon systems having spontaneous magnetic properties [252], principally because of the absence of open shell d orbitals (d^n configuration) with unpaired electrons. The discussion on carbon based magnetic material came to the fore after the serendipitous and controversial discovery of magnetism by Makarova et. al. in 2001 [253]. This was followed by several reports on graphene [254] and graphite systems [255], hydrogenated carbon nanotubes [256], non-irradiated nano-diamonds [257] etc. showing room temperature ferromagnetism. Even before the study of C60, ferromagnetic interactions were identified in crystals of galvinoxyl, tanolsuberate, nitronylnitroxides, Verdazyl radicals etc. [258] Much like trityl groups, models for organic ferro-magnets and high spin organic structures reported so far were conjugated π-systems [259, 260]. This prompted us to explore the magnetic properties of the crystalline material 1, 2-bis(tritylthio)ethane, by carrying out a room temperature and low temperature magnetic hysteresis loop (MH loop) measurements.

The study of magnetic properties was performed at room temperature (300 K) and at low temperature (2 K) with a maximum applied magnetic field of 12 kOe and 70 kOe, respectively. Interestingly, the nano-crystals displayed a dual magnetic behaviour both at 300 K (Ferro-Dia) and 2 K (Ferro-Para). At 300 K, nano crystals displayed typical

ferromagnetic hysteresis loop behavior in the low field region from -4 to +4 kOe (Inset of Figure 3a). In the high field region (up to 12 kOe), a field induced transition from ferromagnetism to a strong diamagnetism is observed (Figure 3a). The dominance of diamagnetic contribution of the sample over the ferromagnetic order gives rise to the downward (upward) bends at both ends of the MH loop, ie at high applied fields. The anomalous transition from a magnetically ordered state to a disordered state with respect to an increase in the applied field is unusual and the mechanism is not fully understood yet. Dual magnetic property with similar MH loops had been reported earlier by two different groups [261, 262]. Lee et al. showed an abrupt transition from ferromagnetism to diamagnetism for proton-irradiated graphene at a critical field of 7 kOe [262]. However, in our case, the transition is not abrupt, but a gradual transition from ferromagnetism to diamagnetism upon increase in field beyond 4 kOe, an observation quite similar to an earlier report from Boukhvalov et al. on O_2 adsorbed graphite [261]. Similar or lesser values of susceptibility have been reported in proton irradiated irradiated fullerene [262] and hydrogenated graphene [254]. The ferromagnetic ordering reported here has a maximum magnetization of 0.014 emu/g at 4 kOe and a coercivity of approximately 215 Oe.

In order to understand the magnetic ordering at low-temperature MH loop measurements were carried out at 2 K using SQUID magnetometer. Low temperature data exhibited a magnetic transition between ferromagnetism and paramagnetism in response to an increase in the applied magnetic field (Figure 5.7 b). Similar and consistent with the room temperature observation, 1, 2- bis(tritylthio)ethane shows a clear ferromagnetic ordering at low temperature (2 K), evident from the smooth hysteresis loop observed between -4 and +4 kOe (Inset of Figure 5.7 b). The ferromagnetic moment was maximum at 4 kOe, with a value of 0.049 emu/g (0.005 μ_B/molecule) and coercivity of 145 Oe. The increase in magnetic moment at lower temperatures is a usual observation in ferromagnets because at near 0 K, the entropy is minimal which leads to the pronounced ordering of the magnetic moments. At higher field region, the magnetization shows a linear increase with increase in the applied field. This indicates a field induced transition from ferromagnetic ordering to a paramagnetic ordering. The maximum magnetization obtained due to paramagnetic ordering was 0.24 emu/g (0.025 μ_B/molecule) at a field of 70 kOe. In the earlier reported case of proton irradiated C_{60}, the highest ferromagnetic and paramagnetic moments obtained at 2 K were 0.023 μ_B/C_{60} and 0.16 μ_B/C_{60} respectively [262]. As a part of the standard procedure to confirm the intrinsic nature

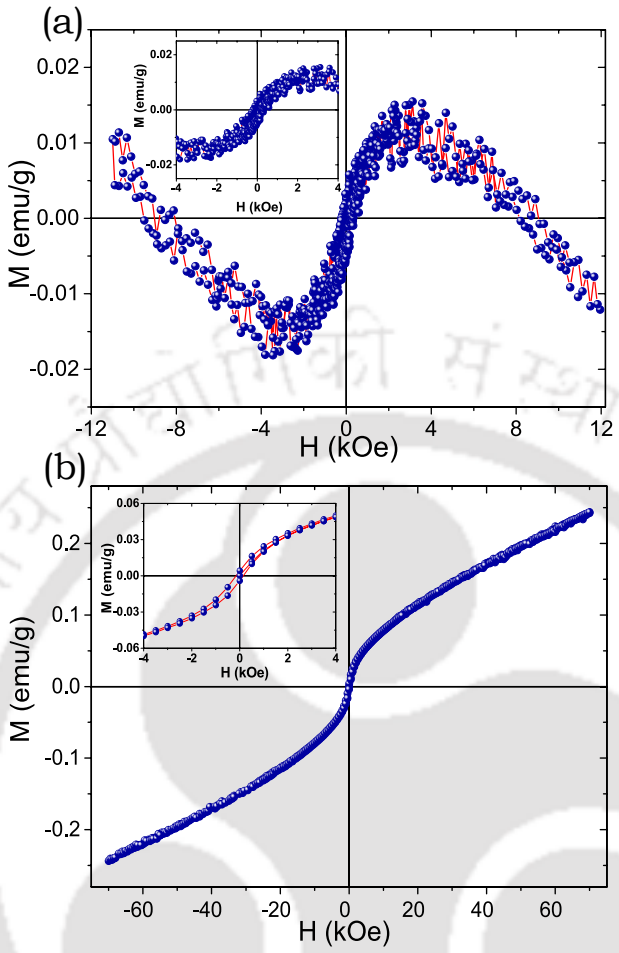

Figure 5.7: Magnetic hysteresis loops of 1,2-bis(tritylthio)ethane. a) Magnetization measurements at 300 K in the range of -12 kOe<H < +12 kOe, showing dual magnetic behavior; ferro at lower magnetic fields and dia at higher fields. b) Magnetization measurements at 2 K in the range of -70 kOe<H < +70 kOe showing dual magnetic behavior, ferro at lower magnetic fields and para at higher magnetic fields. Ferromagnetic behavior at 300 K and 2 K, in the range of -4 kOe<H<+4 kOe are shown in the insets.

of the dual magnetic property of the material, M-H measurements for the bare sample holder and Teflon tape were conducted, and the external diamagnetic contributions were subtracted from the data. Moreover, the experiments were verified to be repeatable in two different Vibrating Sample Magnetometers under identical conditions, along with Superconducting Quantum Interference Device (SQUID) at 2 K. Notably, reagents and solvents used for the synthesis and nano-assembly formation of 1,2-bis(tritylthio)ethane crystals reported here are purely organic, with no presence of any metallic component. Like electric current induced magnetization reversal [263], this peculiar way of magnetic

responsivity at different applied magnetic fields may find applications in future magnetic data storage technology [264]. The resultant inherent magnetism may be directly correlated to the microstructure and the crystalline order of 1, 2-bis(tritylthio)ethane.

Magnetic moment in the molecules is usually generated as a consequence of charges or delocalized electrons in them. As the crystal reported in our study is neutral with no charges, the source of the magnetic response can be attributed to the delocalized π-electron cloud present within the phenyl groups. The presence of H-atoms in the crystal as a source of magnetism is dismissed, as an explicit magnetic ordering is observed in our sample, which won't be possible by the contribution of H-atoms alone.

A unit cell of the crystal comprises of 48 phenyl groups and it is hypothesized that the aromatic phenyl groups within the system can be a source of the obtained magnetic response. Studies have shown that magnetic field when applied in perpendicular direction to the benzene rings, generates an induced current within their delocalized π-electron clouds [265]. Computational investigations by Thomas Heine et al. reported that fields when applied parallel to the plane of the benzene ring has little consequence in producing long-range responses [266]. As the electron delocalization is constrained to be in the plane of the benzene rings, the magnetic moment thus generated will be perpendicular to the benzene containing plane, pointing along the axis of the phenyl moiety. Phenyl group containing molecular crystals such as diphenylalanine [185], naphthalene [267] etc., have been well studied under applied magnetic fields and is known to be responsive only at extremely high field strengths. In contrast, the crystal system reported exhibited a significant ferromagnetic moment both at 300 K and 2 K even at considerably lower applied field strengths. It is also to be noted that, not all phenyl containing organic systems exhibit such strong magnetic reactions with indications to magnetic ordering. The fact that the crystal structure possessing a unique structural orientation of the phenyl groups and the nature of magnetic responses from aromatic system, may be the reason for such magnetic ordering. The forty-eight benzene rings within a single unit cell, has equal number of individual magnetic moments perpendicular to their respective benzene rings. The calculation of the unit vectors parallel to the magnetic moments, not only gives us an idea about the directions of the individual moments within the crystal, but also presents a sense of the magnetic ordering present among these moments. The resultant vector obtained by adding all the 48 unit vectors gives an insight into the nature of net magnetic moment within the unit cell. The cartesian coordinates of the individual atoms can be calculated from the crystal structure obtained via X-ray

diffraction, and the normal vectors perpendicular to the plane of the benzene rings were calculated by employing simple 3D geometry. Table 5.3 lists all the forty-eight moment vectors calculated for the benzene systems.

The values in Table 5.3 shows that the magnetic moment vectors derived from the molecules of 1, 3, 5, 7 and 2, 4, 6, 8 in the unit cell are exactly the same. It also signifies

Table 5.3: List of magnetic moment vectors calculated from all the 48 benzene rings.

S.No	Molecule No.	X	Y	Z
1	1	-0.4361	-0.6430	0.6296
2		-0.9251	-0.1279	-0.3577
3		-0.6105	0.7180	-0.3343
4		0.4673	-0.4581	-0.7562
5		0.5231	0.5732	-0.6307
6		0.6967	-0.4938	0.5203
7	2	0.4361	-0.6430	-0.6296
8		0.9251	-0.1279	0.3577
9		0.6105	0.7180	0.3343
10		-0.4673	-0.4581	0.7562
11		-0.5231	0.5732	0.6307
12		-0.6967	-0.4938	-0.5203
13	3	-0.4361	-0.6430	0.6296
14		-0.9251	-0.1279	-0.3577
15		0.6105	0.7180	-0.3343
16		0.4673	-0.4581	-0.7562
17		0.5231	0.5732	-0.6307
18		0.6967	-0.4938	0.5203
19	4	0.4361	-0.6430	-0.6296
20		0.9251	-0.1279	0.3577
21		0.6105	0.7180	0.3343
22		-0.4673	-0.4581	0.7562

Continued on next page

Table 5.3 – *Continued from previous page*

S.No	Molecule No.	X	Y	Z
23		-0.5231	0.5732	0.6307
24		-0.6967	-0.4938	-0.5203
25		-0.4361	-0.6430	0.6296
26		-0.9251	-0.1279	-0.3577
27	5	0.6105	0.7180	-0.3343
28		0.4673	-0.4581	-0.7562
29		0.5231	0.5732	-0.6307
30		0.6967	-0.4938	0.5203
31		0.4361	-0.6430	-0.6296
32		0.9251	-0.1279	0.3577
33	6	0.6105	0.7180	0.3343
34		-0.4673	-0.4581	0.7562
35		-0.5231	0.5732	0.6307
36		-0.6967	-0.4938	-0.5203
37		-0.4361	-0.6430	0.6296
38		-0.9251	-0.1279	-0.3577
39	7	-0.6105	0.7180	-0.3343
40		0.4673	-0.4581	-0.7562
41		0.5231	0.5732	-0.6307
42		0.6967	-0.4938	0.5203
43		0.4361	-0.6430	-0.6296
44		0.9251	-0.1279	0.3577
45	8	0.6105	0.7180	0.3343
46		-0.4673	-0.4581	0.7562
47		-0.5231	0.5732	0.6307
48		-0.6967	-0.4938	-0.5203

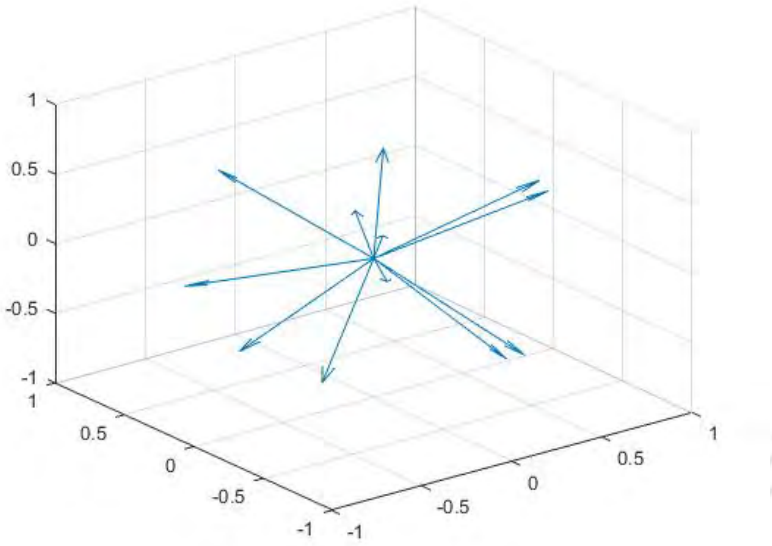

Figure 5.8: Twelve unique magnetic moments plotted in 3D

that among all the eight molecules present within a single unit cell, only two unique conformations exists, which leads to twelve unique orientations of phenyl groups in the crystal (Figure 5.8). Further analysis also reveals that the X and Z components of the magnetic moments originated from these two molecular conformations are antisymmetric with respect to each other whereas, only the Y components remains symmetric. For each X and Z moment component in one group, there exists an equal but opposite moment component in the other group.

On the other hand, for the set of Y components it remains the same for every molecule. A visual depiction of this symmetric and antisymmetric nature of the vector components are presented using pairwise component plots in Figure 5.9. It can be seen that the X vs Y and Z vs Y plots are symmetric about the Y-axis, while the X vs Z plot is antisymmetric in nature. Consequently, on decomposing each magnetic moment vector into its respective orthogonal moments parallel to X, Y and Z axis, all the X and Z moments are antiferromagnetically ordered but the Y moments are ferromagnetically ordered. This is a clear indication of ordering present among the magnetic moments, as is also corroborated by the resultant vector having only a Y component and zero X and Z components. The nature of ordering of the moments is analogous to canted weak ferromagnetism or antiferromagnetism [268] as observed in magnetic materials such

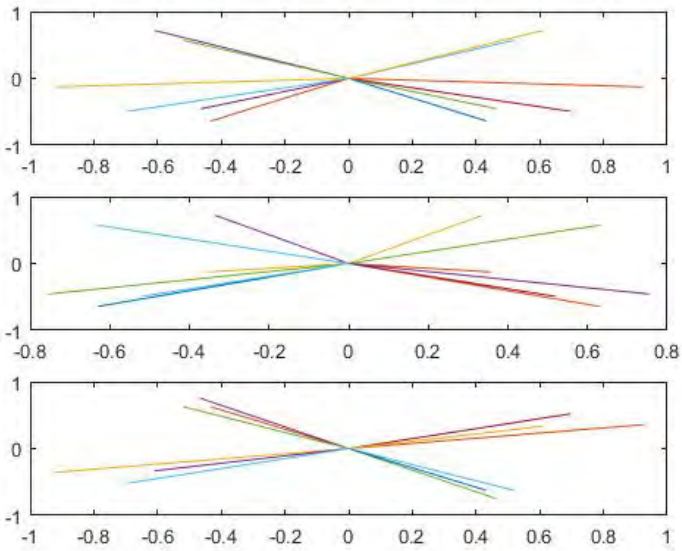

Figure 5.9: Pairwise plots of the moment vectors. 3a.X vs Y, 3b. Z vs Y, 3c. X vs Z respectively from top to bottom. Fig 3a and 3b are symmetric with respect to Y and Fig 3c is antisymmetric about the origin.

as haematite. Canted ferromagnets are those materials whose magnetic moments due to canting do not entirely cancel each other, thus allowing the materials to exhibit a net residual moment. To conclude, the magnetisation curves of 1, 2-bis(tritylthio)ethane obtained both at room temperature and very low temperature points toward a weak ferromagnetic ordering of magnetic moments present in the material. A qualitative explanation of the origin of magnetic response was provided based on the good number of aromatic moieties present within the crystal. The unusual diamagnetic anisotropy exhibited by aromatic molecules has proven to be important for spectroscopic applications, imaging, and deriving the structural and compositional data of organic molecules. The non-localised π-electron cloud of aromatic molecules has also led to the synthesis of a multitude of coordination complexes with interesting properties. Organic magnetic materials that take advantage of the magnetic responses of aromatic moieties are unpopular, and the results reported may serve as a clue for research into a new species of organic magnetic materials.

Over the years, conducting organic materials has gained more attention due to the charge transport and their potential applications in organic device fabrication. Among organic molecules organic crystals formed through molecular ordering which

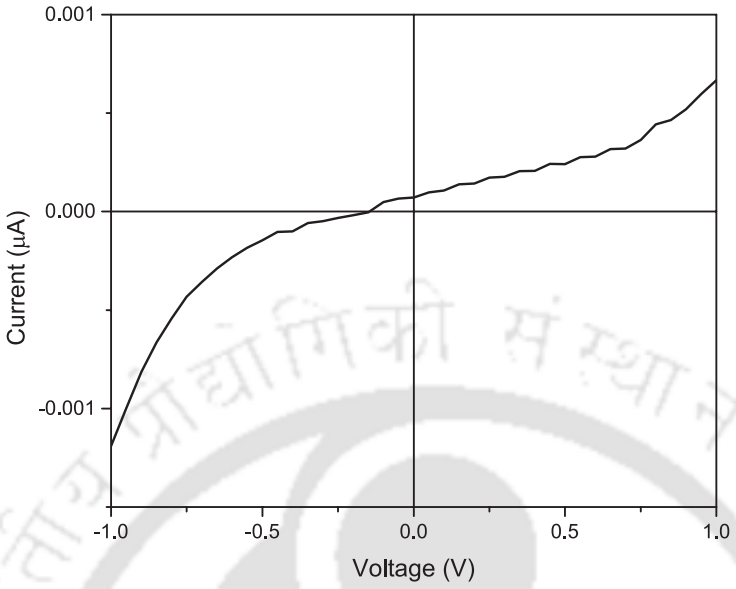

Figure 5.10: The *I-V* characteristics of the nanoassemblies of 1, 2-bis(tritylthio)ethane

permits the overlapping of $\pi - \pi$ orbitals have shown the high charge mobilities [83, 84, 136]. Scientists were in search of such new molecules and considering the difficulty in synthesizing single crystals, alternative ways of synthesizing low-cost electronic materials were explored. To fabricate the organic materials into devices like organic FETs, charge carrier mobility is an important parameter. In order to obtain conductivity, many different types of synthesis methods have been adopted in organic molecules. Self-assembly through stacking in aromatic molecules and π-conjugated molecules showed different carrier mobility based on the types of intermolecular $\pi - \pi$ stacking, as the $\pi - \pi$ stacking distance determines the electron coupling and charge density [269]. As conductivity is directly proportional to charge carrier mobility, we tried exploring the conductivity, and capacitance property of the reported crystal system.

Few preliminary studies on the conductive nature of the sample have been performed. The electrical measurements of the compound have been measured in the range of -1 to +1 V. A simple and fast method was used for the formation of the crystals. The crystals dissolved in ethyl ether was drop casted on the electrode, and Figure 5.10 shows the *I-V* characteristics of the nanoassemblies measured under ambient conditions. The sample was found to be conductive in nature. Other preliminary measurements using impedance analyzer gave a capacitance value of 4.6 pF and a dielectric constant of 88.6 nF/m at

a frequency of 10 kHz. As charge mobility is a property measured with the sample of different geometries and techniques with different length scales, it is difficult to compare the values obtained from different techniques. A few of the organic compounds namely triphenylmethane [270] and polymers [271] fabricated through different methods exhibited the property of capacitance in the range of pF. The reported values are based on the drop cast method, and the experiment has to be optimized by depositing the samples in the form thin film for further characterization and fabrication of organic devices.

5.5 Conclusion

The challenge to generate and perfect nano and micro level stable molecular architectures through self-assembly lies in two mutually fulfilling exercises; i) synthesis of individual building blocks with the right composition and ii) design and fabrication of assembled architectures [272, 273]. The single crystal organic compound we report here self-assembles to a flower-like morphology, thus becoming a very rare organic nano-flower. It also qualifies to be the first organic crystal with an inherent dual magnetic behavior at 300 K and 2 K. Earlier studies on model systems suggested the possibility of organic ferromagnetism in fully conjugated π-systems, though a complete mechanistic understanding still seems elusive. In addition to that preliminary characterization of electrical properties revealed the conductive nature of the material. Molecules with such magnetic and electrical properties are of considerable fundamental interest, especially in light of the recent developments in magneto-electronics and spintronics [230]. Overall, this work presents the potential utility of stable tritylthioethane derivatives and it's usage in the design of bio-nanomaterials, where molecular recognition is primarily mediated through aromatic $\pi - \pi$ interactions. To the best of our knowledge, the organic compound we are reporting here is the first pure organic crystalline compound showing ferromagnetism both at room and low temperatures.

CHAPTER 6

STIMULUS RESPONSIVE HYBRID NANO-ASSEMBLIES

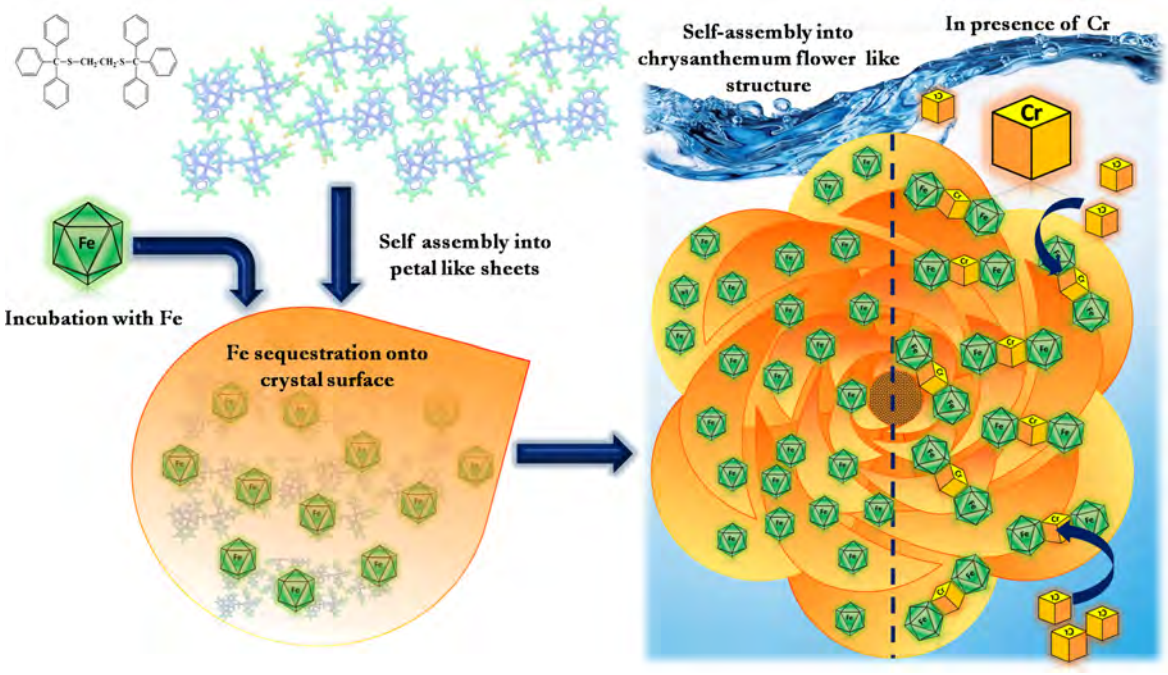

6.1 Summary

Synthesis of novel, cost-effective and eco-friendly materials is still a challenge in applications oriented to exercise heavy metal removal. Magnetite and its hybrid materials has been effective nanoadsorbents with the advantage of simultaneously removing and reducing heavy metals from water. Agglomeration has been a major concern for fabricating magnetite nanoparticles as a nanoadsorbent. In our work, we have fabricated the organic nanoflower of 1, 2-bis(tritylthio)ethane as a potential stimulus responsive material by coating them with magnetite nanoparticles. The superparamagnetic material, was further tested for its potential utility in water remediation as a nano-based adsorbent for the removal of heavy metals like chromium.

6.2 Introduction

Water, which is vital for all forms of life, is contaminated by its improper utilization and environmental changes. Anthropogenic activities leading to the contamination of water bodies have created adverse effects on environment and human health. Heavy metal contamination in water, has been a serious concern for many decades, majorly affecting the densely populated countries [274, 275]. Among heavy metals, chromium is widely used and discharged in water bodies, by industries related to chrome plating, leather tanning and paint manufacturing. Though developed nations, has policies to regulate the discharge level of chromium in waterbodies, it is still a major issue in the developing countries. The environmental protection agency of United states has set a maximum discharge limit of 50 ppm of chromium in the surface water. Even in the presence of very low concentrations, heavy metals such as chromium poses a serious threat to human health [276].

Chromium exists as different species among which, Cr (III) and Cr (VI) are the most stable states. The oxidation states of the metal species determine the bioavailability, toxicity, and fate of the metal in the environment. For example, the trivalent state of chromium is an essential trace nutrient which naturally occurs in the environment. It is thermodynamically stable, less mobile and relatively nontoxic due to the formation of insoluble oxy-hydroxides. In contrast, hexavalent chromium is considered to be highly toxic owing to its strong oxidizing potential and speciation as a weakly sorbing anionic chromate (CrO_4^{2-}) or dichromate ($Cr_2O_7^{2-}$). Hence, reduction of Cr(VI) to Cr(III)

is an important mechanism for minimizing the health hazards caused by chromium contamination.

Various methods such as photo-catalytical oxidation, chemical coagulants, electrochemical techniques, bioremediation, ion-exchange, reverse osmosis, and adsorption have been adapted for water treatment [274, 277–280]. Usual methods of chromium removal are two-step process, where Cr(VI) is first reduced into non-toxic form (Cr(III)), followed by the removal of Cr(III) by precipitation or sorption method. In comparison to the conventional methods, adsorption process follows a one step-procedure for reducing and removing the heavy metals. Among different adsorption procedures, nano-adsorbents are found to be the more efficient and recent developments in nanotechnology has introduced many efficient and innovative techniques for heavy metal removal [136, 281].

Magnetic solid-phase extraction techniques have been reported to be efficient owing to their capability to get isolated from the sample by using an external magnetic field [282, 283]. Magnetite nanoparticles with small size and high surface area, ensures high extraction efficiency within a short period of time [283]. But the particles with high surface area easily undergo aggregation in the solution which could decrease their efficiency. Most of the magnetite-based nanomaterials used in the adsorption have been surface functionalized or modified [284], which in turn is a complicated and intensive process. In this study, magnetically decorated assemblies of 1, 2-bis(tritylthio)ethane at the nanoscale is reported. The nanoassembly formed by the organic crystals which are stable at wide range of pH, are fabricated into functional hybrid material by coating them with magnetite. Interestingly, upon magnetite coating the nanoassemblies resulted in a hybrid material that display super-paramagnetic behavior as analyzed by Vibrating Sample Magnetometer (VSM). Altogether our material, with an inherent dual magnetic property (Chapter 5) and with ferrofluid coating, can find its applications as magnetic switches upon variation of magnetic field. The magnetite hybrid material was further tested for their potential utility in water remediation systems as a nano-based adsorbent for removal of heavy metals like chromium.

6.3 Materials and Methods

6.3.1 Materials

All the chemicals and solvents used for experiments are of reagent grade. Amino acid Fmoc-His(trt)-OH and solvents trifluoroacetic acid,thioanisole, and 1,2-ethanedithiol were purchased from Sigma-Aldrich. Diethyl ether, m-cresol, Iron (II) sulfate heptahydrate and ferric nitrate were purchased from Merck. Sodium dichromate dihydrate was purchased from Sisco Research Laboratories Pvt. Ltd. Trityl Chloride was purchased from Spectrochem.

6.3.2 Synthesis and Crystallization of 1,2-bis(tritylthio)ethane

Method 1: The compound was synthesized by treating trityl group released from the side chain of Fmoc-His(trt)-OH, with 1,2-Ethane dithiol, m-cresol and thioansiole in the presence of trifluoroacteic acid (1:2:2:20). Crystallization and purification was done using diethyl ether as a solvent.

Method 2: Tritryl chloride was treated with 1,2-Ethane dithiol, m-cresol and thioansiole in the presence of trifluoroacteic acid (1:2:2:20). Crystallization and purification of the crystals was performed using diethyl ether as a solvent.

Method 3: In the third method of synthesis, tritryl chloride was treated with 1,2-Ethane dithiol and trifluoroacteic acid (1:9). To the mixture diethyl ether was added for crystallizing and purifying 1,2-bis(tritylthio)ethane.

6.3.3 Synthesis and Coating of Magnetite Nanoparticles

Magnetite was synthesized by co-precipitation method. For co-precipitation, an alkaline medium by mixing aqueous solutions of $FeSO_4$ and $Fe(NO_3)$ has been prepared. An anionic surfactant was added for stabilization and the final mixture was heated at 75°C. Magnetite obtained was washed with distilled water and dried at 60°C. To immobilize magnetite on the surface of the nanoassemblies, magnetite nanoparticles was dispersed at a concentration of 0.214% in ethyl ether, and 1,2-bis(tritylthio)ethane was added to it at a concentration of 2 mg/ml. The reaction mixture was continuously vortexed until

the sample got crystallized in the magnetite solution. The crystallized material was washed with dd.H_2O to remove the unbound magnetite nanoparticles. The coating on the nanotubes was confirmed by FE-SEM and FE-TEM analysis.

6.3.4 pH Stability

Different pH solutions were prepared by dissolving HCl and NaOH. The crystals were added to different pH solutions and was vortexed for 48 hrs.

6.3.5 Characterization

NMR Analysis

^{1}H NMR was recorded on a Bruker 600 MHz NMR spectrometer. NMR spectra were recorded in deuterated chloroform ($CDCl_3$), and the chemical shifts were reported relative to TMS (δ=0 ppm) as an internal reference. Spin multiplicity was abbreviated as follows: s = singlet, d = doublet and t = triplet. ^{1}H NMR (600 MHz, $CDCl_3$) δ (ppm): 7.32–7.31 (d, 12 H), 7.25–7.22 (t, 12 H), 7.20–7.17 (t, 6 H), 2.1 (s, 4 H).

Electron Microscopic Characterization

The size, morphology and crystallinity of the magnetite nanoparticles were studied using FE-TEM analysis. To check the deposition of magnetite nanoparticles on the surface of organic assemblies, ethyl ether was added to the sample, so as to detach the hybrid samples crystallized along the walls of the glass tube. 20 μl of the sample was loaded for FE-SEM analysis and the morphology of nano-assemblies was analyzed using Zeiss (Model: Sigma) Field-Emission Scanning Electron Microscope at 3 kV. Samples were coated with gold for enhancing the conductivity. For FE-TEM analysis 10 µl of the vortexed sample was dropped on the 300 mesh copper grid covered with strong carbon film. Samples were viewed in JEOL transmission electron microscope, Model: JEM 2100F, operating at 200 kV.

Elemental Analysis

On crystallization, the samples were characterized using FE-SEM-EDX for elemental analysis (Model: Sigma). FE-TEM and EDX mapping were done using JEOL transmission

electron microscope, Model: JEM 2100, for showing the distribution of magnetite on the sample surface.

Magnetic Measurements

Magnetic properties of 1,2-bis(tritylthio)ethane assemblies, magnetite and magnetite coated assemblies were examined using Vibrating Sample Magnetometer, LakeShore Model 7410. Magnetic curves were recorded at a temperature of 28º C with maximum applied field of 12 kOe. The saturation magnetization (MS) and coercivity (H_C) values have been extracted from the magnetic hysteresis (MH) loop measurements using IDEAS VSM software.

Adsorption Studies on Heavy Metal Removal

Stock concentration for the adsorption studies were prepared by dissolving $Na_2Cr_2O_7$ at a concentration of 50 mg/ml in dd.H_2O. Adsorption experiments were conducted at a concentration of 1 mg/ml. Samples were vortexed continuously and the samples were loaded for analysis after 24 h.

6.4 Results and Discussion

A new trityl based organic crystal 1,2-bis(tritylthio)ethane is synthesized, which self –assembles to form plate and nanoflower like morphologies. The procedure for synthesis and characterization of the single crystal and nanoassemblies are discussed in the previous chapter. In the next phase of the study, to fabricate the nanoassembly (flower) as a stimulus-responsive material, the trityl system was coated with magnetite nanoparticles synthesized using the co-precipitation method [285, 286]. This line of enquiry would be particularly interesting in the design and development of organic-inorganic hybrid materials with tunable physical properties. Magnetite (Fe_3O_4) has been chosen as an oxide of choice, owing to its desirable properties like amphoteric surface activity, easy dispersion ability and high surface to volume ratio and application in wide areas [287]. The composites used in environmental applications should be non-toxic, biodegradable and cost-effective.

Superparamagnetic magnetite nanoparticles are synthesized by chemical co-precipi-

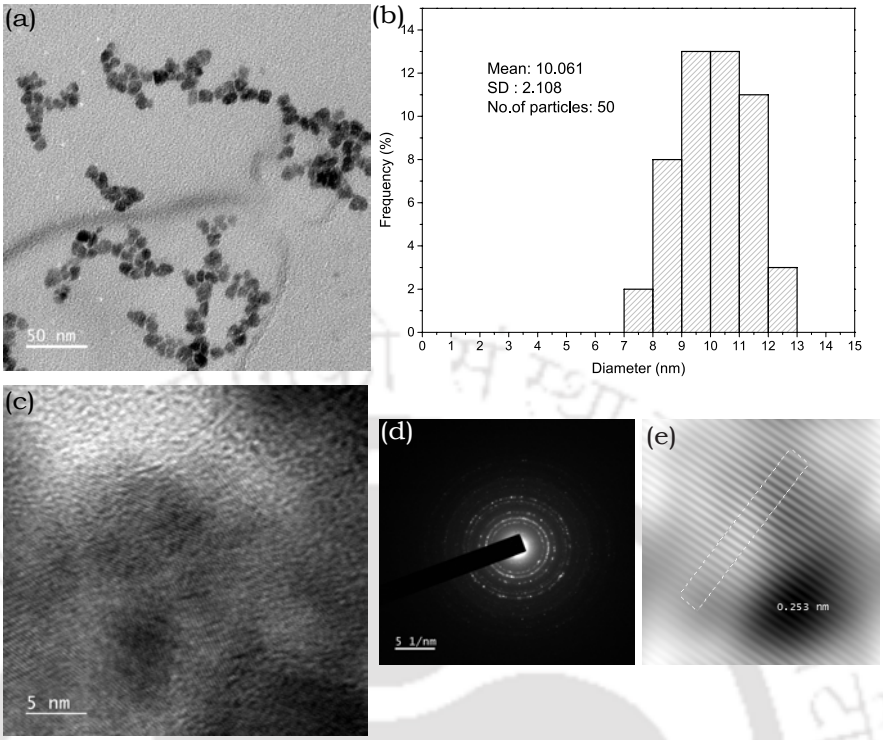

Figure 6.1: Morphological characterization of magnetite nanoparticles using TEM analysis. Synthesized magnetite nanoparticles (a) and its distribution analysis (b). HR-TEM analysis (c) and SAED pattern showing the polycrystalline nature of the synthesized nanoparticles and (e) and the interplanar distance of magnetite nanoparticles (d= 2.5 Å).

-tation method. Among the different types of established synthesis protocols, co-precipitation method is preferred owing to the simplicity of the procedure and cost-effectiveness. To check the dispersity of the synthesized magnetite nanoparticles in diethyl ether, the solvent used for crystallization of 1,2-bis(tritylthio)ethane, the nanoparticles were dispersed at a concentration of 0.214% in ethyl ether. The size and monodispersity of the magnetite nanoparticles was confirmed through FETEM analysis (Figure 6.1). The morphology of the magnetite nanoparticles was observed to be dispersed with an average diameter of 10 nm (On averaging 50 nanoparticles). The statistical sizedistribution of the synthesized nanoparticles was in the range of 7-13 nm. The nature of the magnetic properties depends upon the size of the magnetite nanoparticles, and usually superparamagnetism is observed in nanoparticles with a diameter of less than 20 nm [288]. The ring type pattern of selective area electron diffraction shows the polycrystalline nature of the magnetite nanoparticles. And the interplanar distance of 2.5 Å calculated by HR-TEM analysis co-relates with the previously reported studies [289].

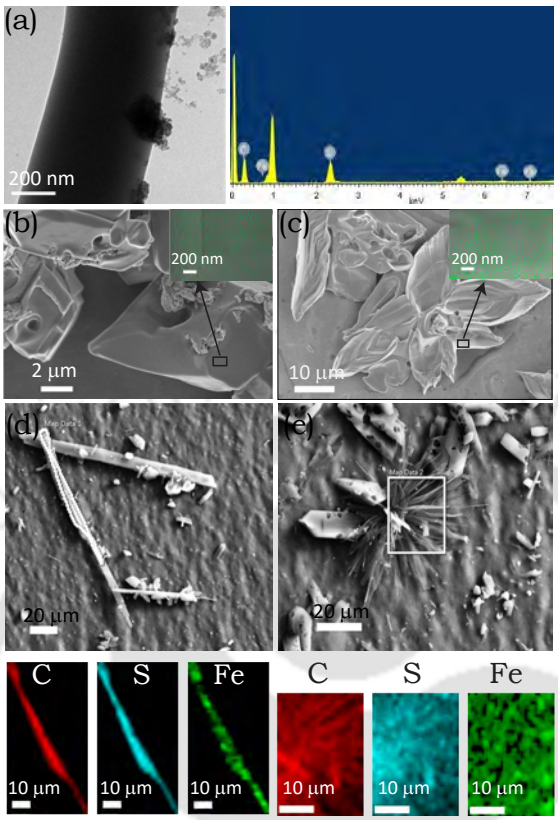

Figure 6.2: Characterization of magnetite coated 1, 2-bis(tritylthio)ethane assemblies. TEM analysis (a) showing the impregnation of magnetite on to the nano-assembled plate-like structure, and its EDX confirming the attachment of magnetite. FE-SEM micrograph of the magnetite coated plate (b) and flower-like morphologies (c) with insets showing the enlarged view of the coated areas. Magnetite nanoparticles in the insets are false colored (green) for better understanding. Elemental mapping of the highlighted areas in the nanoassemblies (d,e) further confirms the dispersion of magnetite on the entire surface.

Magnetite as adsorbents finds it limitations in continuous flow systems, since bare magnetite nanoparticles are highly susceptible to oxidation and tend to agglomerate in aqueous solutions. Stabilization of the nanoparticles is generally attained by surface functionalization [284]. Here we have grown the crystals in ferrofluid, and the adherence of magnetic material by means of non-covalent interaction [290] is evident from the electron microscopic images. 1, 2-bis(tritylthio)ethane is grown in a solution of magnetite, dispersed in diethyl ether and the adherence of magnetite on the samples is evident from the electron microscopic images. High Resolution Transmission Electron Microscopic (HR-TEM) analysis with Energy-dispersive X-ray spectroscopy (EDX) (Figure 6.2 a) clearly reveals the attachment of the synthesized magnetite to the plate like assemblies.

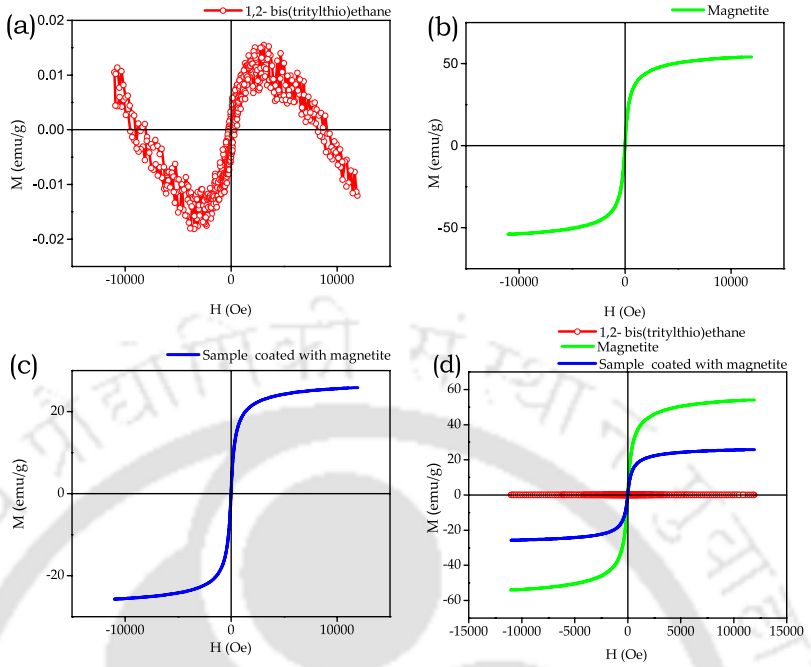

Figure 6.3: Room-temperature hysteresis loops. a, 1,2-bis(tritylthio)ethane showing dual magnetic behavior. b-c, Magnetization curves of magnetite(b) and magnetite coated assemblies(c), d, comparison of magnetic behavior of 1,2-bis(tritylthio)ethane, magnetite and magnetite coated material.

FE-SEM analysis (Figure 6.2b, c) of both the plate and flower like morphologies show the distribution of coated material on the surface. Dispersion of magnetite on the entire surface of the plate and flower like morphologies is further verified by elemental mapping via energy-dispersive X-ray spectroscopy (EDS) mapping (Figure 6.2d, e), where, Fe is found to be distributed over the entire surface, demonstrating the successful impregnation of metals resulting in an organic-inorganic hybrid nanoflower.

The magnetic measurements of the nanoparticles, crystals of 1,2-bis(tritylthio)ethane, and the hybrid material was performed at room temperature (Figure 6.3). Figure 6.3a shows the dual magnetic behavior of the organic crystal as explained in Chapter 5. The magnetization value (M_S) of the magnetite nanoparticles is observed to be $M_S \approx 56$ emu/g and it is in accordance with that of earlier reports on the magnetite nanoparticles of various particle sizes (M_S = 21 - 65 emu/g) [290]. The nanoparticles display a magnetization curve with zero coercivity and remanence, a typical curve for superparamagnetic behavior. The rate of magnetization is determined by the size, crystalline structure and space between the nanoparticles [291]. The size and shape of the hysteresis curve are of

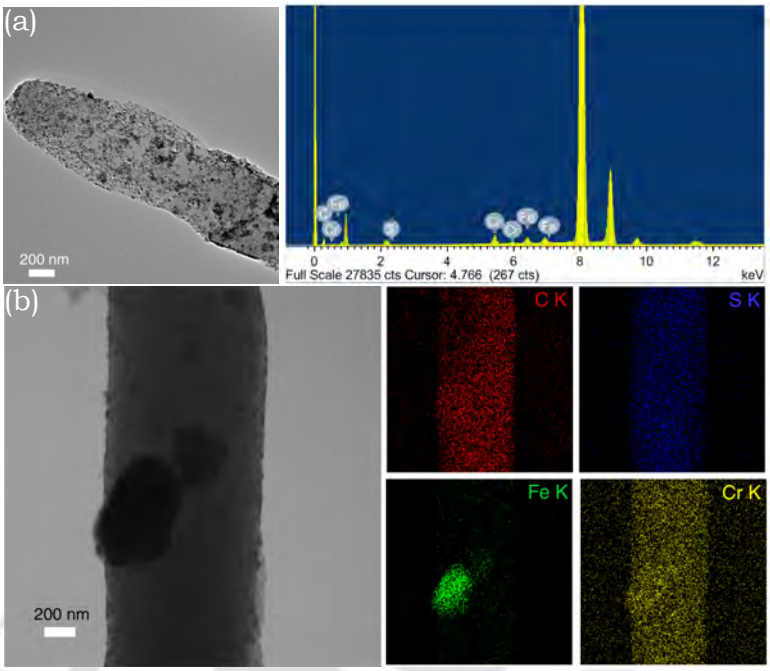

Figure 6.4: Elemental distribution on the surface of nanoassemblies probed by EDS-mapping. TEM and EDX spectra of Chromium (Cr) sequestered hybrid material (a). Backscattered electron image shown in the top left panel of figure b, to verify elemental composition. Elemental spot maps of C, S, Fe and Cr, measured by STEM-EDX, are shown in the following panels of (b), confirming the Cr sequestration on to the hybrid nano assembly.

considerable importance in terms of applications as the energy loss in the system of the material is cycled around its hysteresis. The magnetic energy loss which arises partly from the hysteresis loss can be reduced by reducing the area enclosed by the hysteresis loop. From the figure of our magnetite coated sample (Figure 6.3 c), it is clear that the area enclosed by the MH loop became very small and the loop is thin and narrow which is a specific criterion for a soft ferromagnetic material. Moreover, almost zero coercivity and zero remanence were observed at room temperature, indicating that the newly synthesized magnetite coated 1,2-bis(tritylthio)ethane is a superparamagnetic material. Due to the interaction with the magnetite nanoparticle, the magnetic moment of the naïve material increased largely to a value of 25.6 emu/g from 14 x 10^{-3} emu/g and the coercivity reduced from 140 Oe to almost zero (Figure 6.3 c). Figure 6.3 d shows the MH loop of the magnetite coated 1, 2-bis(tritylthio)ethane along with that of pure 1, 2-bis(tritylthio)ethane and magnetite for comparison. Superparamagnetic property of a

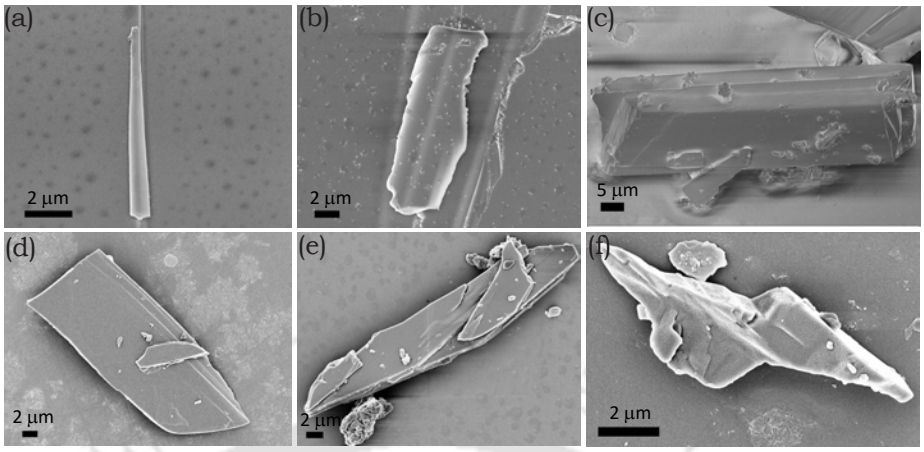

Figure 6.5: FESEM analysis showing the stability of 1,2-bis(tritylthioethane) at extreme acidic and basic conditions. (a) pH 1 (b) pH 2 (c) pH 3 (d) pH 4 (e) pH 9 and (f) pH 10.

magnetic nanoparticle is critical for their application in biomedical and bioengineering fields, because it prevents the magnetic nanoparticles from aggregation and enables them to re-disperse rapidly when the magnetic field is removed [292]. Also the high value of magnetization of the hybrid materials makes them susceptible to magnetic field and enables their easy separation in liquid solutions. Thus, this kind of magnetic responsivity can apply for bioseparation, magnetic drug delivery, magnetic resonance imaging (MRI), environmental applications etc.

To investigate the application of stimulus responsive nature of the magnetite coated hybrid material in water remediation, by adsorbing heavy metal chromium. The organic material has a tendency to crystallize along the walls of the glass tubes. Taking advantage of this property, the organic compound was allowed to crystallize in a magnetite containing solution. Chromium solution of 50 ppm concentration was added to the hybrid material that crystallized along the glass tube. After 24 hours of continuous vortexing, the samples were analyzed for the adsorption of chromium. Field Emission Transmission Electron Microscope (FE-TEM) analysis and EDX spectra (Figure 6.4a) of the sample confirm the presence of Cr getting attached on to the surface. STEM–EDS mapping were performed to further confirm the adsorption of minerals. Elemental mappings for C, S, Fe and Cr on the hybrid material are shown in figure 6.4b. The plate like architectures providing large surface area for the adsorption of magnetite, also exhibited higher specificity towards Cr metal removal. The result of STEM EDS-mapping shown in Figure 6.4 reveals the distribution of carbon and sulfur in 1,2 –bis (tritylthio) ethane, with Fe, and

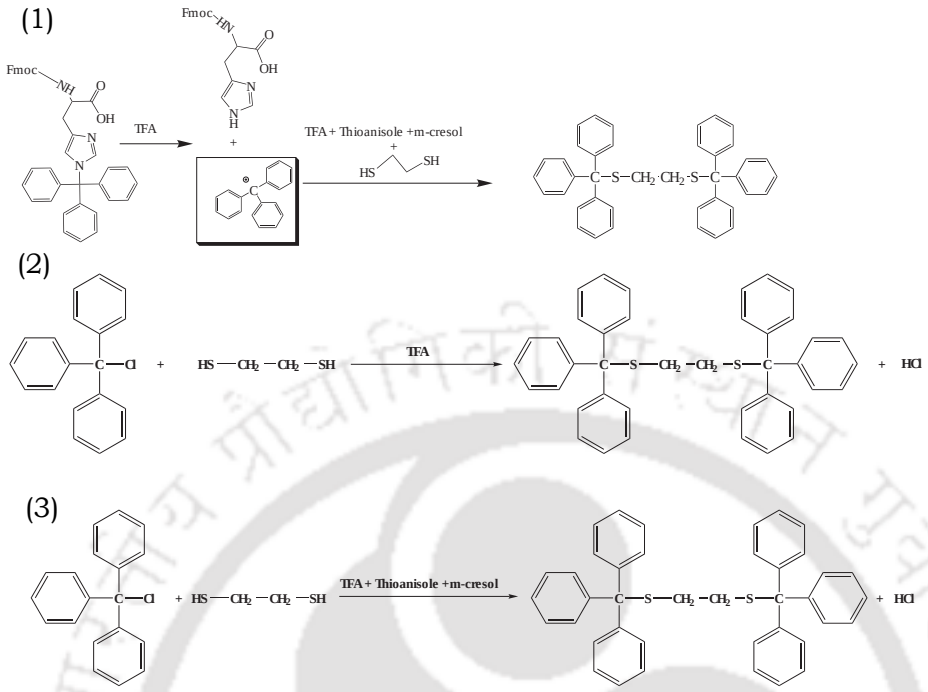

Figure 6.6: Comparison of different methods adopted for the synthesis 1,2-bis(tritylthioethane) (1) Synthesis method using trityl protected amino acids. Methods (2 &3) New protocols optimized for the synthesis of 1,2-bis(tritylthioethane) using trityl chloride as the starting material.

Cr sequestrated on its surface. For effective heavy metal removal at all conditions, it is necessary that basic material should not degrade at extreme pH conditions. To ensure the stability of the organic assemblies, at acidic and basic conditions, the sample was exposed to pH solutions of pH 1,2,3,4,9 and 10. The morphological analysis after continuous vortexing for 24 hrs, revealed that no structural change or morphological damage was observed in the nanostructures (Figure 6.5). The structures remained intact and suggests the possibility of its applicability to the aqueous solutions at wide range of pH.

One possible limitation of the nano-adsorbents reported so far is its cost-effectiveness. One of the essential criteria for developing a material for its extensive application for heavy metal removal, it is its cost-effectiveness and capacity of heavy metal removal. Considering the cost-effectiveness and eco-friendly nature, agricultural wastes, plant products and microbes are used as biosorbents. In the reported protocol for the synthesis of 1,2-bis(tritylthioethane) crystals, amino acid with trityl protected group is used as a starting material. So as to reduce the cost of synthesis, we have designed and optimised

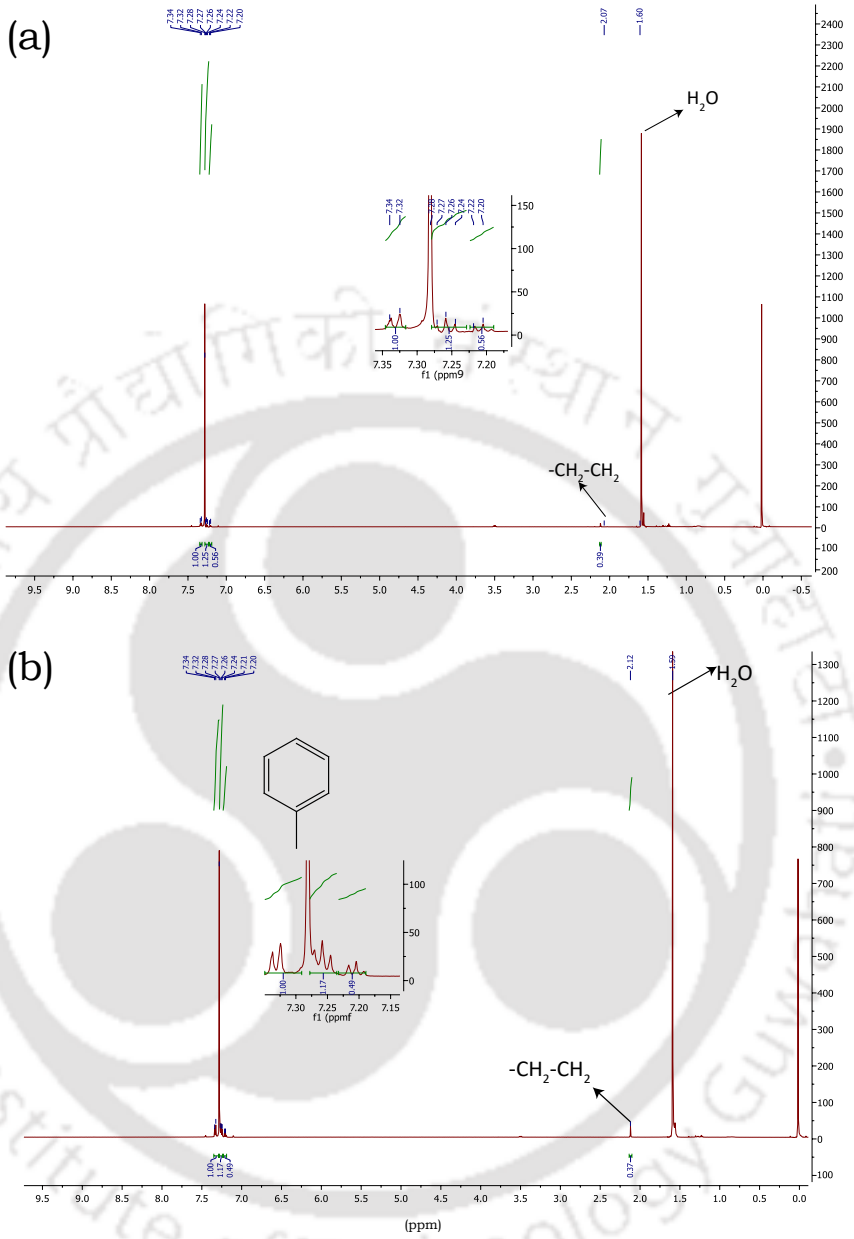

Figure 6.7: ^{1}HNMR analysis of 1,2-bis(tritylthioethane) crystals synthesized by the methods 2(a) and 3(b)

protocols for synthesizing the organic crystals using trityl chloride as the starting material. Two different methods of synthesis have been optimized for the synthesis and crystallization of 1,2-bis(tritylthioethane) (Figure 6.6). Proton NMR of the synthesized crystals has been recorded to verify the purity of the crystals (Figure 6.7). The optimized protocol, an alternative route for crystal synthesis provides an economically viable

approach in addressing the heavy metal contamination. Through this experiment, we intend to demonstrate the potential of a pure organic nanoflower, in acting as a nanoadsorbent for water remediation. Extensive studies on adsorption rate and the kinetics of metal removal has to be performed so as to fabricate the hybrid material as a device for heavy metal removal.

6.5 Conclusion

Overall, this work presents the potential utility of stable tritylthioethane derivatives and it's usage in the design of hybrid nanomaterials. In comparison to the otherwise cumbersome procedures of magnetite impregnation, we designed a simple one-step procedure for the formation of hybrid material. Also we could successfully demonstrate its adaptability to an organic-inorganic hybrid material which responds to an applied magnetic field. The ability to externally control the properties of magnetic materials would be highly desirable from fundamental and technological point of view, particularly in view of recent developments in magneto electronics and spintronics [230]. Furthermore, the presented methodology detailing the procedure for removal of a typical heavy metal reported here, is expected to be an efficient, cost effective and environment friendly approach, owing to the large surface area of both magnetite and the crystalline nanoassemblies. Moreover, magnetite synthesized by different methods has been found effective in removing heavy metals such as As(III), As(V), Cu(II), Zn(II), Pb(II), Hg(II), Ni(II), Co(II), Cu(II) and Cd(II) [293]. The hybridized material provides a new perspective in heavy metal removal and can in principle be fabricated as a tool for the wide spectrum removal of other heavy metals as well.

CHAPTER 7

SINGLE CRYSTAL NANOSTRUCTURES OF (4-(TRITYLTHIO)BUTYLTHIO)TRIPHENYLMETHANE

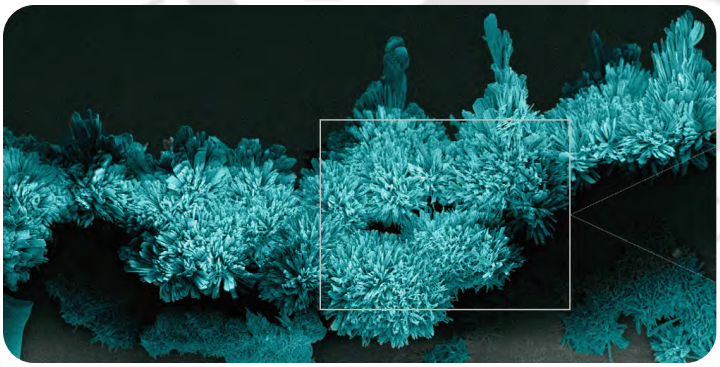

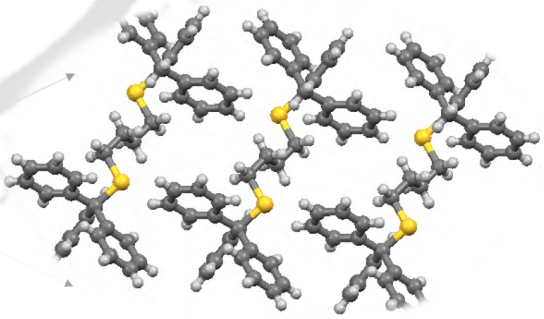

7.1 Summary

We report synthesis, and crystallization of a newly synthesized triphenyl methyl derivative (4-(tritylthio)butylthio)triphenylmethane and its nano-level assembly forming a rare organic nano-flower. Only fewer studies have been done on the design and synthesis of triphenyl based nanostructures despite their wide range applications in different fields. As a consequence of its applicability due its acid labile nature, it is highly desirable to synthesize and fabricate nanolevel assemblies based on trityl systems. The study demonstrates the formation of crystal structures formed by small organic molecule at the nano and micro level with aromatic systems as the principal factor governing molecular recognition and assembly.

7.2 Introduction

Organic nanomaterials with phenyl systems have great potential for diverse applications in organic electronics, energy storage devices, sensors and environmental applications like heavy metal removal, due to their inherent physical properties [40, 186, 188]. In the self-assembly process of organic molecules, the shape and physical properties of the supramolecular structures are mainly governed by non-covalent interactions [294, 295]. Therefore, a thorough understanding of the non-covalent interactions at the structural level is crucial for the rational design of new and improved structures. Many studies are carried out to understand the structure, in particular at the supramolecular level, which is a prerequisite for the rational design of improved self-assembled systems [296]. Also from literature, it is evident that the operative noncovalent interactions can facilitate the rational design of more effective organic systems. Noncovalent weak intermolecular interactions, which can be fine-tuned through the toolbox of synthetic chemistry, not only determines the molecular packing of the individual subunits but also dictates the resulting physical properties of the materials [297]. There is a growing emphasis on the study of self-assembly of small organic molecules as they find applications in fields ranging from medicine to molecular electronics.

Triphenyl derivatives due to their acid labile nature have been successfully used as protecting groups, dyes, mass tags and in many other applications [243]. But the formation of nanostructures through phenyl systems has been poorly investigated. However, only few reports on the nanostructures formed by triphenyl derivatives have been

reported [40, 41]. The driving force for the formation of nanostructures in such systems is the face-to-face and T-shaped aromatic stacking interactions among the phenyl groups. Trityl nanostructures formed through aromatic $\pi - \pi$ stacking have shown ferromagnetic ordering at low magnetic fields and conductivity even at low voltage ranges (Chapter 5). The properties are believed to be exhibited due to the unique orientation of the phenyl groups within the crystal system.

To get a better insight into the physical properties and potential application of trityl based crystal systems, we tried synthesizing a family of molecules that belong to the larger class of trityl systems. Here, we report the synthesis, crystallization, self-assembly, and characterization of new organic molecule (4-(tritylthio)butylthio) triphenylmethane.

7.3 Materials and Methods

7.3.1 Materials

All commercially available products were used without further purification unless otherwise indicated. All the chemicals and solvents used for experiments are of reagent grade. Amino acid Fmoc-His(trt)-OH and solvents Trifluoroacetic acid, Thioanisole, and 1,4-butanedithiol were purchased from Sigma-Aldrich. Diethyl ether and m-cresol were purchased from Merck.

7.3.2 Synthesis of (4-(tritylthio)butylthio)triphenylmethane

The compound was synthesized by treating trityl group released from the side chain of Fmoc-His(trt)-OH with 1,4-butane dithiol, m-cresol and thioansiole in the presence of trifluoroacteic acid (1:2:2:20). Synthesized crystals was purified by successive recrystallization process using diethyl ether as a solvent. Melting points were recorded on a Stuart smp30 melting point apparatus.

7.3.3 NMR Analysis

^{1}H NMR was recorded on a Bruker 600 MHz NMR spectrometer. NMR spectra were recorded in deuterated chloroform ($CDCl_3$), and the chemical shifts were reported relative to TMS (δ0 ppm) as an internal reference. Spin multiplicity was abbreviated as follows:

s = singlet, d = doublet and t = triplet. ^{1}H NMR (600 MHz, $CDCl_3$) δ (ppm): 7.32–7.31 (d, 12 H), 7.25–7.22 (t, 12 H), 7.20–7.17 (t, 6 H), 2.1 (s, 4 H) (s, 4 H) 1.34 (s, 8H).

7.3.4 Raman Spectroscopy

Sample containing both sheet and flower like morphologies was drop casted on a glass slide. An optical microscope of X 100 objective lens was used to focus the laser on the crystal structures. Raman spectra of the samples were recorded at room temperature using Horiba Jobin Vyon, Laser Micro Raman System with a laser excitation wavelength of 633 nm.

7.3.5 Single Crystal-X-Ray Diffraction

Crystal data were collected using BRUKER D8 VENTURE SC-XRD with Mo-Kα (λ=0.71703 Å) radiation at room temperature [296(2) K]. The X-ray data collection was monitored by SMART program (Bruker, 2003). The crystal structure was solved by directed methods (SHELXL-97) and refined by a full matrix (SHELXL-97) least square procedure employing 322 reflections that satisfied I > 2σ(I) criterion. Successive refinements based on F^2 lead to reliability factors of R = 0.0372.

7.3.6 Microscopic Characterization

FE-SEM

Ethyl ether was added to the plate-like crystals and vortexed to yield flower-like morphologies. 20 µl of the sample was loaded on the glass substrates and the morphological characterization was done using Field-Emission Scanning Electron Microscope (FESEM) of Zeiss (Model: Sigma) at 3 kV. Samples were sputtered with gold for enhancing the conductivity.

FE-TEM

10 µl of the vortexed sample was placed on the 300 mesh copper grid covered with strong carbon film; SAED and High Resolution Transmission Electron Microscopic (HR-TEM) analysis of the sample was performed on JEOL transmission electron microscope, Model: JEM 2100, operating at 200 kV.

7.4 Results and Discussion

A new trityl based organic compound has been synthesized and crystallized using diethyl ether as a solvent system. The reaction conditions of the molecule have been similar to that of the synthesis of 1, 2-bis(tritylthio)ethane [40]. Using a trityl protected amino acid as a starting material, a solution containing 1,4-butanedithiol, m-cresol, thioanisole, and TFA were added in the ratio of 1:2:2:20. (Figure 7.1 a) The synthesized molecule was purified by recrystallization using diethyl ether as a solvent.

The purity of the synthesized crystal was analyzed using ^{1}HNMR (Figure 7.2). The molecular organization of the crystals was proposed based on the single crystal measurements carried out on a block colorless crystal with dimensions of 0.150 x 0.150 x 0.100 mm^3. The compound crystallizes into a triclinic system with a P-1 space group. An ORTEP view of the crystallized compound is shown in Figure 7.1 b. The unit cell parameters were found to be a = 7.43620(10), b = 7.79360(10), c = 14.4898(2) Å and Z=1 (Figure 7.1 c). The crystal structure has been deposited in the Cambridge Crystallographic Data

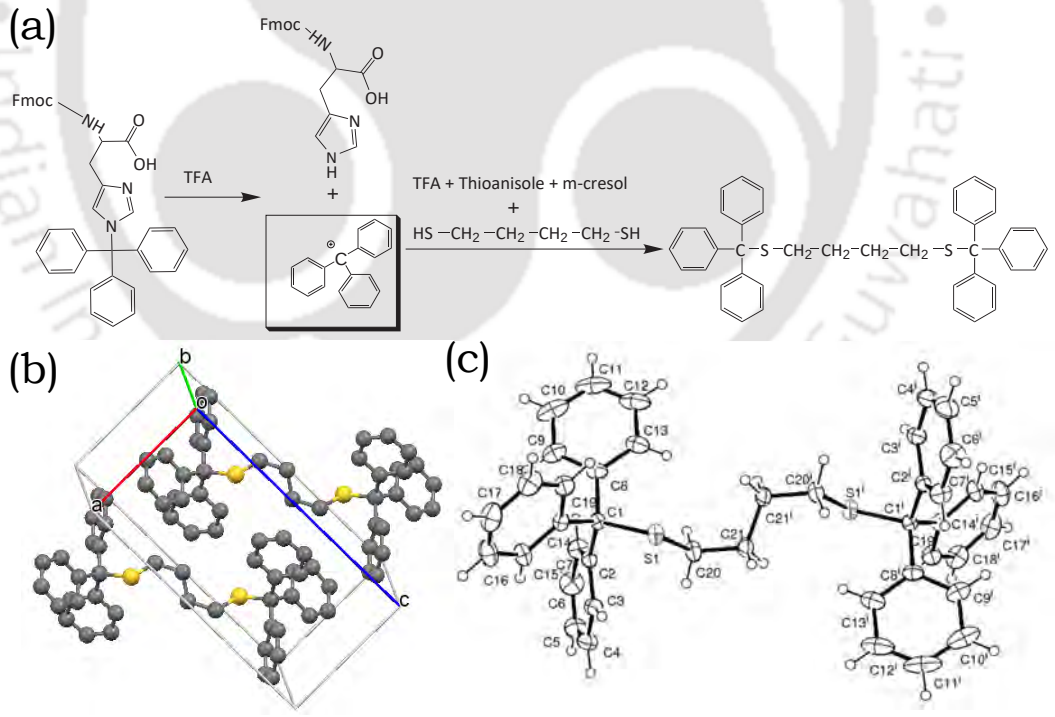

Figure 7.1: Synthesis and crystallization of (4-(tritylthio)butylthio)triphenylmethane. (a) Scheme illustrating the synthesis of (4-(tritylthio)butylthio)triphenylmethane. The schematic unit cell (b) and ORTEP diagram(c) of the crystal structure.

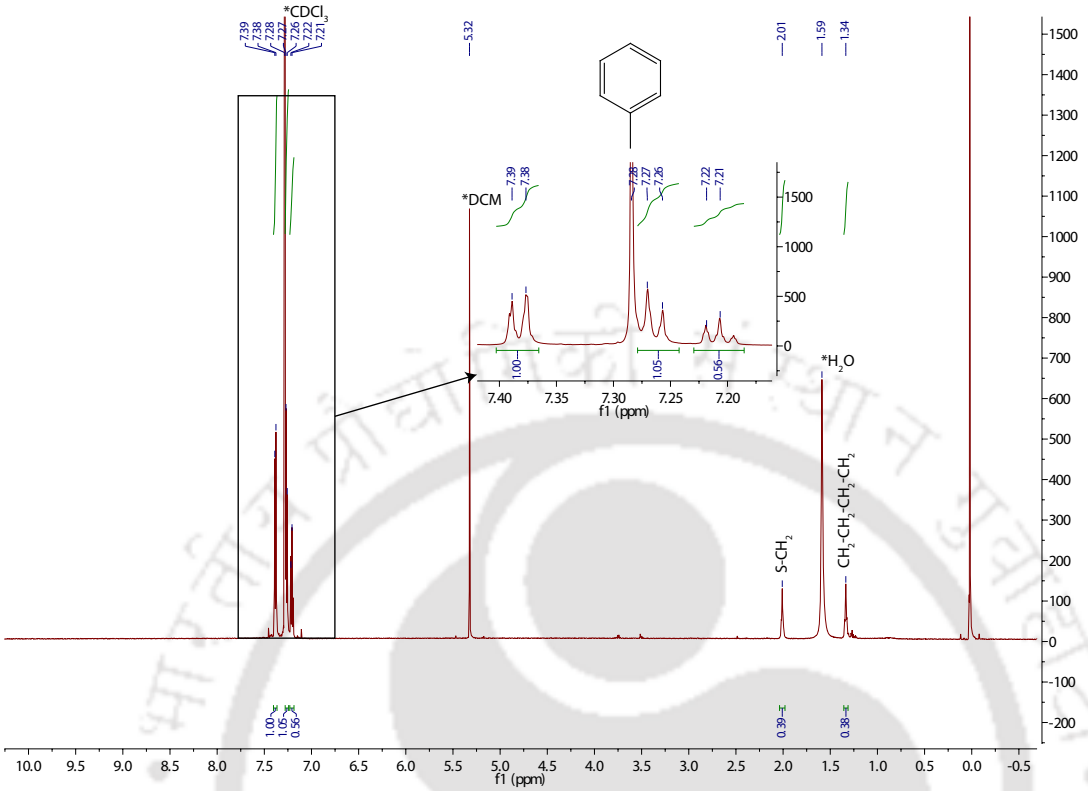

Figure 7.2: ^{1}H NMR characterization of (4-(tritylthio)butylthio)triphenylmethane.

Centre with a CCDC no. of 1869743. The details of the crystal structure and the results of the structure refinement are shown in table 7.1. The melting point of the crystal was found to be 166º C. The decrease in the melting of the crystal structure with respect to the reported 1,2-bis(tritylthio)ethane may be attributed to the number of alkyl systems in the crystal and the crystal packing. One such study was conducted to correlate the melting point and the crystal packing in symmetrical quaternary ammonium salts $(C_nH2_{n+1})4N^+X^-$. The melting point of the crystals decreased with the increase in the number of the alkyl chains. To correlate the packing of the system with the change in the melting point, the single crystal structure of the molecule with the low melting point was studied and it was found that they crystallize in a less-symmetric packing systems [298]. In accordance with the observation, the decrease in the melting point and lesser stability of the crystal structure reported here can be attributed to the increase in the number of alkyl systems and crystallization of the molecule in the least symmetric triclinic system.

For further characterization of the morphologies formed by the crystals it was dissolved in diethyl ether, vortexed and analyzed using FESEM. Figure 7.3 (a,b) shows

Identification code	(4-(tritylthio)butylthio)triphenylmethane
Empirical formula	C_{42} H_{38} S_2
Formula weight	606.84
Temperature	296(2) K
Wavelength	0.71073 Å
Crystal system, space group	Triclinic, P-1
Unit cell dimensions	a = 7.43620(10) Å α = 100.747(2)°. b = 7.79360(10) Å β = 91.7710(10)°. c = 14.4898(2) Å γ = 99.823(2)°.
Volume	811.22(2) $Å^3$
Z, Calculated density	1, 1.242 Mg/m^3
Absorption coefficient	0.194 mm^{-1}
F(000)	322
Crystal size	0.150 x 0.150 x 0.100 mm^3
Theta range for data collection	3.125 to 31.073 °
Index ranges	-10<=h<=10, -11<=k<=11, -21<=l<=21
Reflections collected	31351
Independent reflections	5179 [R(int) = 0.0372]
Completeness to theta = 25.00 °	99.6 %
Absorption correction	Semi-empirical from equivalents
Max. and min. transmission	0.7456 and 0.6876
Refinement method	Full-matrix least-squares on F^2
Data / restraints / parameters	5179 / 0 / 199
Goodness-of-fit on F^2	1.046
Final R indices [I>2sigma (I)]	R1 = 0.0520, wR2 = 0.1244
R indices (all data)	R1 = 0.0799, wR2 = 0.1483
Extinction coefficient	n/a
Largest diff. peak and hole	0.369 and -0.320 e.$Å^{-3}$

Table 7.1: Crystal data and structure refinement for (4-(tritylthio)butylthio)triphenylmethane

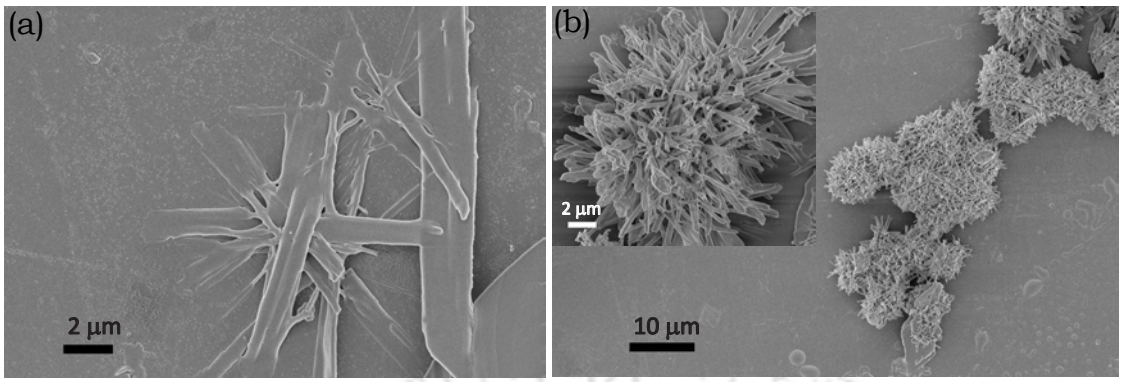

Figure 7.3: Morphological characterization of the nanoassemblies by FE-SEM (a) Plate like and (b) Nanoflower like morphologies with the inset showing high resolution image justifying that the nanoflower is made of plate like morphologies.

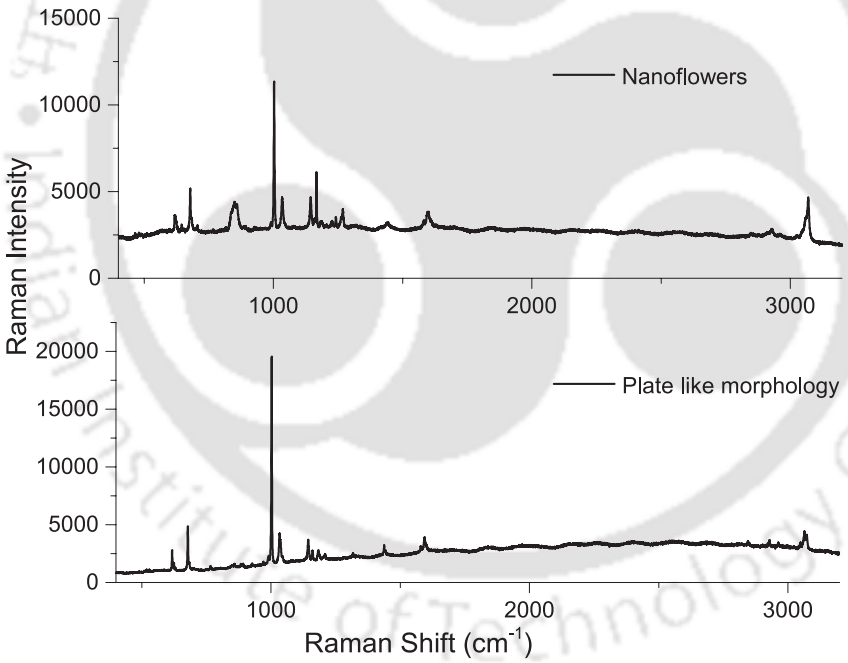

Figure 7.4: Characteristic Raman spectra of plate and nanoflower like morphologies.

the FESEM images of the plate and flower like morphologies formed by the crystals. As shown in the inset of Figure 7.3 b, the plate like morphologies comes together to form flower like morphologies. This was further verified by Raman analysis, where the sample drop casted on glass slides was focused using 100 X optical lens and the laser was

S.No	Sample Peaks (cm^{-1})	Peak assignment
1	618.878 – 685.272	C- S stretch [250]
2	1003.11, 1034.69, 1579.86, 1595.65	Benzene ring [251]
3	1160.32 – 1195.46	CH_2 wag and twist
4	3064.46	CH stretch in aromatic compounds

Table 7.2: Raman peak assignments for the nanostructures.

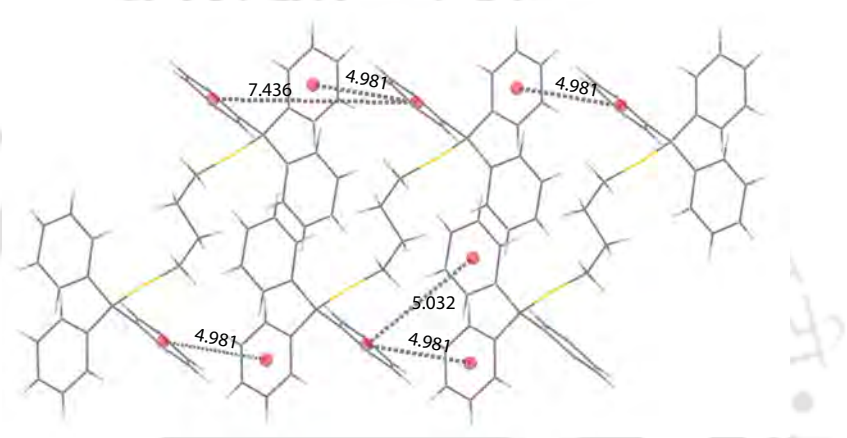

Figure 7.5: (a) Calculation of interatomic distance between the two closest carbon atoms interacting through T-shaped interactions.

irradiated on the plate and flower like morphologies. Raman spectroscopy has been used to identify the vibrational modes resulting from the different functional groups present in the system. Figure 7.4 shows the Raman analysis of plate and flower like morphologies showing the same signature region and the peak assignments of the functional groups is given in table 7.2. In comparison to the earlier reported structures from 1,2-bis(tritylthio)ethane, though there is an increase in the number of alkyl groups, connecting the two triphenyl systems from ethane to butane, the molecules through intermolecular aromatic $\pi - \pi$ stacking interactions self-assembled to form plate and flower like morphologies. As mentioned earlier in chapter 5, multiple phenyl embraces are important feature of such molecular system to engage each other through a supramolecular interaction network.

(4-(tritylthio)butylthio)triphenylmethane with six phenyl rings, can form multiple phenyl embraces (MPE). From Figure 7.5, it is evident that $\pi - \pi$ stacking interactions are mediated through orthogonal i.e. edge-to-face, or T-shaped interactions as observed

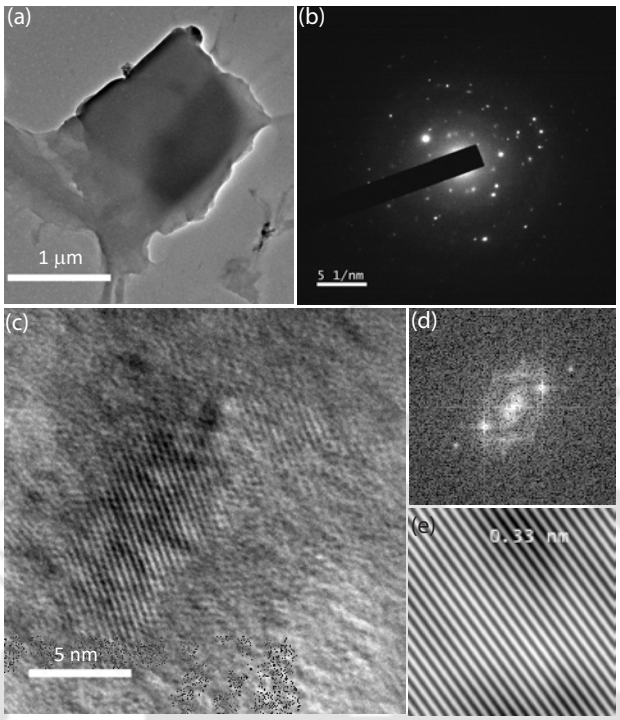

Figure 7.6: (a) FETEM analysis of the plate like structure (b) Single crystal phase of the nanostructures confirmed by SAED pattern (c) HRTEM analysis of another plate like crystal (d) Corresponding Fast-Fourier transform (FFT) pattern of the region seen in (c) and the lattice distance between the planes.

in the previously reported crystal structures [13, 40]. The red spheres represent the centroids of the benzene rings and the grey dashed-line indicates the T-shaped edge-to-face interaction among the benzene rings. The nanoassembly is a result of aromatic stacking interactions between the phenyl rings of the molecules. The packing of the molecules along the a axis involves aromatic $\pi - \pi$ stacking interaction (centroid-centroid 4.98 Å). The strong $\pi - \pi$ stacking may favor the formation of plate like morphologies which in turn come together to form flower like structures. The distance calculated between the two cores of the neighboring aromatic moieties are approximately within the range of 4.06 and 7.08, the distance required for the interaction between typical T-shaped phenyl embraces between the closest and farthest carbon atoms. Obtained values are in good agreement with the earlier reports of the distance and energy estimates in the case of benzene dimer [11].

Detailed structural characterization of the organic nanoassemblies were further achieved by Field Emission Transmission Electron Microscopy (FETEM) and Selective

Area Electron Diffraction (SAED) to verify their crystallinity. Figure 7.6 (a) shows the FETEM analysis of plate like structures and its corresponding selected area electron diffraction (SAED) (Figure 7.6 b) pattern showing its single-crystal characteristics at the nano-level. Figure 7.6 (c, d) shows the HRTEM analysis of the plate like structures and its corresponding FFT used to calculate the lattice distance. The lattice distance calculated was 3.3 Å (Figure 7.6 e), can be indexed to [-202] plane as calculated from the simulated PXRD pattern from the S-XRD data. To the best of our knowledge, this is the second triphenyl based systems to form crystalline assemblies at the nanolevel. The advantage of the synthesis and crystallization methods reported lies in the facile and mild reaction conditions yielding highly crystalline nanostructures. The proposed method can be adapted to synthesize new molecules based on trityl systems.

7.5 Conclusion

In conclusion, a new organic compound (4-(tritylthio)butylthio)triphenylmethane is synthesized and crystallized using diethyl ether at room temperature. Single crystal XRD of the molecule revealed that the molecule crystallizes in triclinic systems. The systematic self-assembly of the molecule is mediated by aromatic $\pi - \pi$ interactions, which results in the formation of plate and flower like morphologies. Structural characterization of the nanostructures through SAED and HR-TEM experiments shows that the morphology is crystalline at the nano-level. As triphenyl systems are known for exhibiting weak ferromagnetic behavior, the molecule can also be explored for magnetic properties. The molecules formed through aromatic $\pi - \pi$ stacking can be an interesting candidate for optical and electronic properties with future applications.

CHAPTER 8

DIHISTIDINE NANOASSEMBLIES

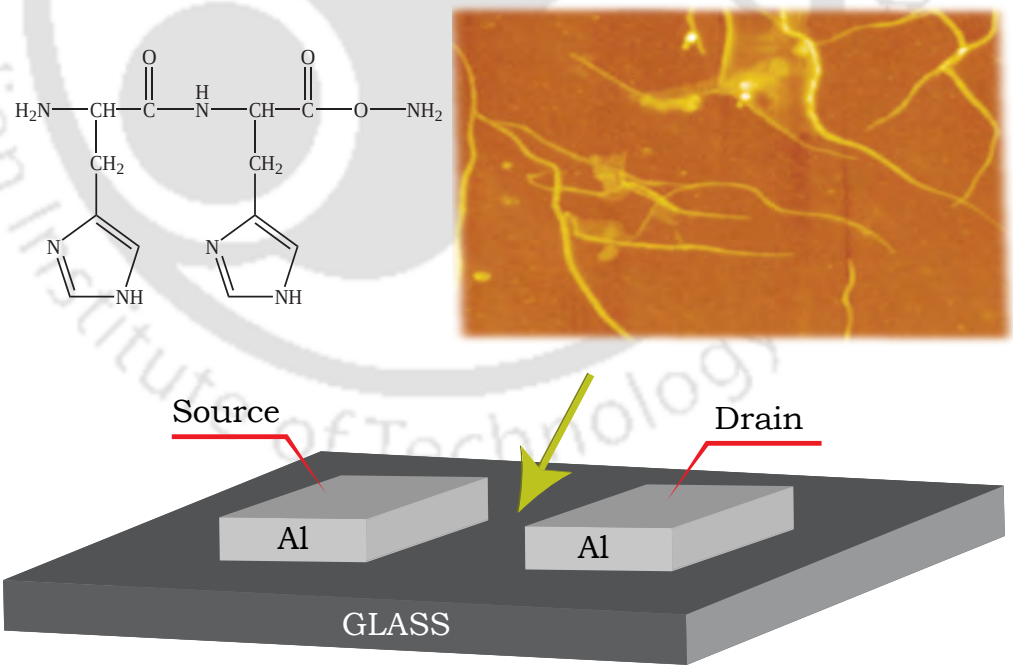

8.1 Summary

Supramolecular assembly has enabled the design and synthesis of a variety of functional materials with well-defined structures. Peptide based materials can self-assemble into a variety of functional materials through precisely controlled non-covalent interactions between the peptide sub-units. Peptide based conducting nanomaterials have wide range of applicability in nanoelectronics. In this work we report our observation of the self-assembly of histidine dipeptide to form nanofibers, and its preliminary measurement for its conductive nature.

8.2 Introduction

Nature has mastered the building blocks of amino acids into hierarchical structures to maintain the fundamental life processes. Inspired by nature, supramolecular chemistry aims at developing complex systems through non-covalent interactions [299]. The combination of non-covalent interactions and bottom-up approach has enabled the design and fabrication of a variety of functional materials in nanotechnology. Nanoscience and technology have developed into one of the most fascinating and important research frontiers in modern science. The possibility to design and generate nanomaterials with well-defined properties at the nanoscale requires controlled organization of the basic building units. A number of molecular self-assembled systems with peptides as basic building blocks have been designed and developed [300]. Yet, the development of peptide based materials into tangible product pipelines are still in their infancy. Peptides with the property of small size, chemical diversity, and facile synthetic methods are important to facilitate the possibility of incorporation of desired functional groups or non-natural amino acids. The flexibility in design makes them excellent starting points for fabricating smart functional materials. Though initially being involved in discovering therapeutic strategies to address diseases [301], scientific community has identified their potential to inspire applications in other fields like nano-electronics and tissue engineering [302]. The efforts gained momentum after the discovery of peptide nanotubes formed by peptides with 2-4 amino acids long [22]. In this chapter, we report the generation and physical property measurements of dihistidine based nano-architectures. Although, few histidine based nanostructures have been reported [303], nanoassemblies exclusively made of dihistidine peptides has not been reported so far.

Histidine heads are usually incorporated into sequences to control the self-assembly of peptides through imidazole rings. Peptide amphiphiles with histidine containing sequences are known to form pH responsive hydrogels [304, 305] and also on inclusion of histidine in the sequence, the same PA formed different nanostructures at different pH conditions [306]. Histidine with an aromatic imidazole side chain are known for its catalytic functions as they are capable of forming cation-π interactions in its protonated form and co-ordination complexes with metallic ions. Such properties are exploited to bind metal ions such as Ni^{2+} with repeats of histidine [307]. Histidine-rich peptide nanotubes have also been used as templates for growing Cu nanocrystals, where the growth of the Cu nanocrystals were optimized by controlling the conformation of the histidine rich peptide by pH changes [200]. In addition to that amino acids like histidine and tryptophan are known to play an important role in photosystems for relaying electrons through proton coupled mechanism [308].

Though proteins are considered to be insulators, long-range electronic conductivity is present in few biological systems. Notable examples of such electron transport in enzymes [309] and protein wires of bacteria [310] has inspired the study of conductivity in protein based materials and fabrication of bioelectronic materials [187]. But the translation of such prototypes to nanodevices is still challenging, because of the difficulty in controlling the self-assembly process. Hence, peptides are used as toolkits to simplify the sequence specific behaviors and to control the self-assembly and folding process. Tryptophan containing peptides showing conductivity has been reported before [311]. Based on the previous reports on self-assembling short peptides [312], and understanding the importance of histidine in proton transfer mechanisms [308], the possibility of conductivity in histidine based nanoassemblies was explored. A preliminary analysis of electrical characterization of the peptide fibers revealed that they are conducting in nature.

8.3 Materials and Methods

8.3.1 Materials

Peptide synthesis was performed using Nova PEG Rink Amide Resin purchased from Nova Biochem. Dimethylformamide (DMF), m-cresol, piperidine and Hydroxybenzotriazole (HOBt) were purchased from Merck. Fmoc-His-(trt)-OH, N, N-Diisopropylethylamine

(DIPEA), N,N,N′,N′-Tetramethyl-O-(1H-benzotriazol-1-yl)uronium hexafluorophosphate, O-(Benzotriazol-1-yl)-N,N,N′,N′-tetramethyluronium hexafluorophosphate (HBTU), thioanisole, 1, 2-Ethanedithiol and TFA were purchased from Sigma Aldrich. Ethanol was purchased from Helix India.

8.3.2 Peptide Synthesis

HH-NH_2 peptides were synthesized by standard Fmoc Solid Phase Peptide Synthesis (SPPS) methods using Rink-Amide Resin. The process of SPPS starts by stepwise attachment of the protected amino acids to the resin. Required amount of resin (Nova-Biochem) was soaked overnight in DMF for swelling up process. The Fmoc group of the swelled up resin is removed using 20% Piperidine in DMF (Merck) and the pH is adjusted to 7 for the attachment of amino acids. Fmoc-protected amino acids are activated using 3 equivalents of amino acid, HOBT, HBTU, and six equivalents of DIPEA. The activated amino acid is added to the resin, so that during the coupling process the activated carboxyl terminal gets attached to the deprotected N-terminal of the resin. Attachment of the first amino acid is followed by the deprotection of its N-terminal for the next amino acid attachment. The process is repeated until the completion of the sequence. On completion of the sequence, Fmoc group of the amino acid at the N-terminal is removed and the resin is dried using diethyl ether. To the dried resin, deprotection mixture containing the solvents namely EDT, m-cresol, Thioanisole, and TFA was added in a ratio of (1:2:2:20) and incubated for 15 hrs. The peptide sequence cleaved from the resin is precipitated using diethyl ether and were studied as TFA salts. The peptides were characterized using a Shimadzu HPLC, equipped with a C-18 reverse-phase chromatographic column and the mass was confirmed by MALDI (Bruker, AUTOFLEX SPEED).

8.3.3 Preparation of Peptide Nanoassemblies

Peptide was dissolved in dd.H_2O and further diluted to a concentration of 4 mg/ml and 8 mg/ml in ethanol. One-day aged peptide solutions were used for the experiments.

8.3.4 Characterization

Atomic Force Microscopy

For AFM analysis 20 μl of one-day old sample was loaded on freshly cleaved mica. AFM topography images were acquired using Asylum MFP-3D origin by Oxford instruments. All imaging was performed in tapping mode using non-contact tips with spring constant of 26 k(N/m) and resonant frequency of 324 kHz. Scan rates employed were 0.5-1 Hz. Data were analyzed using the Asylum research software.

Field Emission-Scanning Electron Microscopy

A 20 μl peptide solution with a concentration of 4 mg/ml was drop casted on a glass substrate. Sample was air dried and coated with gold for enhancing the conductivity. Analysis was performed at 3 kV using FE-SEM model Sigma 300.

Attenuated Total Reflectance–Fourier Transform Infrared Spectroscopy

ATR-FTIR was recorded for the peptide solution with a concentration of 4mg/ml. Analysis were done in the range of 400 – 4000 cm^{-1} with a resolution of 4 cm^{-1} (64 scans were averaged) using ATR-FTIR spectrometer (IRAffinity-1S, Shimadzu, Japan).

Electrical Characterization

Conductance measurements were recorded in a two-terminal sensor device. The device containing the main electrode was fabricated on the glass substrate. The glass substrates were initially cleaned in piranha solution (3:1 H_2SO_4:H_2O_2) followed by repeated washing in deionized water and then dried under vacuum at 100 ºC. By masking technique, aluminum electrodes of 150 nm thickness were deposited on the dried glass substrate by thermal evaporation under high vacuum <10^{-6} mbar to make a blank channel with 40 µm length (L) and 800 µm width (W). From the sample, 20 μl was drop casted on the channel between the electrodes. The sample was dried under room temperature and the electrical measurements were carried out under ambient conditions using a Keithley 4200-SCS semiconductor parameter analyzer.

8.4 Results and Discussion

The dihistidine peptide reported in this work was synthesized using solid phase peptide synthesis and the purity of the molecule was determined by analytical HPLC and by MALDI-TOF as shown in Figure 8.1. The dihistidine peptide was initially dissolved in dd.H_2O and further diluted in ethanol to the required wroking concentrations. Field Emission-Scanning Electron Microscopy was used to study the nanoassemblies formed by the peptides. The peptides formed very short and thin fibers (Figure 8.2 a). Such fibrillar structures formed by dihistidine containing peptides at different pH were earlier reported [303].

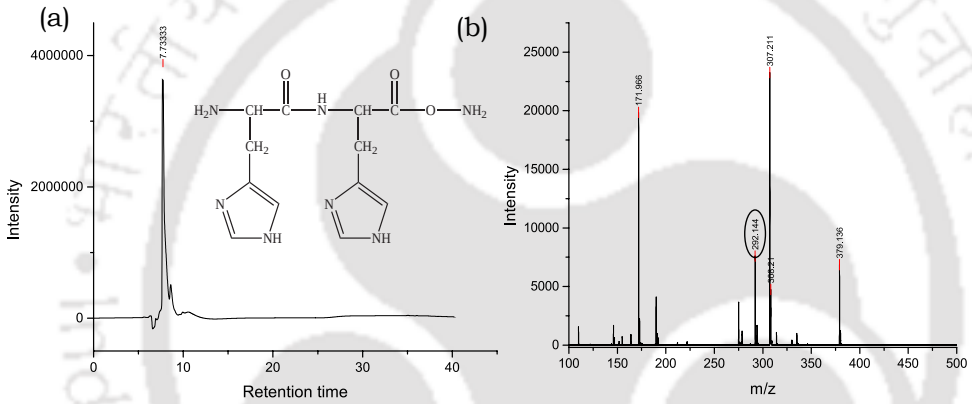

Figure 8.1: (a) Chemical structure of the dipeptide synthesized (b) HPLC and MALDI analysis of the synthesized peptide.

As the fibers formed were very thin in dimensions and was sensitive to electron beam of high voltages, AFM imaging was used to calculate the height and diameter of the nanofibers. Height profiles of the observed nanofibers, exhibited a minimum of 5 nm and a maximum of 20 nm. The diameter of the nanofibers was found to be 50 – 80 nm in diameter. Along with the nanofibers, a thin film like structure with a height of ≈ 5 nm was observed in the background (Figure 8.2 b, c).

Peptide fibrils like amyloids play a key role in the formation of amyloid diseases [147] and other nanofibers like actin filaments and microtubules constituting the cytoskeleton plays a functional role in the body [313, 314]. Peptide designed based on such functional structures self-assembling into fibers and hydrogels have been used for applications in wide areas such as drug delivery and tissue engineering, due to the biocompatibility and high water retention property [315]. The self-assembly of peptide like structures

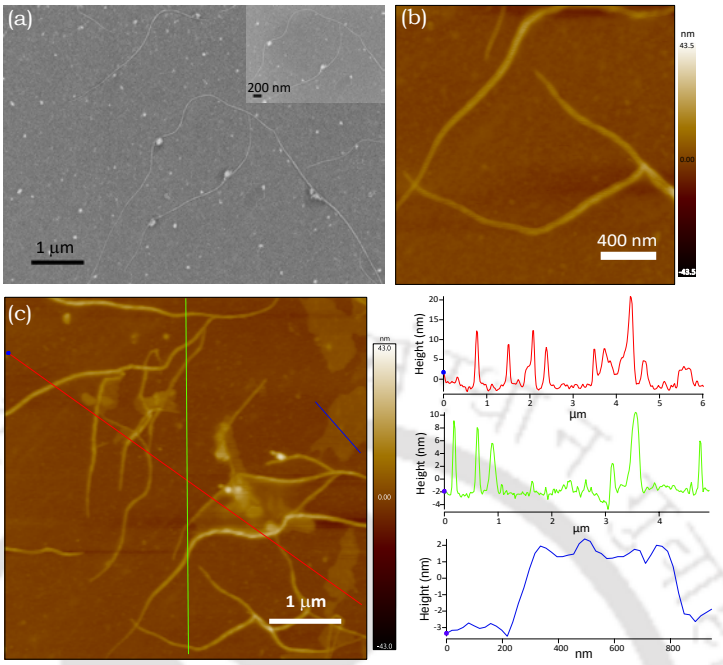

Figure 8.2: (a) Scanning electron micrographs of dihistidine nanofibers with the inset showing a high resolution image. (b) AFM images of nanofibers and (c) Z-height line scan across the fibers and thin films and their respective profiles.

into nanofibers is driven by various non-covalent interactions like H-bonding, aromatic $\pi-\pi$ stacking and van der Waals interactions. To get an insight into the conformation of the peptide assemblies, ATR-FTIR analysis was done. Structural information of the nanoassemblies were analyzed in the amide I band region (1600-1700 cm^{-1}). The resulting amide I band corresponds to C=O stretching vibrations of the single peptide bond in the dihistidine peptide and the peak observed at 1647 cm^{-1} corresponds to random coil structure (Figure 8.3) [316]. In previous reports, change in the secondary structures from helix to coiled-coil to random coil, has been observed at different pH conditions. The protonation of the His side chain is believed to play a key role in triggering the electrostatic destabilization of the helical fibrils [317].

One dimensional nanostructures like nanofibers or nanowires from synthetic compounds are known to exhibit electronic properties in a single dimension [318]. In organic systems, self-assembled structures fabricated out of π-conjugated aromatic units forming crystalline nanofibers has served as a potential candidate material for electronic devices [319]. As peptide systems comes with the property of diversity and functional tunability, a number of peptide conjugated hybrid systems possessing electronic properties were designed

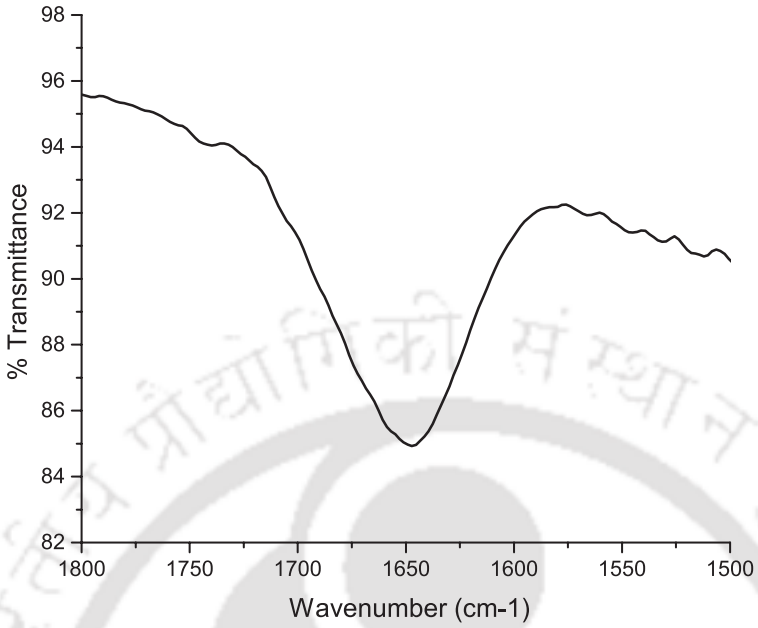

Figure 8.3: FTIR analysis of the amide region of the peptide assemblies.

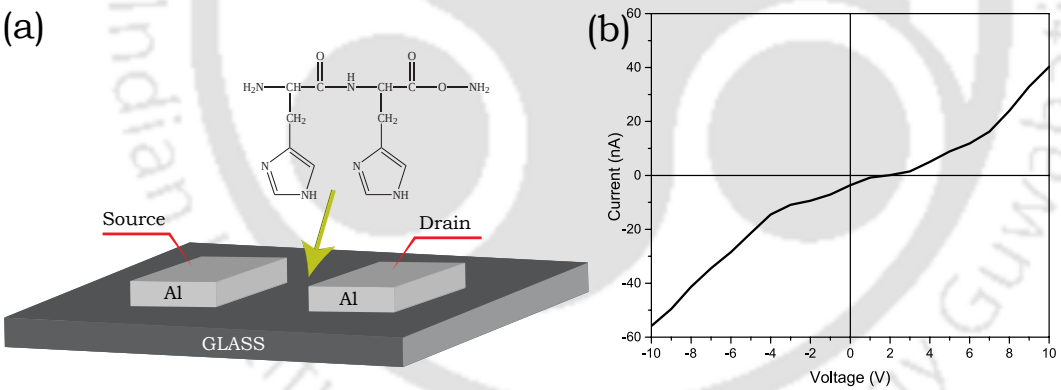

Figure 8.4: (a) Schematic representation of the device configuration used for conductivity measurements. (b) Current – Voltage *(I-V)* characteristics of the dihistidine nanoassemblies.

and fabricated [320, 321]. In particular, π-conjugated peptide nanostructures showing electronic properties have been used as semiconducting layers in Organic FETs [322].

For the fabrication of biocompatible device or precisely, human implantable devices, biomolecules are chosen over inorganic material, owing to their biocompatibility and reduced toxicity. Biological systems with electronic properties act as an interface between synthetic electronic devices and biological molecules [323] to fabricate biocompatible

bioelectronics devices like real time sensors, wearable and implantable devices [324, 325] etc. However, finding an ideal material with the property of biocompatibility along with functional diversity to bridge the two fields, remains a challenge [324]. Among all materials, proteins, and peptides with an inherent property of self-assembly and molecular recognition satisfy the criteria to form diverse architectures with different functionalities [326]. To exploit the obtained nanostructures as functional materials in bioelectronics applications, understanding of their electronic behavior is required. Nanofibrils formed by amyloid sequences and α-helical peptide have shown to have the property of conductivity. Histidine peptides were known to participate in redox reactions of the conductive peptides in nature. To characterize the conductive nature of the peptides, *I-V* curve of the dried dihistidine nanofibers were measured. The peptides were drop casted in the glass substrate with aluminum electrodes of thickness 200 nm (Figure 8.4 a) which acts as source and drain of the electrodes. The samples were allowed to dry and conductance measurements were done using Keithley 4200-SCS semiconductor parameter analyzer at a voltage range of +10 to -10 V. A typical *I-V* curve of the dihistidine nanoassemblies is shown in (Figure 8.4 b). The *I-V* curve is not passing through origin and is showing some current at V=0. Though it can be claimed that material is showing capacitance of some kind, s series of experiments with different scan rates has to be performed to ensure the material property.

While our work reports a preliminary analysis of the conductivity in nanostructures, to study the electron transport properties of the peptides and mechanism behind its conductivity, it requires a series of follow-up experiments to be performed. Also, the observed properties suggest that, the peptide material can be used further, for exploring its electrical properties for fabrication of nanodevices. While histidine-containing sequences are known for impregnating metal ions, the nanostructures can also be used as model systems to impregnate metal ions. The study also suggests the possibility of exploring histidine-containing sequences for conductivity studies and bioelectronic interface material.

8.5 Conclusion

The study reports the formation of nanofibers formed exclusively by histidine containing sequences. Our finding suggests the possibility of long-range electronic conduction in histidine based nanoassemblies. Supramolecular structure of the peptide nanofibers

formed by the histidine sequence may be due to the mechanism of π-stacking interactions of the aromatic side chains. *I-V* curve measurements of the nanofibers show that they are conductive in nature. Initial findings of the experiment suggest that histidine based synthetic peptides can act as a promising platform for studying structure-property relationship in conducting biomaterials. Peptides featuring histidine with various lengths and stereochemistry, can be explored for its physical properties. Histidine rich peptides known to form specific interactions with certain metal ions also has the potential to change conformations at varying pH, concentration and other experimental conditions. Given the potential applicability of synthetic peptides as materials in electronic devices, conducting nanofibers can be assembled in a controlled fashion by tuning assembly inducing parameters.

CHAPTER 9

CONCLUSIONS AND FUTURE POSSIBILITIES

This thesis work employed the fundamental concepts in the design and synthesis of molecules to induce self-assembly formed through aromatic $\pi-\pi$ interactions intended to control their nano-level structure, stability and physical properties. In the fourth chapter, we attempted symmetry as a design concept in controlling nano-level architecture of self-assembling peptide systems. Symmetry along with two other design variables namely aromatic $\pi-\pi$ interactions and overall size of the molecule were used as design parameters in six model molecular systems. From the results obtained, we can conclude that the symmetry of basic building block dictate the topology and self-assembly in model systems. The model system with the most symmetrical subunit forms the most crystalline and stable structure, whereas the one with the minimum number of symmetry elements forms amorphous aggregates. In the fifth chapter, we reported the synthesis of a new triphenyl organic molecule 1, 2-bis(tritylthio)ethane, which crystallizes in a monoclinic system and also self-assembles to form plate and nanoflower like morphologies. The morphologies which are crystalline even at the nano-scale are mediated though T-shaped and face-to-face aromatic interactions. The crystal

containing phenyl embraces arranged in a unique molecular orientation, prompted us to explore the magnetic and electrical properties of the organic assemblies. Being the first crystalline organic nanoflower reported so far, it also happens to be the molecule to exhibit dual magnetic properties both at 300 K and 2 K. On electrical measurements the samples were found to be conducting. In the sixth chapter, we fabricated hybrid organic-inorganic materials by coating the surface of the organic nanoassemblies with superparamagnetic magnetite nanoparticle. The resulting superparamagnetic hybrid material with magnetite on its wide surface area, was used for the impregnation of chromium. Our experimental results also indicate that the designed method is advantageous as (i) it is an environment friendly material with no secondary pollutants, (ii) has wide range pH stability, (iii) requires easy operational procedures and (iv) posses excellent adsorption capacity. Triphenyl systems reported for its wide range of applications are not investigated to its potential for the formation of nanoassemblies. The protocol used for synthesizing 1, 2-bis(tritylthio)ethane, was extended to synthesize another triphenyl molecule. The new molecule (4-(tritylthio)butylthio)triphenylmethane, crystallizes in a triclinic system with a P-1 space group. Though the crystals were found to be less stable than 1, 2-bis(tritylthio)ethane, yet it self-assembled through aromatic interactions to form plate and nano-flower like morphologies. In the eighth chapter, to understand the role of imidazole containing aromatic systems in self-assembly, we synthesized dishistidine peptide, and it self-assembled to form conducting nanofibers. The proposed study has discussed methods to control and fabricate nanoassemblies formed by organic and peptide systems, but it is far from complete in different aspects of controlling the architecture and executing their applications in different fields. Few insights gained from the thesis work are mentioned below:

Concept of symmetry: The concept of symmetry can be extended to other peptide sequences with new symmetrical elements. 1, 2-bis(tritylthio)ethane: Preliminary electrical studies on 1, 2-bis(tritylthio)ethane revealed that the material is conducting and its capacitance is in the range of pF. With the given knowledge, the characterization can be extended for the fabrication of organic crystals into potential devices or as active layers in organic devices.

Applications of organic-inorganic hybrid systems: Nano adsorbents are a new class of materials for developing a cost-effective technology for removal of a broad spectrum of heavy metals from metal-contaminated wastewater. Impregnation of heavy metal on the hybrid materials by means of electron microscopic studies have been shown. To

develop the material as a potential nanoadsorbent, a detailed study on the mechanism and kinetics of chromium removal has to be performed. Further, the kinetic studies can be employed in fabricating devices for heavy metal removal. And as the organic material used is inherently conducting, it can be fabricated into a sensor for heavy metal detection. Magnetite nanoparticles are reported to be effective in removing heavy metals such as As(III), As(V), Cu(II), Zn(II), Pb(II), Hg(II), Ni(II), Co(II), Cu(II) and Cd(II). In the next level of study, the hybrid materials with magnetite on its surface can be fabricated as a tool for removal of a wide spectrum of heavy metals as well.

Synthesis of a family of triphenyl groups based on the proposed synthesis methods: The facile method reported for the synthesis and crystallization of triphenyl systems can be used as a key to the synthesis of new trityl based organic systems.

Histidine based nanoassemblies: Histidine nanofibers being conductive can be used as an experimental platform for exploring its possibility as a bioelectronic interface material. Peptide sequences are versatile in nature, hence peptides sequences featuring histidine with various lengths and stereochemistry can be synthesized and characterized for its physical properties. Histidine containing sequences can be fabricated into smart materials as they change conformations at varying pH, concentration and other experimental conditions. The possibility of exploring the potential of imidazole rings to form specific interactions with metal ions, can collaborate different fields of study to design technologically useful products like nanoreactors, nanocatalysts etc. In the future, the fabricated nanoassemblies can be implemented as potential materials for various applications in the field of nanotechnology.

Patents

International Patent Filed

1. Patent No.PCT/IN2018/050452. Dated 13.07.2017. Title: A device for non-invasive treatment of neurodegenerative diseases.

Indian Patents Filed

2. Patent No.243/KOL/2015. Dated 09.03.2015. Title: Generation and usage of Di-histidine based stimulus responsive nanostructures. Published on Oct 2016.
3. Patent No.10258/2016-KOL. Dated 31.03.2016. Title: Magnetic hydrocarbon crystals.

Papers Published in Referred Journals

1. Jahnu Saikia, Gaurav Pandey, **Sajitha Sasidharan**,Ferrin Antony,Harshal B. Nemade, Sachin Kumar,Nitin Chaudhary,and Vibin Ramakrishnan. ACS Chemical Neuroscience. (2019).doi:10.1021/acschemneuro.8b00490. **Publisher**: American Chemical Society

2. **Sajitha Sasidharan**, Shyni P. C., Nitin Chaudhary, and Vibin Ramakrishnan*. Single Crystal Organic Nanofowers. Scientific Reports. (2017), doi:10.1038/s41598-017-17538-0. **Publisher**: Nature Publishing Group

3. Gaurav Pandey, Jahnu Saikia, **Sajitha Sasidharan**, Deep C. Joshi, Subhash Thota, Harshal B. Nemade, Nitin Chaudhary, and Vibin Ramakrishnan*. Modulation of Peptide Based Nano-Assemblies with Electric and Magnetic Fields. Scientific Reports. (2017), doi:10.1038/s41598-017-02609-z. **Publisher**: Nature Publishing Group

4.**Sajitha Sasidharan**, Prakash Kishore Hazam and Vibin Ramakrishnan*. Symmetry Directed Self-Organization in Peptide Nano-Assemblies through Aromatic pi-pi Interactions. The Journal of Physical Chemistry B. (2017) 121, 404−411. DOI: 10.1021/acs.jpcb.6b09474. **Publisher**: American Chemical Society

Conferences and Workshops Attended

List of Conferences Attended

1. Poster Presentation at 6th International Conference on Multifunctional, Hybrid and Nanomaterials organized by Elseviers from 11-15 March 2019 at Meliá Sitges, Sitges, Spain

2. Oral Presentation at the International Conference on Nanotechnology: Ideas, Innovations and Initiatives-2017 organized at IIT Roorkee, India. Title: Hybrid magnetic organic –inorganic nanoadsorbents for sequestration of chromium.

3. Poster presentation at the Institute level in the International Conference on Materials Chemistry (MC13) organized by RSC in Liverpool, United Kingdom from 10-13 July 2017.Title: Magnetically decorated organic nanoflowers.

4. Poster presentation at the Institute level in Research Conclave 2017 held at IIT Guwahati, India.Title: Molecular self-assembly for fabricating nanostructured materials-Design and applications.

5. Poster presentation at the "International Conference on Advances in Biological Systems and Material Science in NanoWorld" (ABSMSNW-2017), held at IIT- BHU, Varanasi, India. Title: Symmetry Directed Self Organization in Peptide Nano-assemblies through Aromatic $\pi - \pi$ Interactions.

Accomplishments

1. Secured 3rd position in Oral Presentation at the International Conference on Nanotechnology: Ideas, Innovations and Initiatives-2017 organized at IIT Roorkee, India.

2. Recipient of the International grant by Department of Science and Technology Travel (SERB – DST) to attend the International Conference on Materials Chemistry (MC13) organized by RSC in Liverpool, United Kingdom from 10-13 July 2017.

3. Secured 2nd position in the poster presentation at the institute level in Research Conclave 2017 held at IIT Guwahati, India.

4. Best Poster award at the "International Conference on Advances in Biological Systems and Material Science in NanoWorld" (ABSMSNW-2017), held at IIT-BHU, Varanasi, India.

BIBLIOGRAPHY

[1] Thirumalai, D., Liu, Z., O'Brien, E. P. & Reddy, G. Protein folding: from theory to practice. Current Opinion in Structural Biology 23, 22-29, (2013).

[2] Drake, S. Discoveries and opinions of Galileo. (Doubleday New York, 1957).

[3] Haesen, S., Nistor, A. I. & Verstraelen, L. On growth and form and geometry. I. Kragujevac Journal of Mathematics 36, 5-25 (2012).

[4] Thompson, D. A. W. *On Growth and Form*. (Cambridge University Press, 1992).

[5] Feynman, R. P. in Handbook of Nanoscience, Engineering, and Technology, Third Edition 26-35 (CRC Press, 2012).

[6] Taniguchi, N., ARAKAWA, C. & KOBAYASHI, T. in Proceedings of the International Conference on Production Engineering, 18-23, 1974-8.

[7] Binnig, G., Rohrer, H., Gerber, C. & Weibel, E. Surface studies by scanning tunneling microscopy. Physical review letters 49, 57 (1982).

[8] Binnig, G., Quate, C. F. & Gerber, C. Atomic force microscope. Physical review letters 56, 930 (1986).

[9] Kroto, H. W., Heath, J. R., O'Brien, S. C., Curl, R. F. & Smalley, R. E. C60: Buckminsterfullerene. Nature 318, 162 (1985).

[10] k Drexler, E. Engines of Creation: The Coming Era of Nanotechnology. (Oxford University Press, 1992).

[11] Sinnokrot, M. O., Valeev, E. F. & Sherrill, C. D. Estimates of the ab initio limit for $\pi - \pi$ interactions: the benzene dimer. Journal of the American Chemical Society 124, 10887-10893, (2002).

[12] Hunter, C. A. & Sanders, J. K. M. The nature of .pi.-.pi. interactions. Journal of the American Chemical Society 112, 5525-5534, (1990).

[13] Rozycka-Sokolowska, E. et al. Triphenylmethanethiol as a Precursor for the Simultaneous Formation of Bis (Triphenylmethyl) Sulfide, Bis (Triphenylmethyl) Trisulfide, and Bis (Triphenylmethyl) Peroxide: Crystal Structures and Hirshfeld Surface Analyses. Phosphorus, Sulfur, and Silicon and the Related Elements 188, 462-468 (2013).

[14] Meyer, E. A., Castellano, R. K. & Diederich, F. Interactions with Aromatic Rings in Chemical and Biological Recognition. Angewandte Chemie International Edition 42, 1210-1250, (2003).

[15] Tamamis, P. et al. Self-assembly of phenylalanine oligopeptides: insights from experiments and simulations. Biophysical journal 96, 5020-5029 (2009).

[16] Teow, Y., Asharani, P. V., Hande, & M. P. Valiyaveettil, S. Health impact and safety of engineered nanomaterial. *Chemical Communications* 47, 7025-7038, (2011).

[17] Claessens, C. G. & Stoddart, J. F. π–π interactions in self-assembly. Journal of Physical Organic

Chemistry 10, 254-272, (1997).

[18] Gillard, R. E., Raymo, F. M. & Stoddart, J. F. Controlling Self-Assembly. Chemistry – A European Journal 3, 1933-1940, (1997).

[19] Matta, C. F., Castillo, N. & Boyd, R. J. Extended Weak Bonding Interactions in DNA: π-Stacking (Base−Base), Base−Backbone, and Backbone−Backbone Interactions. The Journal of Physical Chemistry B 110, 563-578, (2006).

[20] McGaughey, G. B., Gagne, M. & Rappe, A. K. pi-Stacking interactions. Alive and well in proteins. The Journal of biological chemistry 273, 15458-15463 (1998).

[21] Collings, P. J. Liquid crystals: nature's delicate phase of matter. (Princeton University Press, 2002).

[22] Yan, X., Zhu, P. & Li, J. Self-assembly and application of diphenylalanine-based nanostructures. Chemical Society Reviews 39, 1877-1890, (2010).

[23] Waters, M. L. Aromatic interactions in model systems. Current Opinion in Chemical Biology 6, 736-741, (2002).

[24] Geng, Y., Li, H.-B., Wu, S.-X. & Su, Z.-M. The interplay of intermolecular interactions, packing motifs and electron transport properties in perylene diimide related materials: a theoretical perspective. Journal of Materials Chemistry 22, 20840-20851, (2012).

[25] Rest, C., Kandanelli, R. & Fernández, G. Strategies to create hierarchical self-assembled structures via cooperative non-covalent interactions. Chemical Society Reviews 44, 2543-2572, (2015).

[26] Haino, T., Fujii, T., Watanabe, A. & Takayanagi, U. Supramolecular polymer formed by reversible self-assembly of tetrakisporphyrin. Proceedings of the National Academy of Sciences 106, 10477-10481, (2009).

[27] Toledano, S., Williams, R. J., Jayawarna, V. & Ulijn, R. V. Enzyme-Triggered Self-Assembly of Peptide Hydrogels via Reversed Hydrolysis. Journal of the American Chemical Society 128, 1070-1071, (2006).

[28] Hunter, C. A., Lawson, K. R., Perkins, J. & Urch, C. J. Aromatic interactions. Journal of the Chemical Society, Perkin Transactions 2, 651-669, (2001).

[29] Anslyn, E. V. & Dougherty, D. A. Modern physical organic chemistry. (University science books, 2006).

[30] Sun, S. & Bernstein, E. R. Aromatic van der Waals Clusters: Structure and Nonrigidity. The Journal of Physical Chemistry 100, 13348-13366, (1996).

[31] Li, Z.-T.& Wu, L.-Z. Hydrogen bonded supramolecular structures. Vol. 87 (Springer, 2015).

[32] Palma, M. et al. Self-assembly of hydrogen-bond assisted supramolecular azatriphenylene architectures. Soft Matter 4, 303-310, (2008).

[33] Grimsdale, A. C. & Mullen, K. The chemistry of organic nanomaterials. Angewandte Chemie (International ed. in English) 44, 5592-5629, (2005).

[34] Sorrenti, A., Illa, O. & Ortuno, R. M. Amphiphiles in aqueous solution: well beyond a soap bubble. Chem Soc Rev 42, 8200-8219, (2013).

[35] Lin, Y. et al. Rationally designed helical nanofibers via multiple non-covalent interactions: fabrication and modulation. Soft Matter 6, 2031-2036, (2010).

[36] Zhang, G.& Liu, M. Interfacial Assemblies of Cyanine Dyes and Gemini Amphiphiles with Rigid Spacers: Regulation and Interconversion of the Aggregates. The Journal of Physical Chemistry B 112, 7430-7437, (2008).

[37] Gillissen, M. A. J. et al. Triple Helix Formation in Amphiphilic Discotics: Demystifying Solvent Effects in Supramolecular Self-Assembly. Journal of the American Chemical Society 136, 336-343, (2014).

[38] Fernández, G., García, F. & Sánchez, L. Morphological changes in the self-assembly of a radial oligo-phenylene ethynylene amphiphilic system. Chemical Communications, 6567-6569, (2008).

[39] Gomberg, M. An Instance of Trivalent Carbon: Triphenylmethyl. Journal of the American Chemical Society22, 757-771 (1900).

[40] Sasidharan, S., P. C, S., Chaudhary, N. & Ramakrishnan, V. Single Crystal Organic Nanoflowers. Scientific Reports 7, 17335, (2017).

[41] Singh, W. P. & Singh, R. S. A new class of organogelators based on triphenylmethyl derivatives of primary alcohols: hydrophobic interactions alone can mediate gelation. Beilstein journal of organic chemistry 13, 138-149, (2017).

[42] Buhleier, E., Wehner, W. & Vögtle,F. ' CASCADE'-AND′ NONSKID-CHAIN-LIKE' SYNTHESES OF MOLECULAR CAVITY TOPOLOGIES. Chemischer Informationsdienst 9, no-no,(1978).

[43] Bosman, A. W., Janssen, H. M. & Meijer, E. W. About Dendrimers: Structure, Physical Properties, and Applications. Chemical Reviews 99, 1665-1688, (1999).

[44] Hawker, C. & Fréchet, J. M. J. A new convergent approach to monodisperse dendritic macromolecules. Journal of the Chemical Society, Chemical Communications, 1010-1013, (1990).

[45] Hawker, C. J. & Frechet, J. M. J. Preparation of polymers with controlled molecular architecture. A new convergent approach to dendritic macromolecules. Journal of the American Chemical Society 112, 7638-7647, (1990).

[46] Boas, U. & Heegaard, P. M. Dendrimers in drug research. Chemical Society Reviews 33, 43-63 (2004).

[47] Hawker, C. J., Wooley, K. L. & Fréchet, J. M. J. Unimolecular micelles and globular amphiphiles: dendritic macromolecules as novel recyclable solubilization agents. Journal of the Chemical Society, Perkin Transactions 1, 1287-1297, (1993).

[48] Wallimann, P., Seiler, P. & Diederich, F. Dendrophanes: Novel Steroid-Recognizing Dendritic Receptors. Preliminary Communication. Helvetica Chimica Acta 79, 779-788, (1996).

[49] Wallimann, P., Marti, T., Fürer, A. & Diederich, F. Steroids in Molecular Recognition. Chemical Reviews 97, 1567-1608, (1997).

[50] Seo, M. et al. Self-Association of Bis-Dendritic Organogelators: The Effect of Dendritic Architecture on Multivalent Cooperative Interactions. Chemistry – A European Journal 16, 2427-2441, (2010).

[51] Wang, W. et al. Dynamic $\pi - \pi$ Stacked Molecular Assemblies Emit from Green to Red Colors. Nano Letters 3, 455-458, (2003).

[52] Grice, A. W. et al. High brightness and efficiency blue light-emitting polymer diodes. Applied Physics Letters 73, 629-631, (1998).

[53] S. S., Praveen, V. K. & Ajayaghosh, A. Functional π-Gelators and Their Applications. Chemical Reviews 114, 1973-2129, (2014).

[54] Yoon, S. M., Hwang, I.-C., Kim, K. S. & Choi, H. C. Synthesis of Single-Crystal Tetra(4-pyridyl)porphyrin Rectangular Nanotubes in the Vapor Phase. Angewandte Chemie International Edition 48, 2506-2509, (2009).

[55] Yin, S., Song, B., Liu, G., Wang, Z. & Zhang, X. Self-Organization of Polymerizable Bolaamphiphiles Bearing Diacetylene Mesogenic Group. Langmuir 23, 5936-5941, (2007).

[56] Surin, M. et al. Correlation between the Microscopic Morphology and the Solid-State Photoluminescence Properties in Fluorene-Based Polymers and Copolymers. Chemistry of Materials 16, 994-1001, (2004).

[57] Yan, P., Chowdhury, A., Holman, M. W. & Adams, D. M. Self-Organized Perylene Diimide Nanofibers. The Journal of Physical Chemistry B 109, 724-730, (2005).

[58] Wang, Z., Li, Z., Medforth, C. J. & Shelnutt, J. A. Self-Assembly and Self-Metallization of Porphyrin Nanosheets. Journal of the American Chemical Society 129, 2440-2441, (2007).

[59] Atula, S. Sonication-assisted supramolecular nanorods of meso-diaryl-substituted porphyrins. Chemical Communications, 724-726 (2008).

[60] Sirringhaus, H. et al. Two-dimensional charge transport in self-organized, high-mobility conjugated polymers. Nature 401, 685 (1999).

[61] Berl, V., Huc, I., Khoury, R. G., Krische, M. J. & Lehn, J.-M. Interconversion of single and double helices formed from synthetic molecular strands. Nature 407, 720, (2000).

[62] Zubarev, E. R., Pralle, M. U., Sone, E. D. & Stupp, S. I. Self-Assembly of Dendron Rodcoil Molecules into Nanoribbons. Journal of the American Chemical Society 123, 4105-4106, (2001).

[63] Desiraju, G. R. Supramolecular Synthons in Crystal Engineering—A New Organic Synthesis. Angewandte Chemie International Edition in English 34, 2311-2327, (1995).

[64] Leiserowitz, L. Molecular packing modes. Carboxylic acids. Acta Crystallographica Section B 32, 775-802, (1976).

[65] Cubberley, M. S. & Iverson, B. L. 1H NMR Investigation of Solvent Effects in Aromatic Stacking Interactions. Journal of the American Chemical Society 123, 7560-7563, (2001).

[66] Sindkhedkar, M. D., Mulla, H. R. & Cammers-Goodwin, A. Three-State, Conformational Probe for Hydrophobic, π-Stacking Interactions in Aqueous and Mixed Aqueous Solvent Systems: Anisotropic Solvation of Aromatic Rings. Journal of the American Chemical Society 122, 9271-9277, (2000).

[67] Shetty, A. S., Zhang, J. & Moore, J. S. Aromatic π-Stacking in Solution as Revealed through the Aggregation of Phenylacetylene Macrocycles. Journal of the American Chemical Society 118, 1019-1027, (1996).

[68] Qiu, Y., Chen, P. & Liu, M. Evolution of Various Porphyrin Nanostructures via an Oil/Aqueous Medium: Controlled Self-Assembly, Further Organization, and Supramolecular Chirality. Journal of the American Chemical Society 132, 9644-9652, (2010).

[69] Zang, L., Che, Y. & Moore, J. S. One-Dimensional Self-Assembly of Planar π-Conjugated Molecules: Adaptable Building Blocks for Organic Nanodevices. Accounts of Chemical Research 41, 1596-1608, 2008).

[70] Kasai, H. et al. A novel preparation method of organic microcrystals. Japanese Journal of Applied Physics 31, L1132 (1992).

[71] Nalwa, H. S. et al. Fabrication of organic nanocrystals for electronics and photonics. Advanced Materials 5, 758-760, (1993).

[72] Fu, H.-B. & Yao, J.-N. Size Effects on the Optical Properties of Organic Nanoparticles. Journal of the

American Chemical Society 123, 1434-1439, (2001).

[73] Xiao, D. et al. Size-Tunable Emission from 1,3-Diphenyl-5-(2-anthryl)-2-pyrazoline Nanoparticles. Journal of the American Chemical Society 125, 6740-6745, (2003).

[74] Ariga, K., Lvov, Y. & Kunitake, T. Assembling Alternate Dye−Polyion Molecular Films by Electrostatic Layer-by-Layer Adsorption. Journal of the American Chemical Society 119, 2224-2231, (1997).

[75] Wang, Y., Tang, Z., Correa-Duarte, M. A., Liz-Marzán, L. M. & Kotov, N. A. Multicolor Luminescence Patterning by Photoactivation of Semiconductor Nanoparticle Films. Journal of the American Chemical Society 125, 2830-2831, (2003).

[76] Park, J. & Hammond, P. T. Multilayer Transfer Printing for Polyelectrolyte Multilayer Patterning: Direct Transfer of Layer-by-Layer Assembled Micropatterned Thin Films. Advanced Materials 16, 520-525, (2004).

[77] Wang, B. & Rusling, J. F. Voltammetric Sensor for Chemical Toxicity Using [Ru(bpy)$_2$poly(4-vinylpyridine)$_{10}$Cl)]$^+$ as Catalyst in Ultrathin Films. DNA Damage from Methylating Agents and an Enzyme-Generated Epoxide. Analytical Chemistry 75, 4229-4235, (2003).

[78] Hiller, J. A., Mendelsohn, J. D. & Rubner, M. F. Reversibly erasable nanoporous anti-reflection coatings from polyelectrolyte multilayers. Nature Materials 1, 59, (2002).

[79] Van Patten, P. G., Shreve, A. P. & Donohoe, R. J. Structural and Photophysical Properties of a Water-Soluble Porphyrin Associated with Polycations in Solution and Electrostatically-Assembled Ultrathin Films. The Journal of Physical Chemistry B 104, 5986-5992, (2000).

[80] Dobrawa, R., Lysetska, M., Ballester, P., Grüne, M. & Würthner, F. Fluorescent Supramolecular Polymers: Metal Directed Self-Assembly of Perylene Bisimide Building Blocks. Macromolecules 38, 1315-1325, (2005).

[81] Tang, T., Qu, J., Müllen, K. & Webber, S. E. Molecular Layer-by-Layer Self-Assembly of Water-Soluble Perylene Diimides through $\pi-\pi$ and Electrostatic Interactions. Langmuir 22, 26-28, (2006).

[82] Nelson, S. F., Lin, Y.-Y., Gundlach, D. J. & Jackson, T. N. Temperature-independent transport in high-mobility pentacene transistors. Applied Physics Letters 72, 1854-1856, (1998).

[83] Podzorov, V., Sysoev, S. E., Loginova, E., Pudalov, V. M. & Gershenson, M. E. Single-crystal organic field effect transistors with the hole mobility ≈8 cm^2/Vs. Applied Physics Letters 83, 3504-3506, (2003).

[84] Mas-Torrent, M., Durkut, M., Hadley, P., Ribas, X. & Rovira, C. High Mobility of Dithiophene-Tetrathiafulvalene Single-Crystal Organic Field Effect Transistors. Journal of the American Chemical Society 126, 984-985, s(2004).

[85] Sirringhaus, H., Tessler, N. & Friend, R. H. Integrated optoelectronic devices based on conjugated polymers. Science 280, 1741-1744 (1998).

[86] Bao, Z., Dodabalapur, A. & Lovinger, A. J. Soluble and processable regioregular poly(3-hexylthiophene) for thin film field-effect transistor applications with high mobility. Applied Physics Letters 69, 4108-4110, (1996).

[87] Horowitz, G. Field-effect transistors based on short organic molecules. Journal of Materials Chemistry 9, 2021-2026 (1999).

[88] Lanzani, G., Cerullo, G., Stagira, S., Silvestri, S. D. & Garnier, F. Ultrafast spectroscopy of dark states

in solid state sexithiophene. The Journal of Chemical Physics 111, 6474-6480, (1999).

[89] Taur, Y. & Ning, T. H. Fundamentals of modern VLSI devices. (Cambridge university press, 2013).

[90] Datar, A. et al. Linearly Polarized Emission of an Organic Semiconductor Nanobelt. The Journal of Physical Chemistry B 110, 12327-12332, (2006).

[91] Schwab, A. D. et al. Photoconductivity of Self-Assembled Porphyrin Nanorods. Nano Letters 4, 1261-1265, (2004).

[92] Schenning, A. P. H. J. & Meijer, E. W. Supramolecular electronics; nanowires from self-assembled π-conjugated systems. Chemical Communications, 3245-3258, (2005).

[93] Grem, G., Leditzky, G., Ullrich, B. & Leising, G. Blue electroluminescent device based on a conjugated polymer. Synthetic Metals 51, 383-389, (1992).

[94] Hepp, A. et al. Light-emitting field-effect transistor based on a tetracene thin film. Phys Rev Lett 91, 157406, (2003).

[95] Gazit, E. A possible role for pi-stacking in the self-assembly of amyloid fibrils. Faseb j 16, 77-83, (2002).

[96] Reches, M. & Gazit, E. Casting Metal Nanowires Within Discrete Self-Assembled Peptide Nanotubes. Science 300, 625-627, (2003).

[97] Reches, M. & Gazit, E. Formation of Closed-Cage Nanostructures by Self-Assembly of Aromatic Dipeptides. Nano Letters 4, 581-585, (2004).

[98] Meital, R. & Ehud, G. Designed aromatic homo-dipeptides: formation of ordered nanostructures and potential nanotechnological applications. Physical Biology3, S10 (2006).

[99] Kool, E. T. Hydrogen bonding, base stacking, and steric effects in dna replication. Annu Rev Biophys Biomol Struct 30, 1-22, (2001).

[100] Shiels, J. C., Tuite, J. B., Nolan, S. J. & Baranger, A. M. Investigation of a conserved stacking interaction in target site recognition by the U1A protein. Nucleic Acids Res 30, 550-558 (2002).

[101] Nolan, S. J., Shiels, J. C., Tuite, J. B., Cecere, K. L. & Baranger, A. M. Recognition of an Essential Adenine at a Protein−RNA Interface: Comparison of the Contributions of Hydrogen Bonds and a Stacking Interaction. Journal of the American Chemical Society 121, 8951-8952, (1999).

[102] Gazit, E. Self-assembled peptide nanostructures: the design of molecular building blocks and their technological utilization. Chemical Society Reviews 36, 1263-1269 (2007).

[103] Guler, M. O. & Stupp, S. I. A Self-Assembled Nanofiber Catalyst for Ester Hydrolysis. Journal of the American Chemical Society 129, 12082-12083, (2007).

[104] Ulijn, R. V. & Smith, A. M. Designing peptide based nanomaterials. Chemical Society Reviews 37, 664-675, (2008).

[105] Andersen, N. H. Protein Structure, Stability, and Folding. Methods in Molecular Biology. Volume 168 Edited by Kenneth P. Murphy (University of Iowa College of Medicine). Humana Press: Totowa, New Jersey. 2001. ISBN 0-89603-682-0. Journal of the American Chemical Society 123, 12933-12934, (2001).

[106] Kahn, S. E., Andrikopoulos, S. & Verchere, C. B. Islet amyloid: a long-recognized but underappreciated pathological feature of type 2 diabetes. Diabetes 48, 241-253 (1999).

[107] Tenidis, K. et al. Identification of a penta- and hexapeptide of islet amyloid polypeptide (IAPP) with

amyloidogenic and cytotoxic properties. J Mol Biol 295, 1055-1071, (2000).

[108] Kayed, R. et al. Conformational transitions of islet amyloid polypeptide (IAPP) in amyloid formation in vitro. J Mol Biol 287, 781-796, (1999).

[109] Azriel, R. & Gazit, E. Analysis of the minimal amyloid-forming fragment of the islet amyloid polypeptide. An experimental support for the key role of the phenylalanine residue in amyloid formation. The Journal of biological chemistry 276, 34156-34161, (2001).

[110] Tjernberg, L. O. et al. Arrest of beta-amyloid fibril formation by a pentapeptide ligand. The Journal of biological chemistry 271, 8545-8548 (1996).

[111] Findeis, M. A. et al. Modified-peptide inhibitors of amyloid beta-peptide polymerization. Biochemistry 38, 6791-6800,(1999).

[112] Soto, C. et al. Beta-sheet breaker peptides inhibit fibrillogenesis in a rat brain model of amyloidosis: implications for Alzheimer's therapy. Nature medicine 4, 822-826 (1998).

[113] Balbach, J. J. et al. Amyloid fibril formation by A beta 16-22, a seven-residue fragment of the Alzheimer's beta-amyloid peptide, and structural characterization by solid state NMR. Biochemistry 39, 13748-13759 (2000).

[114] Haggqvist, B. et al. Medin: an integral fragment of aortic smooth muscle cell-produced lactadherin forms the most common human amyloid. Proc Natl Acad Sci U S A 96, 8669-8674 (1999).

[115] Han, H., Weinreb, P. H. & Lansbury, P. T., Jr. The core Alzheimer's peptide NAC forms amyloid fibrils which seed and are seeded by beta-amyloid: is NAC a common trigger or target in neurodegenerative disease? Chemistry & biology 2, 163-169 (1995).

[116] Kedar, I., Ravid, M. & Sohar, E. In vitro synthesis of "amyloid"fibrils from insulin, calcitonin and parathormone. Israel journal of medical sciences 12, 1137-1140 (1976).

[117] Benvenga, S., Trimarchi, F.& Facchiano, A. Homology of calcitonin with the amyloid-related proteins. Journal of endocrinological investigation 17, 119-122, (1994).

[118] Vidal, R. et al. A stop-codon mutation in the BRI gene associated with familial British dementia. Nature 399, 776, (1999).

[119] Ciunik, Z., Berski, S., Latajka, Z. & Leszczyński, J. New aspects of weak C-H$\cdots$ π bonds: intermolecular interactions between alicyclic and aromatic rings in crystals of small compounds, peptides and proteins. Journal of molecular structure 442, 125-134 (1998).

[120] Burley, S. & Petsko, G. A. Aromatic-aromatic interaction: a mechanism of protein structure stabilization. Science 229, 23-28 (1985).

[121] Sasidharan, S., Hazam, P. K. & Ramakrishnan, V. Symmetry-Directed Self-Organization in Peptide Nanoassemblies through Aromatic π–π Interactions. The Journal of Physical Chemistry B 121, 404-411, (2017).

[122] Pauling, L. & Corey, R. B. The pleated sheet, a new layer configuration of polypeptide chains. Proc Natl Acad Sci U S A 37, 251-256 (1951).

[123] Zhang, S., Holmes, T., Lockshin, C. & Rich, A. Spontaneous assembly of a self-complementary oligopeptide to form a stable macroscopic membrane. Proceedings of the National Academy of Sciences 90, 3334-3338 (1993).

[124] Chiti, F. & Dobson, C. M. Protein misfolding, functional amyloid, and human disease. Annu. Rev.

Biochem. 75, 333-366 (2006).

[125] Aggeli, A. et al. Hierarchical self-assembly of chiral rod-like molecules as a model for peptide β-sheet tapes, ribbons, fibrils, and fibers. Proceedings of the National Academy of Sciences 98, 11857-11862 (2001).

[126] Caplan, M. R., Schwartzfarb, E. M., Zhang, S., Kamm, R. D. & Lauffenburger, D. A. Control of self-assembling oligopeptide matrix formation through systematic variation of amino acid sequence. Biomaterials 23, 219-227 (2002).

[127] Maity, S., Hashemi, M. & Lyubchenko, Y. L. Nano-assembly of amyloid β peptide: role of the hairpin fold. Scientific Reports 7, 2344, (2017).

[128] Matsuura, K., Hayashi, H., Murasato, K. & Kimizuka, N. Trigonal tryptophane zipper as a novel building block for pH-responsive peptide nano-assemblies. Chemical Communications 47, 265-267, (2011).

[129] Aggeli, A. et al. Responsive gels formed by the spontaneous self-assembly of peptides into polymeric β-sheet tapes. Nature 386, 259, (1997).

[130] Crick, F. The packing of [alpha]-helices: simple coiled-coils. Acta Crystallographica 6, 689-697, (1953).

[131] Pauling, L. & Corey, R. B. Compound Helical Configurations of Polypeptide Chains: Structure of Proteins of the α-Keratin Type. Nature 171, 59, (1953).

[132] Aravinda, S. et al. Aromatic-aromatic interactions in crystal structures of helical peptide scaffolds containing projecting phenylalanine residues. Journal of the American Chemical Society 125, 5308-5315 (2003).

[133] Zhao, X. & Zhang, S. Molecular designer self-assembling peptides. Chemical Society Reviews 35, 1105-1110, (2006).

[134] Ranganathan, D., Haridas, V. & Karle, I. L. Cystinophanes, a Novel Family of Aromatic-Bridged Cystine Cyclic Peptides: Synthesis, Crystal Structure, Molecular Recognition, and Conformational Studies. Journal of the American Chemical Society 120, 2695-2702, (1998).

[135] Ranganathan, D., Haridas, V., Gilardi, R. & Karle, I. L. Self-Assembling Aromatic-Bridged Serine-Based Cyclodepsipeptides (Serinophanes): A Demonstration of Tubular Structures Formed through Aromatic $\pi - \pi$ Interactions. Journal of the American Chemical Society 120, 10793-10800, (1998).

[136] Yang, Z., Chiu, T.-C. & Chang, H.-T. Preparation and Characterization of Different Shapes of Silver Nanostructures in Aqueous Solution. The Open Nanoscience Journal 1, 5-12, (2007).

[137] Kol, N. et al. Self-assembled peptide nanotubes are uniquely rigid bioinspired supramolecular structures. Nano letters 5, 1343-1346 (2005).

[138] Reches, M. & Gazit, E. Controlled patterning of aligned self-assembled peptide nanotubes. Nature nanotechnology 1, 195 (2006).

[139] Adler-Abramovich, L. et al. Self-assembled arrays of peptide nanotubes by vapor deposition. Nature nanotechnology 4, 849 (2009).

[140] Yan, X. et al. Reversible transitions between peptide nanotubes and vesicle-like structures including theoretical modeling studies. Chemistry 14, 5974-5980, (2008).

[141] Ryu, J. & Park, C. B. Solid-Phase Growth of Nanostructures from Amorphous Peptide Thin Film:

Effect of Water Activity and Temperature. Chemistry of Materials 20, 4284-4290, (2008).

[142] Dudukovic, N. A. & Zukoski, C. F. Gelation of Fmoc-diphenylalanine is a first order phase transition. Soft Matter 11, 7663-7673 (2015).

[143] Mahler, A., Reches, M., Rechter, M., Cohen, S. & Gazit, E. Rigid, Self-Assembled Hydrogel Composed of a Modified Aromatic Dipeptide. Advanced Materials 18, 1365-1370, (2006).

[144] Reches, M. & Gazit, E. Self-assembly of peptide nanotubes and amyloid-like structures by charged-termini-capped diphenylalanine peptide analogues. Israel Journal of Chemistry 45, 363-371, (2010).

[145] Song, Y. et al. Synthesis of peptide-nanotube platinum-nanoparticle composites. Chemical Communications, 1044-1045, (2004).

[146] Krysmann, M. J. et al. Self-assembly and hydrogelation of an amyloid peptide fragment. Biochemistry 47, 4597-4605 (2008).

[147] Reches, M., Porat, Y. & Gazit, E. Amyloid fibril formation by pentapeptide and tetrapeptide fragments of human calcitonin. Journal of Biological Chemistry 277, 35475-35480 (2002).

[148] Jayawarna, V. et al. Nanostructured Hydrogels for Three-Dimensional Cell Culture Through Self-Assembly of Fluorenylmethoxycarbonyl–Dipeptides. Advanced Materials 18, 611-614, (2006).

[149] Jayawarna, V. et al. Introducing chemical functionality in Fmoc-peptide gels for cell culture. Acta Biomaterialia 5, 934-943, (2009).

[150] Yang, Z., Liang, G. & Xu, B. Enzymatic Hydrogelation of Small Molecules. Accounts of Chemical Research 41, 315-326, (2008).

[151] Zhao, F., Ma, M. L. & Xu, B. Molecular hydrogels of therapeutic agents. Chemical Society Reviews 38, 883-891, (2009).

[152] Fleming, S. & Ulijn, R. V. Design of nanostructures based on aromatic peptide amphiphiles. Chemical Society Reviews 43, 8150-8177, (2014).

[153] Valéry, C. et al. Biomimetic organization: Octapeptide self-assembly into nanotubes of viral capsid-like dimension. Proceedings of the National Academy of Sciences of the United States of America 100, 10258-10262, (2003).

[154] De Santis, P., Forni, E. & Rizzo, R. Conformational analysis of DNA–basic polypeptide complexes: Possible models of nucleoprotamines and nucleohistones. Biopolymers: Original Research on Biomolecules 13, 313-326 (1974).

[155] Ghadiri, M. R., Granja, J. R., Milligan, R. A., McRee, D. E. & Khazanovich, N. Self-assembling organic nanotubes based on a cyclic peptide architecture. Nature 366, 324-327 (1993).

[156] Ghadiri, M. R., Granja, J. R. & Buehler, L. K. Artificial transmembrane ion channels from self-assembling peptide nanotubes. Nature 369, 301-304, (1994).

[157] Horne, W. S., Ashkenasy, N. & Ghadiri, M. R. Modulating Charge Transfer Through Cyclic D,L α-Peptide Self-Assembly. Chemistry (Weinheim an der Bergstrasse, Germany) 11, 1137-1144, (2005).

[158] Chapman, R., Danial, M., Koh, M. L., Jolliffe, K. A. & Perrier, S. Design and properties of functional nanotubes from the self-assembly of cyclic peptide templates. Chemical Society Reviews 41, 6023-6041, (2012).

[159] Silva, R. F., Araújo, D. R., Silva, E. R., Ando, R. A. & Alves, W. A. l-Diphenylalanine Microtubes As a Potential Drug-Delivery System: Characterization, Release Kinetics, and Cytotoxicity. Langmuir

29, 10205-10212, (2013).

[160] Görbitz, C. H. The structure of nanotubes formed by diphenylalanine, the core recognition motif of Alzheimer's β-amyloid polypeptide. Chemical Communications, 2332-2334, (2006).

[161] Görbitz, C. H. Nanotube Formation by Hydrophobic Dipeptides. Chemistry – A European Journal 7, 5153-5159, (2001).

[162] Carny, O., Shalev, D. E. & Gazit, E. Fabrication of Coaxial Metal Nanocables Using a Self-Assembled Peptide Nanotube Scaffold. Nano Letters 6, 1594-1597, (2006).

[163] Adler-Abramovich, L. et al. Thermal and Chemical Stability of Diphenylalanine Peptide Nanotubes: Implications for Nanotechnological Applications. Langmuir 22, 1313-1320, (2006).

[164] Lu, K., Jacob, J., Thiyagarajan, P., Conticello, V. P. & Lynn, D. G. Exploiting Amyloid Fibril Lamination for Nanotube Self-Assembly. Journal of the American Chemical Society 125, 6391-6393, (2003).

[165] Lu, K. et al. Macroscale assembly of peptide nanotubes. Chemical Communications, 2729-2731, (2007).

[166] Huang, R., Qi, W., Su, R., Zhao, J. & He, Z. Solvent and surface controlled self-assembly of diphenylalanine peptide: from microtubes to nanofibers. Soft Matter 7, 6418-6421, (2011).

[167] Huang, R., Wang, Y., Qi, W., Su, R. & He, Z. Temperature-induced reversible self-assembly of diphenylalanine peptide and the structural transition from organogel to crystalline nanowires. Nanoscale Research Letters 9, 653-653, (2014).

[168] Yan, X., Cui, Y., He, Q., Wang, K. & Li, J. Organogels Based on Self-Assembly of Diphenylalanine Peptide and Their Application To Immobilize Quantum Dots. Chemistry of Materials 20, 1522-1526, (2008).

[169] Yang, Z., Gu, H., Zhang, Y., Wang, L. & Xu, B. Small molecule hydrogels based on a class of antiinflammatory agents. Chemical Communications, 208-209, (2004).

[170] Jayawarna, V., Smith, A., Gough, J. E. & Ulijn, R. V. Three-dimensional cell culture of chondrocytes on modified di-phenylalanine scaffolds. Biochemical Society Transactions 35, 535-537, (2007).

[171] Smith, A. M. et al. Fmoc-Diphenylalanine Self Assembles to a Hydrogel via a Novel Architecture Based on $\pi - \pi$ Interlocked β-Sheets. Advanced Materials 20, 37-41, (2008).

[172] Bowerman, C. J. & Nilsson, B. L. A Reductive Trigger for Peptide Self-Assembly and Hydrogelation. Journal of the American Chemical Society 132, 9526-9527, (2010).

[173] Mishra, A., Panda, J. J., Basu, A. & Chauhan, V. S. Nanovesicles Based on Self-Assembly of Conformationally Constrained Aromatic Residue Containing Amphiphilic Dipeptides. Langmuir 24, 4571-4576, (2008).

[174] Mishra, A. & Chauhan, V. S. Probing the role of aromaticity in the design of dipeptide based nanostructures. Nanoscale 3, 945-949, (2011).

[175] Lange, S. C. et al. pH response and molecular recognition in a low molecular weight peptide hydrogel. Organic & Biomolecular Chemistry 13, 561-569, (2015).

[176] Raeburn, J. et al. Fmoc-diphenylalanine hydrogels: understanding the variability in reported mechanical properties. Soft Matter 8, 1168-1174, (2012).

[177] Reddy, S. M., Shanmugam, G., Duraipandy, N., Kiran, M. S. & Mandal, A. B. An additional flu-

orenylmethoxycarbonyl (Fmoc) moiety in di-Fmoc-functionalized L-lysine induces pH-controlled ambidextrous gelation with significant advantages. Soft Matter 11, 8126-8140, (2015).

[178] Ulijn, R. V. Enzyme-responsive materials: a new class of smart biomaterials. Journal of Materials Chemistry 16, 2217-2225, (2006).

[179] Yang, Z., Liang, G., Wang, L. & Xu, B. Using a Kinase/Phosphatase Switch to Regulate a Supramolecular Hydrogel and Forming the Supramolecular Hydrogel in Vivo. Journal of the American Chemical Society 128, 3038-3043, (2006).

[180] Das, A. K., Collins, R. & Ulijn, R. V. Exploiting Enzymatic (Reversed) Hydrolysis in Directed Self-Assembly of Peptide Nanostructures. Small 4, 279-287, (2008).

[181] Pauling, L. The Diamagnetic Anisotropy of Aromatic Molecules. The Journal of Chemical Physics 4, 673-677, (1936).

[182] Worcester, D. L. Structural origins of diamagnetic anisotropy in proteins. Proceedings of the National Academy of Sciences 75, 5475-5477, (1978).

[183] Pauling, L. Diamagnetic anisotropy of the peptide group. Proceedings of the National Academy of Sciences 76, 2293-2294, (1979).

[184] Inouye, H., Fraser, P. E. & Kirschner, D. A. Structure of beta-crystallite assemblies formed by Alzheimer beta-amyloid protein analogues: analysis by x-ray diffraction. Biophysical Journal 64, 502-519, (1993).

[185] A. Hill, R. J. et al. Alignment of Aromatic Peptide Tubes in Strong Magnetic Fields. Advanced Materials 19, 4474-4479, (2007).

[186] Creasey, R. C. G., Shingaya, Y. & Nakayama, T. Improved electrical conductance through self-assembly of bioinspired peptides into nanoscale fibers. Materials Chemistry and Physics 158, 52-59, (2015).

[187] Ing, N. L. & Spencer, R. K. Electronic Conductivity in Biomimetic alpha-Helical Peptide Nanofibers and Gels. 12, 2652-2661, (2018).

[188] Adler-Abramovich, L. & Gazit, E. The physical properties of supramolecular peptide assemblies: from building block association to technological applications. Chemical Society Reviews 43, 6881-6893, (2014).

[189] Ryu, J., Lim, S. Y. & Park, C. B. Photoluminescent Peptide Nanotubes. Advanced Materials 21, 1577-1581, (2009).

[190] Smith, J. F., Knowles, T. P. J., Dobson, C. M., MacPhee, C. E. & Welland, M. E. Characterization of the nanoscale properties of individual amyloid fibrils. Proceedings of the National Academy of Sciences 103, 15806-15811, (2006).

[191] Sedman, V. L. et al. Tuning the mechanical properties of self-assembled mixed-peptide tubes. Journal of microscopy 249, 165-172, (2013).

[192] Kuner, P. et al. Controlling polymerization of β-amyloid and prion-derived peptides with synthetic small molecule ligands. Journal of Biological Chemistry 275, 1673-1678 (2000).

[193] Twyman, L. J. & Allsop, D. A short synthesis of the β-amyloid (Aβ) aggregation inhibitor 3-p-toluoyl-2-[4′-(3-diethylaminopropoxy)-phenyl]-benzofuran. Tetrahedron Letters 40, 9383-9384 (1999).

[194] Lorenzo, A. & Yankner, B. A. Beta-amyloid neurotoxicity requires fibril formation and is inhibited

by congo red. Proceedings of the National Academy of Sciences 91, 12243-12247 (1994).

[195] Merlini, G. et al. Interaction of the anthracycline 4'-iodo-4'-deoxydoxorubicin with amyloid fibrils: inhibition of amyloidogenesis. Proc Natl Acad Sci U S A 92, 2959-2963 (1995).

[196] Zhou, M., Ulijn, R. V. & Gough, J. E. Extracellular matrix formation in self-assembled minimalistic bioactive hydrogels based on aromatic peptide amphiphiles. Journal of tissue engineering 5, 2041731414531593-2041731414531593, (2014).

[197] Laromaine, A., Koh, L., Murugesan, M., Ulijn, R. V. & Stevens, M. M. Protease-Triggered Dispersion of Nanoparticle Assemblies. Journal of the American Chemical Society 129, 4156-4157, (2007).

[198] Yemini, M., Reches, M., Gazit, E. & Rishpon, J. Peptide Nanotube-Modified Electrodes for Enzyme−Biosensor Applications. Analytical Chemistry 77, 5155-5159, (2005).

[199] Khalily, M. A., Ustahuseyin, O., Garifullin, R., Genc, R. & Guler, M. O. A supramolecular peptide nanofiber templated Pd nanocatalyst for efficient Suzuki coupling reactions under aqueous conditions. Chemical Communications 48, 11358-11360, (2012).

[200] Banerjee, I. A., Yu, L. & Matsui, H. Cu nanocrystal growth on peptide nanotubes by biomineralization: Size control of Cu nanocrystals by tuning peptide conformation. Proceedings of the National Academy of Sciences 100, 14678-14682, (2003).

[201] Battaglia, M., Buckingham, A. & Williams, J. The electric quadrupole moments of benzene and hexafluorobenzene. Chemical Physics Letters 78, 421-423 (1981).

[202] Ramakrishnan, C. & Ramachandran, G. N. Stereochemical Criteria for Polypeptide and Protein Chain Conformations: II. Allowed Conformations for a Pair of Peptide Units. Biophysical Journal 5, 909-933, (1965).

[203] Berman, H. M. et al. The Protein Data Bank. Nucleic Acids Research 28, 235-242, (2000).

[204] Hartgerink, J. D., Granja, J. R., Milligan, R. A. & Ghadiri, M. R. Self-Assembling Peptide Nanotubes. Journal of the American Chemical Society 118, 43-50, (1996).

[205] Valery, C. et al. Biomimetic organization: Octapeptide self-assembly into nanotubes of viral capsid-like dimension. Proceedings of the National Academy of Sciences 100, 10258-10262, (2003).

[206] Holmes, T. C. et al. Extensive neurite outgrowth and active synapse formation on self-assembling peptide scaffolds. Proceedings of the National Academy of Sciences 97, 6728-6733, (2000).

[207] Amdursky, N., Molotskii, M., Gazit, E. & Rosenman, G. Elementary Building Blocks of Self-Assembled Peptide Nanotubes. Journal of the American Chemical Society 132, 15632-15636, (2010).

[208] Guo, C., Luo, Y., Zhou, R. & Wei, G. Triphenylalanine peptides self-assemble into nanospheres and nanorods that are different from the nanovesicles and nanotubes formed by diphenylalanine peptides. Nanoscale 6, 2800-2811, (2014).

[209] Rubin, D. J. et al. Structural, Nanomechanical, and Computational Characterization of d,l-Cyclic Peptide Assemblies. ACS Nano 9, 3360-3368, (2015).

[210] Li, Q., Jia, Y., Dai, L., Yang, Y. & Li, J. Controlled Rod Nanostructured Assembly of Diphenylalanine and Their Optical Waveguide Properties. ACS Nano 9, 2689-2695, (2015).

[211] Goodsell, D. S., & Olson, A. J. Structural Symmetry and Protein Function. Annual Review of Biophysics and Biomolecular Structure 29, 105-153, (2000).

[212] Horcas, I. et al. WSXM: A software for scanning probe microscopy and a tool for nanotechnology.

Review of Scientific Instruments 78, 013705, (2007).

[213] Chakrabarti, P. & Pal, D. The interrelationships of side-chain and main-chain conformations in proteins. Progress in Biophysics and Molecular Biology 76, 1-102 (2001).

[214] Shi, Z., Olson, C. A., Rose, G. D., Baldwin, R. L. & Kallenbach, N. R. Polyproline II structure in a sequence of seven alanine residues. Proceedings of the National Academy of Sciences 99, 9190-9195, (2002).

[215] Ramakrishnan, V., Ranbhor, R. & Durani, S. Existence of Specific "Folds" in Polyproline II Ensembles of an "Unfolded" Alanine Peptide Detected by Molecular Dynamics. Journal of the American Chemical Society 126, 16332-16333, (2004).

[216] Ramakrishnan, V., Ranbhor, R., Kumar, A. & Durani, S. The Link between Sequence and Conformation in Protein Structures Appears To Be Stereochemically Established. The Journal of Physical Chemistry B 110, 9314-9323, (2006).

[217] Munishkina, L. A., Henriques, J., Uversky, V. N. & Fink, A. L. Role of Protein−Water Interactions and Electrostatics in α-Synuclein Fibril Formation. Biochemistry 43, 3289-3300, (2004).

[218] Vetri, V. & Foderà, V. The route to protein aggregate superstructures: Particulates and amyloid-like spherulites. FEBS Letters 589, 2448-2463, (2015).

[219] Topping, T. B. & Gloss, L. M. The impact of solubility and electrostatics on fibril formation by the H3 and H4 histones. Protein Science 20, 2060-2073, 2011).

[220] Foderà, V. et al. Observation of the Early Structural Changes Leading to the Formation of Protein Superstructures. The Journal of Physical Chemistry Letters 5, 3254-3258, (2014).

[221] Foderà, V., Zaccone, A., Lattuada, M. & Donald, A. M. Electrostatics Controls the Formation of Amyloid Superstructures in Protein Aggregation. Physical Review Letters 111, 108105, (2013).

[222] Yang, Z., Liang, G., Ma, M., Gao, Y. & Xu, B. Conjugates of naphthalene and dipeptides produce molecular hydrogelators with high efficiency of hydrogelation and superhelical nanofibers. Journal of Materials Chemistry 17, 850-854, (2007).

[223] Brasseru, R., Killian, J. A., De Kruijff, B. & Ruysschaert, J. M. Conformational analysis of gramicidin-gramicidin interactions at the air/water interface suggests that gramicidin aggregates into tube-like structures similar as found in the gramicidin-induced hexagonal HII phase. Biochimica et Biophysica Acta (BBA) – Biomembranes 903, 11-17, (1987).

[224] Lee, O.-S., Cho, V. & Schatz, G. C. Modeling the Self-Assembly of Peptide Amphiphiles into Fibers Using Coarse-Grained Molecular Dynamics. Nano Letters 12, 4907-4913, (2012).

[225] Kornmueller, K. et al. Tracking morphologies at the nanoscale: Self-assembly of an amphiphilic designer peptide into a double helix superstructure. Nano Research 8, 1822-1833, (2015).

[226] Michaels, T. C. T. & Knowles, T. P. J. Role of filament annealing in the kinetics and thermodynamics of nucleated polymerization. The Journal of Chemical Physics 140, 214904, (2014).

[227] Di Michele, L., Eiser, E. & Foderà, V. Minimal Model for Self-Catalysis in the Formation of Amyloid-Like Elongated Fibrils. The Journal of Physical Chemistry Letters 4, 3158-3164, (2013).

[228] Ryadnov, M. G., Bella, A., Timson, S. & Woolfson, D. N. Modular Design of Peptide Fibrillar Nano- to Microstructures. Journal of the American Chemical Society 131, 13240-13241, (2009).

[229] Boris, I. K. A Review for Synthesis of Nanoflowers. Recent patents on nanotechnology2, 190-200,

(2008).

[230] Ohno, H. et al. Electric-field control of ferromagnetism. Nature 408, 944-946 (2000).

[231] Ge, J., Lei, J. & Zare, R. N. Protein–inorganic hybrid nanoflowers. Nature Nanotechnology7, 428, (2012).

[232] Huang, Y., Ran, X., Lin, Y., Ren, J. & Qu, X. Self-assembly of an organic–inorganic hybrid nanoflower as an efficient biomimetic catalyst for self-activated tandem reactions. Chemical Communications 51, 4386-4389, (2015).

[233] Zhang, S., Chen, H.-S., Matras-Postolek, K. & Yang, P. ZnO nanoflowers with single crystal structure towards enhanced gas sensing and photocatalysis. Physical Chemistry Chemical Physics17, 30300-30306, (2015).

[234] Negrón, L. M. et al. Organic Nanoflowers from a Wide Variety of Molecules Templated by a Hierarchical Supramolecular Scaffold. Langmuir32, 2283-2290, (2016).

[235] Tao, Y. et al. 3D polyaniline nanoflowers self-assembled from single crystal nanoplates. Russian Journal of Physical Chemistry A89, 1449-1451, (2015).

[236] Wu, Z.-F. et al. Amino acids-incorporated nanoflowers with an intrinsic peroxidase-like activity. Scientific Reports6, 22412, (2016).

[237] Su, Y. et al. A peony-flower-like hierarchical mesocrystal formed by diphenylalanine. Journal of Materials Chemistry20, 6734-6740, (2010).

[238] Xiao, Y., Zhang, M., Wang, F.-X. & Pan, G.-B. Hierarchical flower-shaped organic NPB architectures with a durable water-repellent property. CrystEngComm14, 1933-1935, (2012).

[239] Zhu, G. et al. Noncanonical Self-Assembly of Multifunctional DNA Nanoflowers for Biomedical Applications. Journal of the American Chemical Society135, 16438-16445, (2013).

[240] Hu, R. et al. DNA Nanoflowers for Multiplexed Cellular Imaging and Traceable Targeted Drug Delivery. Angewandte Chemie International Edition53, 5821-5826, (2014).

[241] Zhang, L. et al. Self-Assembled DNA Immunonanoflowers as Multivalent CpG Nanoagents. ACS Applied Materials & Interfaces7, 24069-24074, (2015).

[242] Version, B. S. 5.054, and SADABS Version 2.05. Bruker Analytical X-ray Systems Inc., Madison, WI (2003).

[243] Shchepinov, M. S. & Korshun, V. A. Recent applications of bifunctional trityl groups. Chemical Society Reviews32, 170-180, (2003).

[244] Merrifield, R. B. Solid Phase Peptide Synthesis. I. The Synthesis of a Tetrapeptide. Journal of the American Chemical Society85, 2149-2154, (1963).

[245] Gao, H., Yan, F., Li, J., Zeng, Y. & Wang, J. Synthesis and characterization of ZnO nanorods and nanoflowers grown on GaN-based LED epiwafer using a solution deposition method. Journal of Physics D: Applied Physics40, 3654 (2007).

[246] Wang, Y., Li, X., Lu, G., Chen, G. & Chen, Y. Synthesis and photo-catalytic degradation property of nanostructured-ZnO with different morphology. Materials Letters62, 2359-2362, (2008).

[247] Suh, H.-W., Kim, G.-Y., Jung, Y.-S., Choi, W.-K. & Byun, D. Growth and properties of ZnO nanoblade and nanoflower prepared by ultrasonic pyrolysis. Journal of Applied Physics97, 044305, (2005).

[248] Pan, A. et al. ZnO flowers made up of thin nanosheets and their optical properties. Journal of

Crystal Growth282, 165-172, (2005).

[249] Zeng, S. et al. Facile Route for the Fabrication of Porous Hematite Nanoflowers: Its Synthesis, Growth Mechanism, Application in the Lithium Ion Battery, and Magnetic and Photocatalytic Properties. The Journal of Physical Chemistry C112, 4836-4843, (2008).

[250] Lambert, J., Shurvell, H., Lightner, D. & Cooks, R. Organic Structural Spectroscopy Prentice-Hall. Inc. New Jersey (1998).

[251] Lekprasert, B. et al. Investigations of the supramolecular structure of individual diphenylalanine nano-and microtubes by polarized Raman microspectroscopy. Biomacromolecules13, 2181-2187 (2012).

[252] Heisenberg, W. Zur Theorie des Ferromagnetismus. Zeitschrift für Physik 49, 619-636, (1985).

[253] Makarova, T. L. et al. Magnetic carbon. Nature 413, 716-718, (2001).

[254] Eng, A. Y. S. et al. Searching for Magnetism in Hydrogenated Graphene: Using Highly Hydrogenated Graphene Prepared via Birch Reduction of Graphite Oxides. ACS Nano 7, 5930-5939, (2013).

[255] Lee, K. W. & Lee, C. E. Electron spin resonance of proton-irradiated graphite. Phys Rev Lett 97, 137206, (2006).

[256] Friedman, A. L. et al. Possible room-temperature ferromagnetism in hydrogenated carbon nanotubes. Physical Review B 81, 115461 (2010).

[257] Talapatra, S. et al. Irradiation-induced magnetism in carbon nanostructures. Phys Rev Lett 95, 097201, (2005).

[258] Miller, J. S. Organic- and molecule-based magnets. Materials Today 17, 224-235, (2014).

[259] Dougherty, D. A. New high-spin π systems. Pure and applied chemistry 62, 519-524 (1990).

[260] Dougherty, D. A. Cation-π Interactions in Chemistry and Biology: A New View of Benzene, Phe, Tyr, and Trp. Science 271, 163-168, (1996).

[261] Boukhvalov, D., Moehlecke, S., Da Silva, R. & Kopelevich, Y. Effect of oxygen adsorption on magnetic properties of graphite. Physical Review B 83, 233408 (2011).

[262] Lee, K. W., Kweon, H. & Lee, C. E. Field-Induced Transition from Room-Temperature Ferromagnetism to Diamagnetism in Proton-Irradiated Fullerene. Advanced Materials 25, 5663-5667 (2013).

[263] Matsukura, F., Tokura, Y. & Ohno, H. Control of magnetism by electric fields. Nat Nano 10, 209-220, (2015).

[264] Chappert, C., Fert, A. & Van Dau, F. N. The emergence of spin electronics in data storage. Nat Mater 6, 813-823 (2007).

[265] Gomes, J. On the use of the ring current concept. Molecular Physics 40, 765-769 (1980).

[266] Islas, R., Heine, T. & Merino, G. The induced magnetic field. Accounts of chemical research 45, 215-228 (2011).

[267] The magnetic anisotropy of naphthalene crystals. Proceedings of the Royal Society of London. Series A 124, 545-554, (1929).

[268] Park, S.-H. et al. Canted antiferromagnetism and spin reorientation transition in layered inorganic–organic perovskite $(C_6H_5CH_2CH_2NH_3)_2MnCl_4$. Dalton Transactions 41, 1237-1242 (2012).

[269] Shukla, D. et al. Dioxapyrene-Based Organic Semiconductors for Organic Field Effect Transistors.

The Journal of Physical Chemistry C 113, 14482-14486, (2009).

[270] Munn, R. W., Miniewicz, A. & Kuchta, B. Electrical and related properties of organic solids. Vol. 24 (Springer Science & Business Media, 2012).

[271] Sun, S.-S. & Sariciftci, N. S. Organic photovoltaics: mechanisms, materials, and devices. (CRC press, 2005).

[272] Rúa, F. et al. Self-Assembly of a Cyclobutane β-Tetrapeptide To Form Nanosized Structures. Organic Letters9, 3643-3645, (2007).

[273] Adachi, H. et al. Photoresponsive Toroidal Nanostructure Formed by Self-Assembly of Azobenzene-Functionalized Tris(phenylisoxazolyl)benzene. Organic Letters18, 924-927, (2016).

[274] Fu, F. & Wang, Q. Removal of heavy metal ions from wastewaters: A review. Journal of Environmental Management 92, 407-418, (2011).

[275] Tchounwou, P. B., Yedjou, C. G., Patlolla, A. K. & Sutton, D. J. in Molecular, clinical and environmental toxicology 133-164 (Springer, 2012).

[276] ATSDR, S. Toxicological Profile for Chromium. Agency for Toxic Substances and Disease Registry. Public Health Service, US Department of Health and Human Services. http://www. atsdr. cdc. gov/toxprofiles/tp. asp (2012).

[277] Wang, H. & Na, C. Binder-free carbon nanotube electrode for electrochemical removal of chromium. ACS applied materials & interfaces 6, 20309-20316 (2014).

[278] Hashim, M. A., Mukhopadhyay, S., Sahu, J. N. & Sengupta, B. Remediation technologies for heavy metal contaminated groundwater. Journal of Environmental Management 92, 2355-2388, (2011).

[279] Xing, Y., Chen, X. & Wang, D. Electrically Regenerated Ion Exchange for Removal and Recovery of Cr(VI) from Wastewater. Environmental Science & Technology 41, 1439-1443, (2007).

[280] Pan, C., Troyer, L. D., Catalano, J. G. & Giammar, D. E. Dynamics of Chromium(VI) Removal from Drinking Water by Iron Electrocoagulation. Environmental Science & Technology 50, 13502-13510, (2016).

[281] Ali, I. New Generation Adsorbents for Water Treatment. Chemical Reviews 112, 5073-5091, (2012).

[282] Zhao, Q. et al. Rapid Magnetic Solid-Phase Extraction Based on Magnetic Multiwalled Carbon Nanotubes for the Determination of Polycyclic Aromatic Hydrocarbons in Edible Oils. Journal of Agricultural and Food Chemistry 59, 12794-12800, (2011).

[283] Liu, Y. et al. Synthesis of High Saturation Magnetization Superparamagnetic Fe3O4 Hollow Microspheres for Swift Chromium Removal. ACS Applied Materials & Interfaces 4, 4913-4920, (2012).

[284] Wu, W., He, Q. & Jiang, C. Magnetic iron oxide nanoparticles: synthesis and surface functionalization strategies. Nanoscale research letters 3, 397-415, (2008).

[285] Reena Mary, A. P. et al. Synthesis of Bio-Compatible SPION-based Aqueous Ferrofluids and Evaluation of RadioFrequency Power Loss for Magnetic Hyperthermia. Nanoscale research letters 5, 1706-1711, (2010).

[286] Nair, S. S., Thomas, J., Suchand Sandeep, C., Anantharaman, M. & Philip, R. An optical limiter based on ferrofluids. Applied Physics Letters 92, 171908 (2008).

[287] Teja, A. S. & Koh, P.-Y. Synthesis, properties, and applications of magnetic iron oxide nanoparticles. Progress in Crystal Growth and Characterization of Materials 55, 22-45, (2009).

[288] Neamtu, J. &Verga, N. Magnetic nanoparticles for magneto-resonance imaging and targeted drug delivery. Digest Journal of Nanomaterials and Biostructures 6, 969-978 (2011).

[289] Wan, J., Cai, W., Meng, X. & Liu, E. Monodisperse water-soluble magnetite nanoparticles prepared by polyol process for high-performance magnetic resonance imaging. Chemical Communications, 5004-5006, (2007).

[290] El Ghandoor, H., Zidan, H., Khalil, M. M. & Ismail, M. Synthesis and some physical properties of magnetite (Fe_3O_4) nanoparticles. Int. J. Electrochem. Sci 7, 5734-5745 (2012).

[291] Lodhia, J., Mandarano, G., Ferris, N., Eu, P. & Cowell, S. Development and use of iron oxide nanoparticles (Part 1): Synthesis of iron oxide nanoparticles for MRI. Biomedical imaging and intervention journal 6, e12 (2010).

[292] Khan, A. Preparation and characterization of magnetic nanoparticles embedded in microgels. Materials Letters 62, 898-902 (2008).

[293] Einschlag, F. S. G. & Carlos, L. Waste Water-Treatment Technologies and Recent Analytical Developments. (2013).

[294] Lehn, J.-M. Toward Self-Organization and Complex Matter. Science 295, 2400-2403, (2002).

[295] Whitesides, G. M. & Grzybowski, B. Self-Assembly at All Scales. Science 295, 2418-2421, (2002).

[296] Marker, K. et al. Welcoming natural isotopic abundance in solid-state NMR: probing pi-stacking and supramolecular structure of organic nanoassemblies using DNP. Chemical science 8, 974-987, (2017).

[297] Sutton, C., Risko, C. & Brédas, J.-L. Noncovalent Intermolecular Interactions in Organic Electronic Materials: Implications for the Molecular Packing vs Electronic Properties of Acenes. Chemistry of Materials 28, 3-16, (2016).

[298] Mason, D. & Bernstein, J. A Crystal Packing-Melting Point Correlation for Quaternary Ammonium Salts. Molecular Crystals and Liquid Crystals Science and Technology. Section A. Molecular Crystals and Liquid Crystals 242, 179-191 (1994).

[299] Stupp, S. I. & Palmer, L. C. Supramolecular Chemistry and Self-Assembly in Organic Materials Design. Chemistry of Materials 26, 507-518, (2014).

[300] Habibi, N., Kamaly, N., Memic, A. & Shafiee, H. Self-assembled peptide-based nanostructures: Smart nanomaterials toward targeted drug delivery. Nano today 11, 41-60, (2016).

[301] Fosgerau, K. & Hoffmann, T. Peptide therapeutics: current status and future directions. Drug Discovery Today 20, 122-128, (2015).

[302] de la Rica, R. & Matsui, H. Applications of peptide and protein-based materials in bionanotechnology. Chem Soc Rev 39, 3499-3509, (2010).

[303] Hatip Koc, M. et al. Hierarchical Self-Assembly of Histidine-Functionalized Peptide Amphiphiles into Supramolecular Chiral Nanostructures. Langmuir 33, 7947-7956, (2017).

[304] Frisch, H. & Besenius, P. pH-Switchable Self-Assembled Materials. Macromolecular Rapid Communications 36, 346-363, (2015).

[305] Lin, B. F. et al. pH-responsive branched peptide amphiphile hydrogel designed for applications in regenerative medicine with potential as injectable tissue scaffolds. Journal of Materials Chemistry 22, 19447-19454, (2012).

[306] Moyer, T. J. et al. pH and Amphiphilic Structure Direct Supramolecular Behavior in Biofunctional

Assemblies. Journal of the American Chemical Society 136, 14746-14752, (2014).

[307] Valenti, L. E., De Pauli, C. P. & Giacomelli, C. E. The binding of Ni(II) ions to hexahistidine as a model system of the interaction between nickel and His-tagged proteins. Journal of Inorganic Biochemistry 100, 192-200, (2006).

[308] Hammarström, L. & Styring, S. Proton-coupled electron transfer of tyrosines in Photosystem II and model systems for artificial photosynthesis: the role of a redox-active link between catalyst and photosensitizer. Energy & Environmental Science 4, 2379-2388, (2011).

[309] Winkler, J. R. & Gray, H. B. Long-Range Electron Tunneling. Journal of the American Chemical Society 136, 2930-2939, (2014).

[310] Malvankar, N. S. et al. Tunable metallic-like conductivity in microbial nanowire networks. Nature Nanotechnology 6, 573, (2011).

[311] Namgung, S. D. et al. Increased electrical conductivity of peptides through annealing process. APL Materials 5, 086109, (2017).

[312] Nalluri, S. K. M. et al. Conducting Nanofibers and Organogels Derived from the Self-Assembly of Tetrathiafulvalene-Appended Dipeptides. Langmuir 30, 12429-12437, (2014).

[313] Kirschner, M. & Mitchison, T. Beyond self-assembly: from microtubules to morphogenesis. Cell 45, 329-342 (1986).

[314] Pollard, T. D. & Borisy, G. G. Cellular motility driven by assembly and disassembly of actin filaments. Cell 112, 453-465 (2003).

[315] Altunbas, A. & Pochan, D. J. Peptide-based and polypeptide-based hydrogels for drug delivery and tissue engineering. Topics in current chemistry 310, 135-167, (2012).

[316] Kong, J. & Yu, S. Fourier transform infrared spectroscopic analysis of protein secondary structures. Acta biochimica et biophysica Sinica 39, 549-559 (2007).

[317] Zimenkov, Y. et al. Rational Design of a Reversible pH-Responsive Switch for Peptide Self-Assembly. Journal of the American Chemical Society 128, 6770-6771, (2006).

[318] Palmer, L. C. & Stupp, S. I. Molecular Self-Assembly into One-Dimensional Nanostructures. Accounts of Chemical Research 41, 1674-1684, (2008).

[319] Xiao, S. et al. Transferring Self-Assembled, Nanoscale Cables into Electrical Devices. Journal of the American Chemical Society 128, 10700-10701, (2006).

[320] Tovar, J. D. Supramolecular Construction of Optoelectronic Biomaterials. Accounts of Chemical Research 46, 1527-1537, (2013).

[321] Wall, B. D. et al. Variation of Formal Hydrogen-Bonding Networks within Electronically Delocalized π-Conjugated Oligopeptide Nanostructures. Langmuir 30, 11375-11385, (2014).

[322] Besar, K., Ardoña, H. A. M., Tovar, J. D. & Katz, H. E. Demonstration of Hole Transport and Voltage Equilibration in Self-Assembled π-Conjugated Peptide Nanostructures Using Field-Effect Transistor Architectures. ACS Nano 9, 12401-12409, (2015).

[323] Nicolini, C. From neural chip and engineered biomolecules to bioelectronic devices: An overview. Biosensors and Bioelectronics 10, 105-127, (1995).

[324] Someya, T., Bao, Z. & Malliaras, G. G. The rise of plastic bioelectronics. Nature 540, 379, (2016).

[325] Zhang, A. & Lieber, C. M. Nano-Bioelectronics. Chemical Reviews 116, 215-257, (2016).

[326] De Santis, E. & Ryadnov, M. G. Peptide self-assembly for nanomaterials: the old new kid on the block. Chemical Society Reviews 44, 8288-8300, (2015).